



Faculty of Electrical Technology and Engineering

**DEVELOPMENT OF CAPACITIVE WIRELESS POWER TRANSFER
COUPLER FOR UNDERWATER EV CHARGING APPLICATION**

NURUL AIMI SYAFIQAH BINTI TAJUL ARIS

Bachelor of Electrical Engineering Technology with Honours

2025

**DEVELOPMENT OF CAPACITIVE WIRELESS POWER TRANSFER COUPLER
FOR UNDERWATER EV CHARGING APPLICATION**

NURUL AIMI SYAFIQAH BINTI TAJUL ARIS



UNIVERSITI TEKNIKAL MALAYSIA MELAKA

2025

DECLARATION

I declare that this project report entitled Development Of Capacitive Wireless Power Transfer Coupler For Underwater Ev Charging Application is the result of my own research except as cited in the references. The project report has not been accepted for any degree and is not concurrently submitted in candidature of any other degree.



Signature

:

Student Name

:

NURUL AIMI SYAFIQAH BINTI TAJUL ARIS

Date

:

6/1/2025

UNIVERSITI TEKNIKAL MALAYSIA MELAKA

APPROVAL

I hereby declare that I have checked this project report and in my opinion, this project report is adequate in terms of scope and quality for the award of the degree of Bachelor of Electrical Engineering Technology with Honours.

Signature :

Supervisor Name : TS.DR SUZIANA BINTI AHMAD

Date : 6/1/2025

UNIVERSITI TEKNIKAL MALAYSIA MELAKA

DEDICATION

I dedicate this project to my family, whose unwavering support and encouragement have been my guiding light throughout this journey.

To my parents, for their sacrifices and belief in my potential, which have inspired me to strive for excellence.

To my friends and mentors, for their invaluable guidance, motivation, and camaraderie that made this endeavor possible.

Lastly, to all those who dream of making a difference, may this work serve as a steppingstone toward innovation and progress.

اونيورسيتي تيكنيكل مليسيا ملاك
UNIVERSITI TEKNIKAL MALAYSIA MELAKA

ABSTRACT

Wireless power transfer (WPT) has gained significant attention as a promising technology for charging and powering electronic devices without the need for physical connections. Capacitive wireless power transfer makes it possible to transfer power between devices without making direct contact by doing away with the need for physical connectors or cables. The capacitive Power Transfer (CPT) coupler for underwater electric vehicle (EV) charging, addressing the limitations of underwater environments. This project investigates the design, simulation and implementation of a CPT coupler tailored for underwater EV applications addressing the unique limitations posed by varying dielectric properties of different underwater mediums. The study begins with the calculation of parameters for two-plate and four-plate CPT couplers using MATLAB simulations, focusing on capacitance values across air, freshwater and seawater. The results demonstrated consistent alignment with theoretical predictions and validating the simulation approach. Then, the focus shifted on developing capacitive wireless power transfer coupler for underwater EV charging application using printed circuit board. This phase successfully demonstrated the fabrication and assembly process for the coupler achieving the second objective. Lastly, analyzing the development of capacitive wireless power transfer coupler for underwater EV charging application using real time experiment demonstrating efficient power transfer across the tested mediums. The findings of this research highlight the potential of CPT technology in enabling reliable and efficient underwater wireless charging systems with significant implications for electric ship charging and subsea power applications. By doing this, could improve and analyze the efficiency of underwater wireless charging by focusing all electricity on the charging vehicle.

ABSTRAK

Penghantaran kuasa tanpa wayar (WPT) semakin mendapat perhatian sebagai teknologi masa depan yang berpotensi untuk mengecas dan membekalkan tenaga kepada peranti elektronik tanpa memerlukan kabel. Projek ini memfokuskan kepada reka bentuk, simulasi, dan pelaksanaan coupler CPT yang dioptimumkan khusus untuk aplikasi pengecasan kenderaan elektrik (EV) bawah air, dengan mengambil kira cabaran unik seperti sifat dielektrik yang berbeza dalam medium seperti udara, air dan air laut. Kajian ini dimulakan dengan pengiraan parameter coupler CPT 2 plat dan 4 plat menggunakan simulasi MATLAB, di mana nilai parameter dianalisis dalam ketiga-tiga medium tersebut. Hasil simulasi menunjukkan keserasian yang tinggi dengan ramalan teori, sekali gus mengesahkan ketepatan pendekatan simulasi yang digunakan. Seterusnya, melibatkan reka bentuk, fabrikasi, dan pemasangan coupler CPT menggunakan papan litar bercetak yang berjaya memenuhi objektif kedua projek. Akhirnya, ujian dijalankan untuk menganalisis prestasi sistem CPT dalam persekitaran bawah air. Hasil ujian membuktikan bahawa sistem ini mampu memindahkan tenaga dengan merentasi medium yang diuji, sekaligus membuktikan kebolehpercayaan teknologi ini untuk aplikasi dunia sebenar. Penemuan ini menekankan potensi besar CPT dalam menyediakan penyelesaian pengecasan bawah air yang efisien dan stabil, dengan implikasi penting untuk pengecasan kapal elektrik serta aplikasi tenaga dasar laut. Projek ini membuka ruang untuk penambahbaikan lanjut dalam kecekapan dan reka bentuk sistem CPT, serta menyediakan asas kukuh untuk kajian dan pembangunan teknologi pengecasan bawah air pada masa hadapan.

ACKNOWLEDGEMENTS

First and foremost, I express my deepest gratitude to Universiti Teknikal Malaysia Melaka and the faculty of Electrical Technology and Engineering for providing me with the opportunity and resources to undertake this project.

I am sincerely thankful to my project supervisor, Dr Suziana Binti Ahmad, for their guidance, expertise, and constructive feedback throughout this journey. Their mentorship has been invaluable in shaping the direction and outcome of this work. I extend my appreciation to the faculty members and technical staff for their assistance and support during this project.

A heartfelt thanks to my family and friends, whose unwavering encouragement and understanding have been a source of strength and motivation. I am grateful to my peers and colleagues who shared ideas, provided constructive criticism, and collaborated to overcome challenges during this process. This project would not have been possible without the collective efforts and support of all these individuals.

Last but not least, I want to sincerely thank myself. I am proud of myself for believing in my abilities, working hard with dedication, staying strong during tough times and never giving up. I am grateful for my generosity, always trying to give more than I take and for staying true to my values by striving to do the right thing. Most importantly, I thank myself for being honest and true to who I am throughout this journey.

TABLE OF CONTENTS

	PAGE
DECLARATION	
APPROVAL	
DEDICATIONS	
ABSTRACT	i
ABSTRAK	ii
ACKNOWLEDGEMENTS	iii
TABLE OF CONTENTS	iv
LIST OF TABLES	vii
LIST OF FIGURES	viii
LIST OF SYMBOLS	xiv
LIST OF ABBREVIATIONS	xv
LIST OF APPENDICES	xvi
CHAPTER 1 INTRODUCTION	17
1.1 Background	17
1.2 Problem Statement	19
1.3 Project Objective	20
1.4 Scope of Project	20
CHAPTER 2 LITERATURE REVIEW	22
2.1 Introduction	22
2.2 Wireless power Transfer (WPT)	22
2.2.1 Inductive Power Transfer (IPT)	24
2.2.2 Capacitive Power Transfer (CPT)	27
2.2.3 Hybrid Power Transfer (CPT-IPT)	28
2.3 Fundamental of working principle of CPT	32
2.4 Capacitive coupler structure	34
2.4.1 Two-plate couplers	34
2.4.2 Four-plate couplers	35
2.4.3 Six-plate couplers	37
2.5 Application of CPT system	40
2.5.1 Electronic application	40
2.5.2 Transportation application	41
2.5.3 Biomedical	46
2.6 Research, Ideology and Concept of Previous Project	47

2.7	Comparisons of existing WPT underwater in air, fresh water, and seawater	55
2.8	Summary	61
CHAPTER 3 METHODOLOGY		62
3.1	Introduction	62
3.2	Flowchart of overall system	63
3.3	Block diagram	64
3.4	Circuit Modelling	65
	3.4.1 Analysis of sheilded CPT circuit model	65
	3.4.2 LTspice	67
	3.4.3 MATLAB	68
3.5	Simulation in MATLAB	68
	3.5.1 Calculations on CPT structure	69
	3.5.2 Case of WPT under fresh water	70
	3.5.3 Freshwater Adaptation , K	71
	3.5.4 Quality factor , Q	72
	3.5.5 Pseudo-coupling coefficient , kp	72
	3.5.6 KpQ product , kQ	73
	3.5.7 Maximum power transfer efficiency, nmax	73
	3.5.8 Frequency characteristics, fk	74
	3.5.9 Case of WPT under seawater	75
	3.5.10 Maximum power transfer efficiency , nmax	76
	3.5.11 Coupling coefficient, K	76
	3.5.12 Refined Coupling coefficient, K	77
	3.5.13 Frequency dependent transfer function , F	77
3.6	Simulation LTspice	78
	3.6.1 Freshwater	78
	3.6.2 Seawater	80
3.7	Hardware development	83
	3.7.1 System of project	83
	3.7.2 Experimental setup	84
	3.7.3 Experimental setup in Air	87
	3.7.4 Experimental setup in Freshwater	88
	3.7.5 Experimental setup in Seawater	89
	3.7.6 NanoVNA saver	91
	3.7.7 NanoVNA vector network analyzer	92
3.8	Gantt Chart of the project	95
3.9	Summary	97
CHAPTER 4 RESULTS AND DISCUSSIONS		98
4.1	Introduction	98
4.2	Result simulation using MATLAB	98
	4.2.1 Result calculation of capacitance versus distance	99
	4.2.2 Result calculation of nmax (maximum power transfer efficiency) VS frequency	104
	4.2.3 Result calculation of kpQ VS frequency	110
	4.2.4 Result calculation of frequency	115
	4.2.5 Result calculation of F and K	116
4.3	Result on simulation using LTspice	118

4.3.1	LTspice in water	118
4.3.2	LTspice seawater	120
4.4	Measurement and analysis	122
4.4.1	NanoVNA saver	122
4.4.2	NanoVNA vector network analyzer	130
4.5	Summary	133
CHAPTER 5 CONCLUSION AND RECOMMENDATIONS		134
5.1	Conclusion	134
5.2	Future Works	135
5.3	Project potential	136
REFERENCES		137
APPENDICES		142



LIST OF TABLES

TABLE	TITLE	PAGE
Table 2.1	The differences between IPT, CPT and Hybrid (IPT-CPT)	31
Table 2.2	The differences between IPT, CPT and Hybrid (IPT-CPT) based on research papers	32
Table 2.3	The two-plate CPT method structure for long-distance quasi-wireless and electric car charging applications.	35
Table 2.4	The comparison between plate structure and their equation.	39
Table 2.5	Review various applications using CPT system	46
Table 2.6	Comparisons of existing WPT underwater in air, fresh water, and seawater	56
Table 2.7	Application of wireless power transfer (WPT)	57
Table 2.8	Wireless power transfer (WPT)	60
Table 3.1	Comparisons of existing WPT underwater in air, fresh water, and seawater	69
Table 3.2	Parameter are set for calculation.	70
Table 3.3	Parameter are set for calculation.	70
Table 3.4	Parameter for calculation in freshwater	71
Table 3.5	Parameter for calculation in seawater	75
Table 3.6	Parameter for calculation in freshwater	79
Table 3.7	Parameter for calculation in seawater	81
Table 3.7	The tasks or activities and duration to completed BDP 1	95
Table 3.8	The tasks or activities and duration to completed BDP 2	96

LIST OF FIGURES

FIGURE	TITLE	PAGE
Figure 2.1	Display a WPT systems typical system structure	23
Figure 2.2	The generic block diagram of a wireless power system	24
Figure 2.3	The standard IPT system	25
Figure 2.4	Circuit diagram of IPT system	25
Figure 2.5	The inductive power transfer (IPT) system schematic diagram	26
Figure 2.6	Typical CPT system	28
Figure 2.7	Schematic diagram of CPT system	28
Figure 2.8	The coils in configuration (a) are connected in phase while configuration (b) has the coils connected out of phase	30
Figure 2.9	Displays the hybrid IPT and CPT system with SS compensation	31
Figure 2.10	A typical structure of a CPT system	33
Figure 2.11	The structure of a single pair of metal plates in water medium	33
Figure 2.12	The two-plate structure	34
Figure 2.13	Example of a two-plate long-distance quasi-wireless CPT system structure	35
Figure 2.14	The structure of a two-plate compact CPT system use for electric vehicle charging (EV).	35
Figure 2.15	The double-sided LC-compensated two-plate quasi-wireless CPT system	35
Figure 2.16	The equivalent concept of a ground and chassis two-plate CPT system.	35
Figure 2.17	The four-plate parallel structure	36
Figure 2.18	The four-plate stacked structure	36
Figure 2.19	The model of coupling capacitor in seawater conditions	36
Figure 2.20	The six-plate structure of CPT system	37

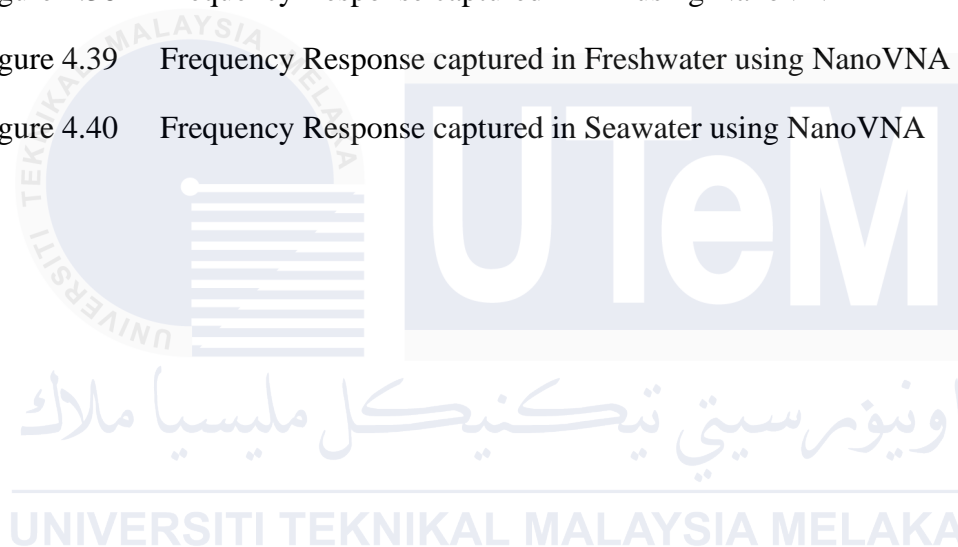
Figure 2.21	The circuit topology of a six-plate CPT system with LCL compensation	38
Figure 2.22	The process of simplifying the capacitor model when $V_2 = V_3 = 0$	38
Figure 2.23	Display strategy for the suggested WPT system with near field capacitively coupling	41
Figure 2.24	Demonstrate the proposed near-field capacitively connected WPT system's experimental setup	41
Figure 2.25	The Corbin Sparrow equipped with an onboard battery charger and an offboard experimental charger's DC charging port	42
Figure 2.26	a) show conformal bumper charging station that has transmitter foil strips attached to a foam rubber	43
Figure 2.27	b) show conformal bumper for charging stations that has transmitter foil strips attached to a foam rubber pad	43
Figure 2.28	The overview of underwater wireless charging system	44
Figure 2.29	The experimental setup for the UWPT system	44
Figure 2.30	The illustration of the drone recharge process using laser beaming	45
Figure 2.31	Power line emulation setup, side view	45
Figure 2.32	Power supply for biomedical implants based on CPT system	46
Figure 2.33	The BD-UCWPT experimental prototype	47
Figure 2.34	The 3-dimensional coupling capacitance	48
Figure 2.35	The connecting CS1 and CS2 capacitance to a flexible distance in a seawater medium	48
Figure 2.36	The Experimental setup for the four-plate CPT system undergoing testing.	49
Figure 2.37	The coupling capacitor structure in the seawater condition.	49
Figure 2.38	Waveforms of experimental voltage and current in coupling capacitors	50
Figure 2.39	a) The experimental configuration incorporating the cross-coupling effect.	51
Figure 2.40	The coupling between 4 plate structure	51

Figure 2.41	Compare the observed capacitance of separation distance in air with the analytical and numerical approaches	51
Figure 2.42	A scaled-down prototype of the capacitive coupler-equipped LC compensated CPT system prototype	52
Figure 2.43	The component requirements and circuit topology of the underwater CPT system with LC compensation	53
Figure 2.44	HFSS-simulated coupling capacitance between the two plates within a wide range of relative distances d	53
Figure 2.45	a) prototype b) measurement setup	54
Figure 2.46	Measurements of the Q-factor and $\tan \delta$ of the frequency characteristics of tap water	54
Figure 3.1	Flowchart of overall project	63
Figure 3.2	Block diagram	64
Figure 3.3	Circuit model for S-CPT coupling capacitance circuit analysis	66
Figure 3.4	Simplified model of shielded-CPT coupling structure	67
Figure 3.5	LTspice Illustration	67
Figure 3.6	MATLAB illustration	68
Figure 3.7	Calculation based on circuit in freshwater	71
Figure 3.8	Calculation based on circuit for seawater	76
Figure 3.9	Schematic of capacitive coupler in freshwater	78
Figure 3.10	Schematic of capacitive coupler in freshwater designed in LTspice	80
Figure 3.11	Schematic of capacitive coupler in seawater	81
Figure 3.12	Schematic of capacitive coupler in seawater designed in LTspice	82
Figure 3.13	The simulation model based on research paper	85
Figure 3.14	The setup circuit connection in freshwater by referring to research paper	85
Figure 3.15	Calculation of inductor coil	85
Figure 3.16	The setup connection for NanoVNA in air	87
Figure 3.17	The setup connection circuit in air	87

Figure 3.18	The condition of parallel plate in freshwater	88
Figure 3.19	The water level with height of 6cm	88
Figure 3.20	The setup connection circuit in freshwater	89
Figure 3.21	The condition of parallel plate in seawater	90
Figure 3.22	The setup connection of NanoVNA for seawater	90
Figure 3.23	The setup connection circuit in seawater	90
Figure 3.24	NanoVNA saver	91
Figure 3.25	NanoVNA vector network analyzer	93
Figure 3.26	The NanoVNA vector network analyzer with its calibration standards for short, open and thru is used for accurate measurements.	93
Figure 4.1	Tabulated data from MATLAB simulation	99
Figure 4.2	The graph of capacitance vs. distance in the air, displaying a sharp decrease in capacitance as distance increase.	100
Figure 4.3	Capacitance vs. distance graph in freshwater, illustrating a more gradual drop than in air.	101
Figure 4.4	Capacitance vs. distance graph in seawater, similar in trend to freshwater but with slightly higher values	102
Figure 4.5	The graph of capacitance vs distance combines the data in air, freshwater and seawater	103
Figure 4.6	Tabulated data from MATLAB simulation for air medium	104
Figure 4.7	The graph maximum power transfer efficiency versus frequency in air medium	105
Figure 4.8	Tabulated data from MATLAB simulation for freshwater medium	105
Figure 4.9	The graph maximum power transfer efficiency versus frequency in freshwater medium	106
Figure 4.10	Tabulated data from MATLAB simulation for seawater medium	107
Figure 4.11	The graph maximum power transfer efficiency versus frequency in seawater medium	108
Figure 4.12	Tabulated data from MATLAB simulation for air ,freshwater and seawater	108

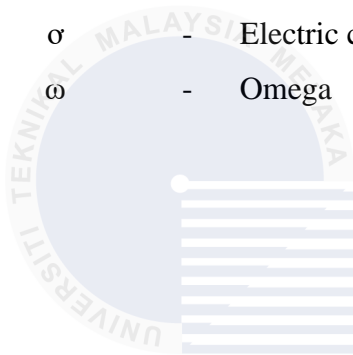
Figure 4.13	The combined graph of maximum power transfer efficiency versus frequency in air, freshwater and seawater	109
Figure 4.14	Tabulated data from MATLAB simulation	110
Figure 4.15	The graph of kQ versus frequency in air medium	111
Figure 4.16	The graph of kQ versus frequency in freshwater medium	112
Figure 4.17	The graph of kQ versus frequency in seawater medium	113
Figure 4.18	The combined graph kQ versus frequency in air, freshwater and seawater	114
Figure 4.19	Value result from MATLAB of calculation for frequency	115
Figure 4.20	Value result from MATLAB of calculation	116
Figure 4.21	Tabulated data from MATLAB simulation of calculation for frequency and F	117
Figure 4.22	The graph of F vs frequency	117
Figure 4.23	LTspice Simulation of a Resonant LC Filter Circuit in water condition	118
Figure 4.24	The circuit designed in LTspice in water condition	119
Figure 4.25	Frequency Response result gain in LTspice under water condition	120
Figure 4.26	LTspice Simulation of a Resonant LC Filter Circuit under seawater condition	120
Figure 4.27	The circuit designed in LTspice in seawater condition	121
Figure 4.28	Frequency Response result gain in LTspice under seawater condition	122
Figure 4.29	Frequency Sweep Analysis Captured Using NanoVNA Saver in air	123
Figure 4.30	S11 Return Loss frequency response data captured by NanoVNA Saver in air	123
Figure 4.31	The S21 gain (dB) frequency response data captured via NanoVNA Saver in air	124
Figure 4.32	Frequency Sweep Analysis Captured Using NanoVNA Saver in water	125
Figure 4.33	S11 Return Loss frequency response data captured by NanoVNA Saver in water.	126

Figure 4.34	The S21 gain (dB) frequency response data captured via NanoVNA Saver in water	127
Figure 4.35	Frequency Sweep Analysis Captured Using NanoVNA Saver in seawater	127
Figure 4.36	S11 Return Loss frequency response data captured by NanoVNA Saver in seawater	128
Figure 4.37	The S21 gain (dB) frequency response data captured via NanoVNA Saver in seawater	129
Figure 4.38	Frequency Response captured in Air using NanoVNA	130
Figure 4.39	Frequency Response captured in Freshwater using NanoVNA	131
Figure 4.40	Frequency Response captured in Seawater using NanoVNA	132



LIST OF SYMBOLS

ϵ_0	-	The permittivity of free space (8.854×10^{-12} F/m)
ϵ_r	-	The relative permittivity
A	-	Area
C	-	Capacitance
d	-	Distance
mm	-	Milimeter
σ	-	Electric conductivity
ω	-	Omega

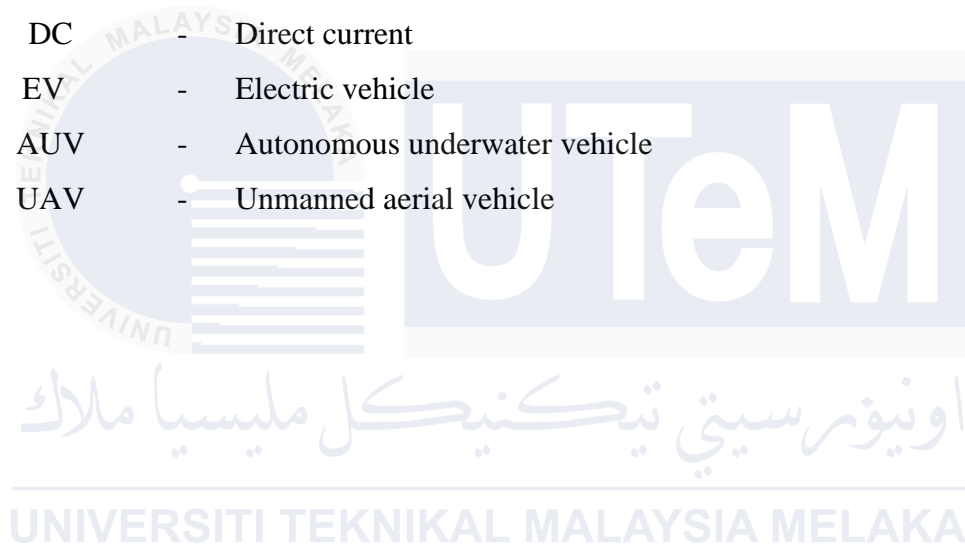


اونيورسيتي تيكنيكل مليسيا ملاك

UNIVERSITI TEKNIKAL MALAYSIA MELAKA

LIST OF ABBREVIATIONS

WPT	-	Wireless power transfer
CPT	-	Capacitive power transfer
CWPT	-	Capacitive wireless power transfer
IPT	-	Inductive power transfer
UWPT	-	Underwater wireless power transfer
AC	-	Alternating current
DC	-	Direct current
EV	-	Electric vehicle
AUV	-	Autonomous underwater vehicle
UAV	-	Unmanned aerial vehicle



LIST OF APPENDICES

APPENDIX	TITLE	PAGE
Appendix A	Example of Appendix A	142
Appendix B	Example of Appendix B	143
Appendix C	Example of Appendix C	144
Appendix D	Example of Appendix D	145
Appendix E	Example of Appendix E	146
Appendix F	Example of Appendix F	147
Appendix G	Example of Appendix G	148
Appendix H	Example of Appendix H	149

CHAPTER 1

INTRODUCTION

1.1 Background

In recent years, there has been an increasing interest in wireless power transfer (WPT) systems which are designed to provide contactless transmission of power to electrical devices in various locations. With the use of innovative technology, wireless power transfer (WPT) can be used to transmit electrical energy from a power source to a receiver without the need for physical cables [1], [2]. Its potential uses in a variety of fields such as consumer electronics, industrial automation, and electric vehicles (EV) have made it more well-known.

There are several types of WPT systems one is capacitive power transfer (CPT) system [3], [4] which are the inductive wireless power transfer (IPT) system [5], [6], [7]. A particular type of WPT called CPT capacitive power transfer (CPT) depends on capacitive coupling between a transmitter and a receiver. CPT transfers power using electric fields instead of magnetic fields like inductive power transfer (IPT). The key components of a CPT system include a power source acting as the transmitter and a load serving as the receiver both of which are equipped with capacitive electrodes [1], [8].

However, current WPT technology mostly concentrates on applications in air and with little research done on applications of the technology underwater. Because of the significant eddy-current loss caused by the high frequency magnetic field, the IPT

technology is not suitable for direct application in water [9]. When compared to the IPT system, CPT technology is an excellent option to enable device charging in underwater environments and on surface of waters [10], [11].

The objective of the project is to investigate the performance of CPT systems underwater in freshwater environments and construct a capacitive coupler for a CWPT system for underwater EV charging application [12], [13] and seawater [14], [15], [16]. Using analytical and numerical methods, electromagnetic simulation software will develop and design the capacitive coupler. In order to minimize electric field leakage between the transmitter and receiver electrodes, the coupler would optimize power transfer efficiency. A printed circuit board and copper plates will be deployed to make the prototype. The proposed capacitive underwater charging concept will be validated through the implementation of a downside prototype [3], [11], [15].

The report begins with an overview of existing underwater EV charging methods and technologies, highlighting the need for innovative solutions then review of capacitive wireless power transfer (CPT) principles and applications, emphasizing its relevance and potential advantages for underwater charging scenarios. In methodology section outlines design, simulation techniques, and the fabrication of capacitive WPT coupler.

1.2 Problem Statement

Underwater capacitive power transfer (CPT) wireless charging of electric vehicles (EVs) is essential for global sustainability, supporting many Sustainable Development Goals (SDGs) of the United Nations. By lowering electronic waste, it specifically helps SDGs 12 and 14. SDG 12 promotes sustainable patterns of production and consumption. Underwater CPT contributes by reducing the need for disposable batteries and electronic waste is minimized while SDG14 focuses on protecting and responsibility in using the oceans and marine life.

Traditional underwater cables can harm marine life as electromagnetic interference from unshielded CPT systems may disturb ecosystems. By containing the electric field, shielded couplers can lessen the interference and increase safety of underwater CPT in underwater environments. It can be challenging to create efficient shielded couplers that transfer power effectively while reducing energy loss. Due to electromagnetic interference and towards emissions, current CPT systems may interfere with nearby electrical equipment as well as marine life.

Shielded couplers are designed to provide safe and effective power transfer between the electric vehicle and the charger by limiting the electric field inside a defined area. In addition to its enhanced performance and reduced environmental effect, underwater CPT is now a more economical and environmentally friendly way to charge electric vehicles. Hence, efficient power transfer systems can extend the lifespan of EV batteries while decreasing the overall environmental impact and promoting more responsible use of resources.

Underwater safety concerns with traditional cable connections make CPT an achievable solution. However, existing systems are inefficient and may even be hazardous because of energy leakage. Shielded couplers can improve the safety and efficiency of

underwater wireless charging by focusing all electricity on the charging vehicle, hence promoting SDG14, and SDG 12.

1.3 Project Objective

The aim of this project is to assess the effectiveness of the proposed six-plate CPT system for underwater applications.

- i) To calculate the parameters of two-plate and four-plate capacitive wireless power transfer (CPT) coupler for underwater EV applications.
- ii) To develop capacitive wireless power transfer coupler for underwater EV charging application using printed circuit board.
- iii) To analyze the development of capacitive wireless power transfer coupler for underwater EV charging application using real-time experiment

1.4 Scope of Project

The scope of this project is defined as follows:

- a) Development of capacitive wireless power transfer coupler for underwater EV charging application using two plate and four plates CPT system for underwater condition.
- b) Development of capacitive wireless power transfer coupler for underwater EV charging application and the system using four metal plates of transmitter and receiver and is controlled electronically in open loop. The tested coupling capacitor is placed in freshwater and salty water condition.

- c) Analysis to validate the underwater coupler high-power capability development of capacitive wireless power transfer coupler for underwater EV charging application involves measured in capacitance and distance.
- d) The simulation work is conducted with the LTspice and MATLAB to simulate the electrical behavior of the system.



CHAPTER 2

LITERATURE REVIEW

2.1 Introduction

This chapter describes the capacitive WPT couplers for underwater EV charging system. Due to its potential uses over various fields, wireless power transfer (WPT) has attracted a lot of attention. Capacitive power transfer (CPT) shows potential as a solution for underwater electric vehicle (EV) charging. This literature review investigates the current state of research and advancements in capacitive couplers specifically designed for underwater electric vehicle (EV) charging. It studies the challenges and solutions surrounding efficient power transfer in submerged environments, highlighting the potential applications and limitations of capacitive coupling technology in these areas. It aims to throw some insight into the ability and potential uses of capacitive couplers in underwater EV charging systems through analysing the findings of previous research.

2.2 Wireless power Transfer (WPT)

Wireless power transfer (WPT) uses cables or wires as physical connections that transmit electrical energy. The study electrically powered transmitter device creates a variable in time electromagnetic field in wireless power transmission systems which transfers power across space to a receiving device. By performing without using over wires and batteries, wireless power transfer technology can improve an electronic device in mobility, convenience, and safety for all users [17]. A typical wireless power transfer (WPT) system consists of two main components as shown in Figure 2.1, transmitter, and a

receiver. The transmitter includes a power source, such as a power amplifier which can generate an alternating magnetic field. The receiver contains a coil that captures this field converting it back into electrical energy for powering devices or charging batteries [17].

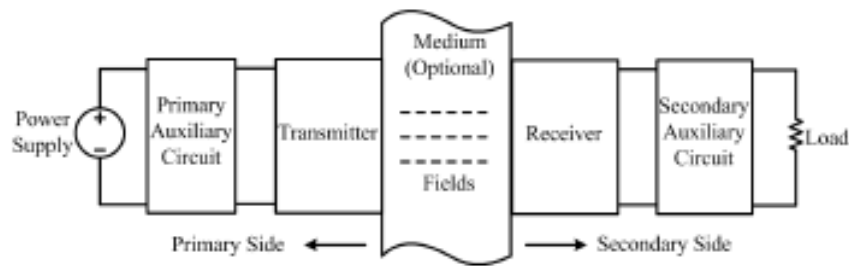


Figure 2.1 Display a WPT systems typical system structure [17].

Since using connecting cables to connect electrical devices is inconvenient, hazardous or not practical wireless power transfer come in convenient. Wireless power techniques are classified into two primary categories which is near field and far field. When using non-radiative or near field techniques, power is transmitted over short periods. This transfers power across small distances by applying magnetic fields including those relating to a magnet. Technologies like wireless power transmission in implanted medical devices like artificial cardiac pacemakers or electric vehicles (EV) are commonly employed for this. It is also used for charging smartwatches, phones, and even electric toothbrushes [17].

In radiative or far field techniques, power beaming are another term for it. Beams of electromagnetic radiation, such as laser or microwave beams, are employed for transmitting power. These methods require to be focused at the intended destination still have long-range transmission of energy potential. Wireless-powered drone aircraft and solar-powered satellites are examples of proposed uses for this kind of technology. For all wireless power systems, limiting the quantity of potentially hazardous electromagnetic fields that humans and other living things are exposed to is an essential consideration [17].

A wireless power system consists of a "transmitter" device that is connected to the mains power line or another power source. Power is transformed into a fluctuating electromagnetic field by it. This field is then received by one or more "receiver" devices, which convert it back into DC or AC electric current for use by an electrical load as seen in Figure 2.2.

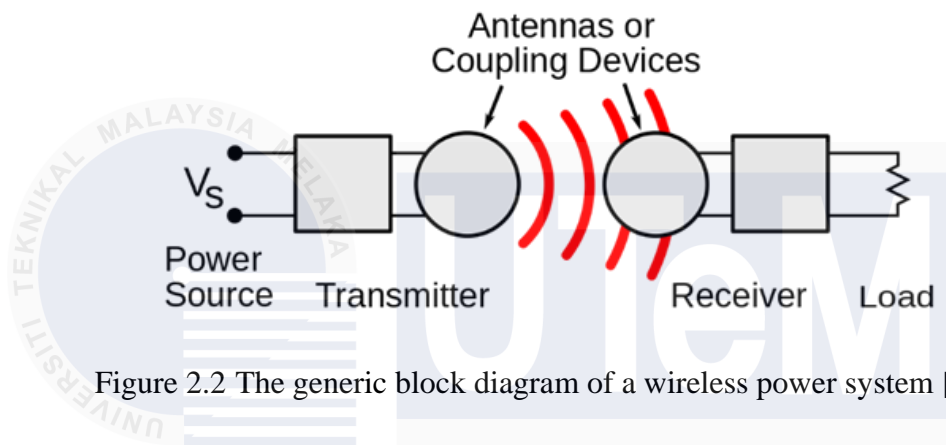


Figure 2.2 The generic block diagram of a wireless power system [17].

2.2.1 Inductive Power Transfer (IPT)

IPT offers several advantages such as eliminating physical connectors such wires, and sockets. Enhancing safety by removing exposed electrical contacts and providing convenience in applications like electric vehicle (EV) charging where plugging in cables can be difficult. It also supports resonant coupling, achieving high efficiency (up to 95%) over relatively long distances [1], [6], [18].

However, IPT has disadvantages including the need for an air gap between coils which limits efficiency of power transfer. The efficiency reduces as the air gap rises. Efficient power transfer requires precise alignment between the coils. Misalignment can significantly reduce the system's performance requirement for precise alignment for

effective power transfer energy during the transfer process, some energy is inevitably loss as heat, and the high initial cost of implementation [5].

Additionally, IPT systems face specific challenges in applications such as roadway charging for EVs, where larger air gaps, higher power levels and the need of consistent between systems from different manufacturers add complexity. IPT offers significant potential for wireless power transfer by providing safety, convenience, and high efficiency in various applications. However, it also presents challenges such as alignment sensitivity, heat dissipation and high initial costs. In order to overcome these obstacles and improve the usefulness and effectiveness of IPT systems in a variety of applications, more developments and innovations are required [1], [6], [19]. As seen in Figure 2.3 and 2.4 [18]

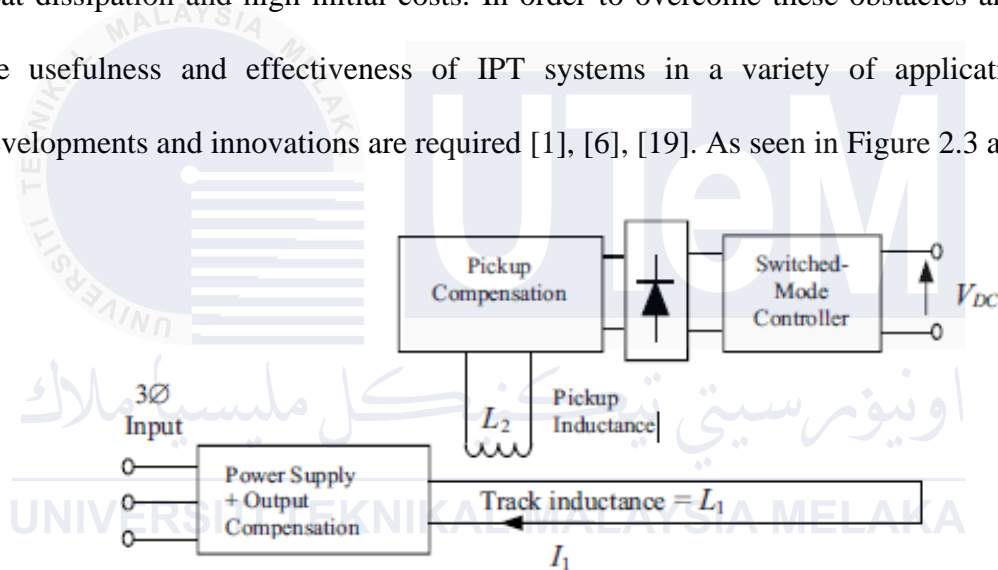


Figure 2.3 The standard IPT system [18].

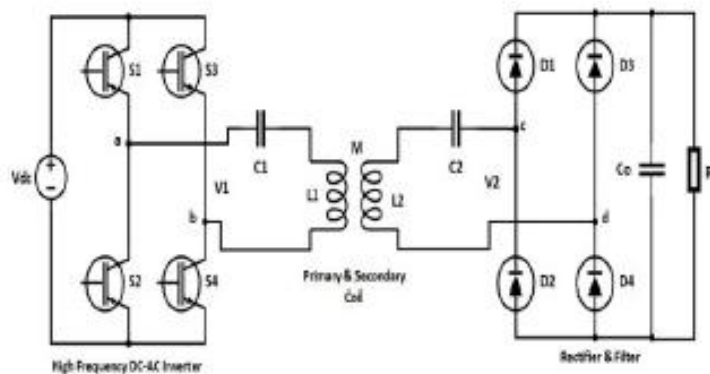


Figure 2.4 Circuit diagram of IPT system [18].

IPT operates on the same fundamental principles as conventional transformers. As seen in Figure 2.5, the primary (transmitter) and secondary (receiver) coils are the two essential parts. An electromagnetic field develops around the primary coil when it is exposed to an alternating current (AC). When the secondary coil is within range of the magnetic field, an alternating voltage is produced. When the induced voltage is rectified, it can be utilised to power electronics or replenish batteries. The coupling coefficient (k) between the inductors and their quality factor (Q) determines how efficiently power is transferred in IPT systems. Resonant coupling, in which the transmitter and receiver are adjusted to the same resonant frequency in order to maximise power transfer and minimise losses, is a common technique used in efficient IPT systems [5], [6], [19], [20].

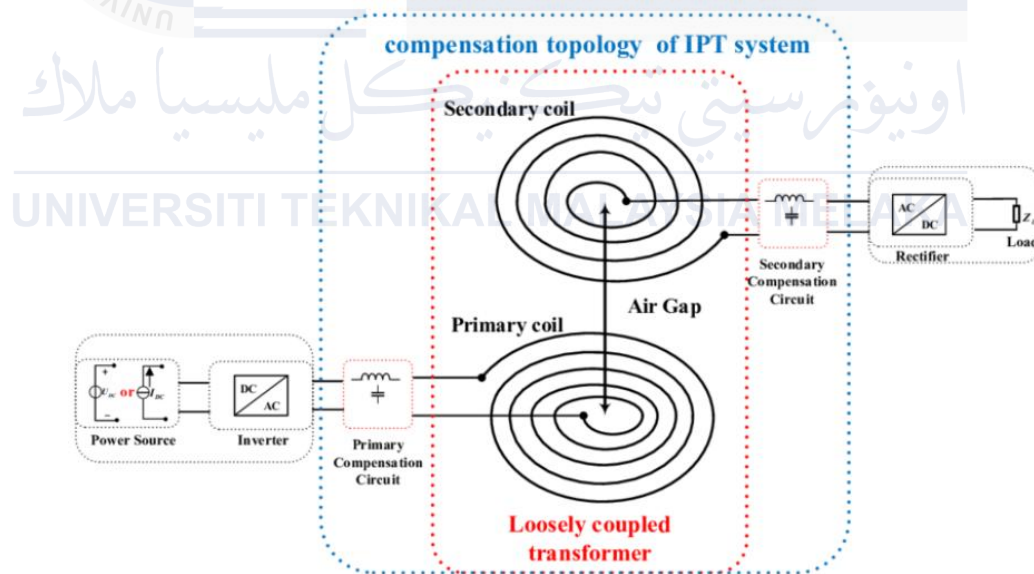


Figure 2.5 The inductive power transfer (IPT) system schematic diagram [20].

2.2.2 Capacitive Power Transfer (CPT)

Capacitive Power Transfer (CPT) systems for underwater applications represent an innovative approach to wireless energy transmission. The working principle of CPT involves the generation of an electric field between a set of electrodes connected to an AC power source. When these electrodes create an alternating electric field, a receiving set of electrodes designed to resonate with this field captures the energy through capacitive coupling. This energy is then converted back into a usable form to power devices or recharge batteries [21], [22], [23], [24].

The ability of CPT to transfer power efficiently over short distances is one of its key characteristics and making it ideal for close-proximity applications its relatively simple and compact design it also potential for miniaturization of the system components which is the components can be miniaturized allowing for smaller and lightweight power transfer setups. Additionally, CPT systems are less susceptible to alignment issues that commonly affect inductive power transfer systems and provide more flexibility in positioning [11], [21], [25].

While, the disadvantages include a generally shorter effective range compared to inductive methods. CPT generally has a shorter effective range compared to inductive power transfer methods which is limiting its use to closer distances well as potential challenges related to the dielectric properties of the underwater environment, which can affect the efficiency and stability of power transfer which posing challenges in maintaining consistent performance. Despite these limitations, CPT systems offer a promising solution for specific underwater applications where compactness and ease of alignment are critical

[21]. As seen in Figure 2.6 show the typical CPT system and in Figure 2.7 show schematic diagram of CPT system [14].

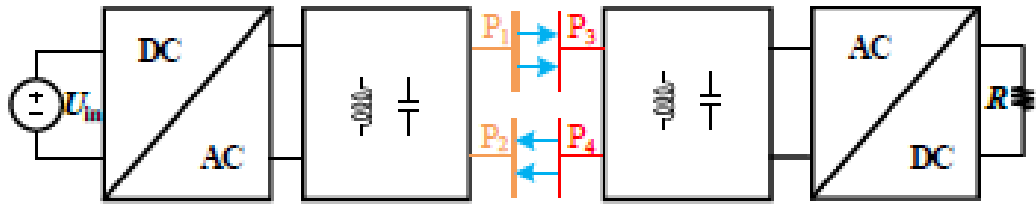


Figure 2.6 Typical CPT system [14].

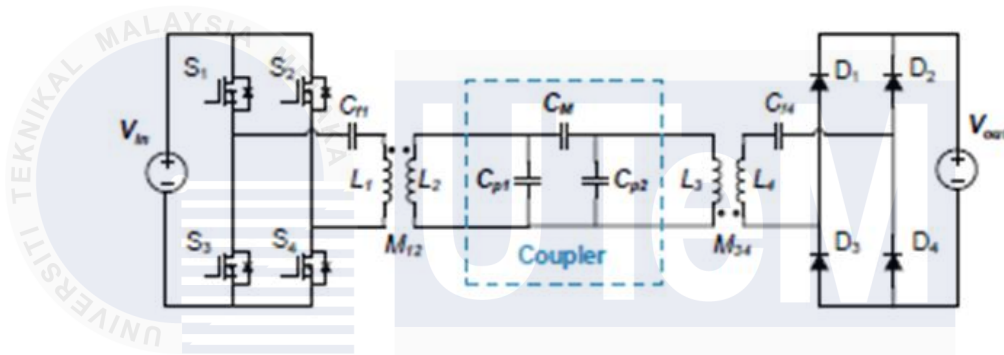


Figure 2.7 Schematic diagram of CPT system [14].

2.2.3 Hybrid Power Transfer (CPT-IPT)

Inductive power transfer (IPT) and capacitive power transfer (CPT) used in hybrid wireless power transfer (WPT) systems provide a beneficial technique for underwater applications. In order to transport energy over a gap, IPT uses magnetic fields created by coils whereas CPT uses electric fields between capacitive plates [19]. Hybrid IPT-CPT systems are able to combine the flexibility and potential for miniaturisation of CPT with the high efficiency and reliability of IPT through the combined use of these two techniques. Using this combination of power transfer can be more flexible and can accommodate various alignment circumstances and distances between the transmitter and receiver [19].

The advantages of this hybrid approach include extended range by combining IPT and CPT, hybrid systems can achieve a greater range than any single technology alone. This is particularly beneficial for underwater applications where the distance that separates the device from the power source can change. It also could enhance efficiency as the system can dynamically leverage the most efficient power transfer method based on the situation by reducing energy losses and improving overall efficiency. Additionally, the system redundancy and fault tolerance are enhanced by ensuring reliable operation even if one component fails [19], [23], [26].

However, the disadvantages of maintaining the interaction between IPT and CPT requires complex control mechanisms which can make development and maintenance more difficult. In addition, system design and control become more complex. Higher initial costs could arise from the increased complexity and requirement for more part such as coils for IPT and plates for CPT. Furthermore, it has an impact on environmental sensitivity because underwater environments may pose particular difficulties due to their variable dielectric qualities and potential for interference from magnetic and electric fields. The efficiency and stability of power transfer may be affected by several variables. In despite these difficulties, the hybrid IPT-CPT system is a promising development in the field of underwater wireless power transfer delivering a reliable and flexible answer for a wide range of underwater applications [19], [26].

Combining Inductive Power Transfer (IPT) and Capacitive Power Transfer (CPT) systems can enhance the efficiency and flexibility of underwater EV charging. The IPT system provides robust and reliable power transfer over short distances, while the CPT system offers safer, high-frequency power transfer suitable for various underwater

environments. Integrating these technologies ensures a more versatile and effective solution for underwater wireless charging of electric vehicles. With its combination of coupling coils and coupling capacitors, the IPT-CPT system transfers power using both magnetic and electric fields [6].

A transmission medium is produced by the alternating magnetic field created by the currents passing through the coils in an IPT system. However, because of the self-inductance of the transfer coil, such currents will stress it with high voltages, and the CPT requires high port voltages to create the electric field needed for the capacitive coupler. So that IPT and CPT can be combined to create a hybrid system to transfer electric power, the voltages stressed on the coil of the IPT system are also possible to use for the CPT system [27]. A generic hybrid system model including inductive power transfer (IPT) and capacitive power transfer (CPT) is shown in Figure 2.8 and Figure 2.9 [27].

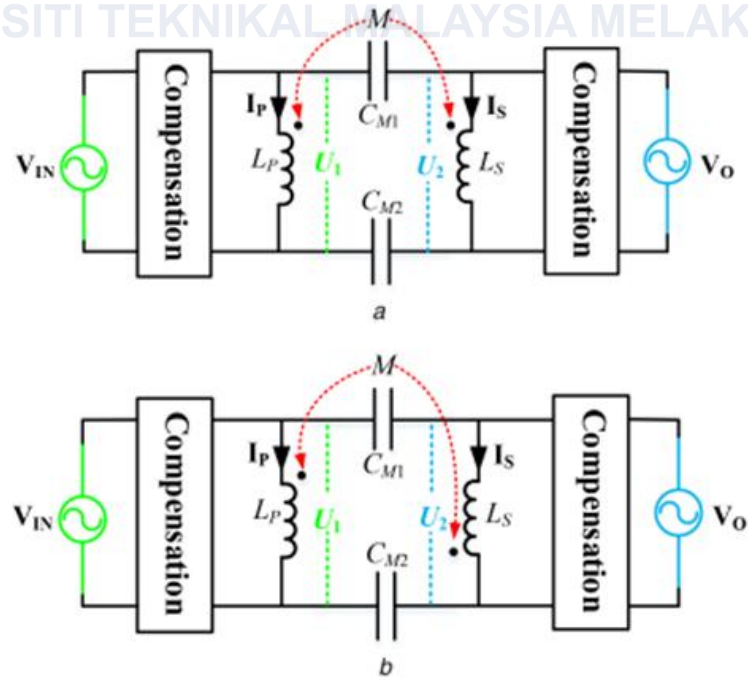


Figure 2.8 The coils in configuration (a) are connected in phase while configuration (b) has the coils connected out of phase [27].

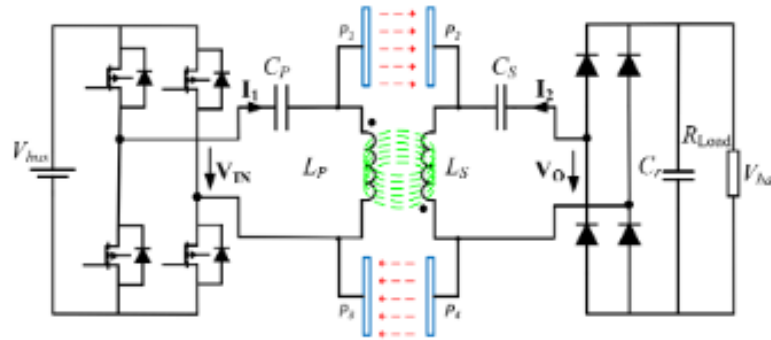


Figure 2.9 Displays the hybrid IPT and CPT system with SS compensation [27].

The IPT coupler coils are linked to four metal plates separately. Similar to the SS compensating employed in the IPT system, two capacitors C_P and C_S are used to connect the sending and receiving side in series to induce resonance in the hybrid system [9].

Table 2.1 The differences between IPT, CPT and Hybrid (IPT-CPT)

Item	System type		
	IPT	CPT	HYBRID (IPT-CPT)
Range	shorter range due to magnetic field limitations [6]	longer ranges due to electric field confinement [21]	Flexible range depending on specific design [9]
Cost	expensive	cost-effective	higher initial costs
Size and weight	Bulky and heavy	Smaller and lighter	lightweight
Output power	High power	Lower power	High power
Efficiency	Higher efficiency	Lower efficiency	High efficiency [27]
Voltage and current	More suitable for applications with high current and low voltage [18]	More suitable for applications with high voltage and low current [22], [23]	Combine both voltage requirement [27]

Table 2.2 The differences between IPT, CPT and Hybrid (IPT-CPT) based on research papers

Item	System type		
	IPT	CPT	HYBRID (IPT-CPT)
Power and Efficiency	3kW,92% [28] 1.5kW, 95.6% [10] 1kW ,80% [18]	100 W, 80.15%. [29] 100W ,50%[14] 3.3kW,75.9% [12] 6.06kW,92.3%[25]	1.1kW, 91.9% [9] 100W,73.6% [30] 3kW ,94.45% [31]
Frequency	85kHz [10] 100kHz [18]	625kHz [29] 500kHz [14] 6.78MHz [32] 13.56MHz [33]	1MHz [30], [31]
Gap	5mm [28] 120mm [10] 300mm [18]	150mm [29] 400mm[14] 200mm [12]	300 mm [9] 18mm [30] 150mm [31]

2.3 Fundamental of working principle of CPT

A CPT system common component is DC power supply, rectifier, load, coupling coupler, high-frequency inverter, transmitter compensation system, and compensation topology as shown in Figure 2.10. A DC power supply is the first component in the basic operating principle of a Capacitive Power Transfer (CPT) system, it then supplies energy to the system. Then, inverter transforms this DC energy into high-frequency AC, which can range from hundreds of kHz to MHz. When the high-frequency AC is sent through a mechanism for compensation that reduces high-order harmonic distortion and raises the voltage to an appropriate level. A coupling mechanism then allows the wireless transmission of energy while the receiver compensation maintains appropriate voltage control and adjustments. Finally, a rectifier transforms the AC back into DC to give the load a steady power supply [3], [16], [21], [29].

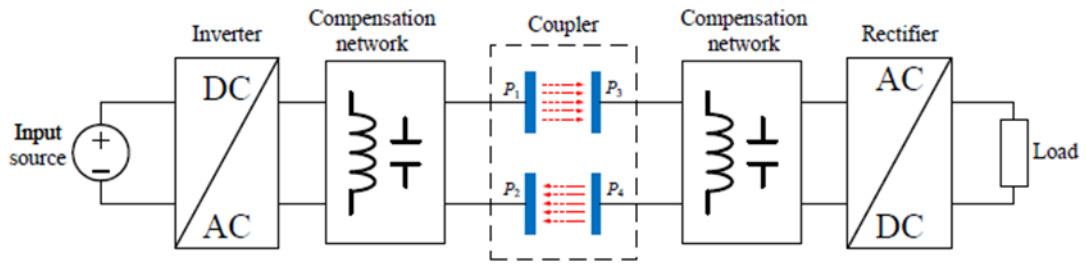


Figure 2.10 A typical structure of a CPT system [29].

Typical underwater CPT couplers are made up of two pairs of insulating layers and metal plates. The metal plates are separated from the water medium with insulating layers [11], [21]. Before studying undersea CPT systems, a single pair of metal plates were examined. An illustration of a single pair of metal plates in a water medium is shown in Figure 2.11. The metal plates are represented by the orange sections, the insulating layer by the green parts, and the water medium by the blue parts. The conductivity of the water medium determines whether it is a conductive conductor or a non-conductive dielectric [4].

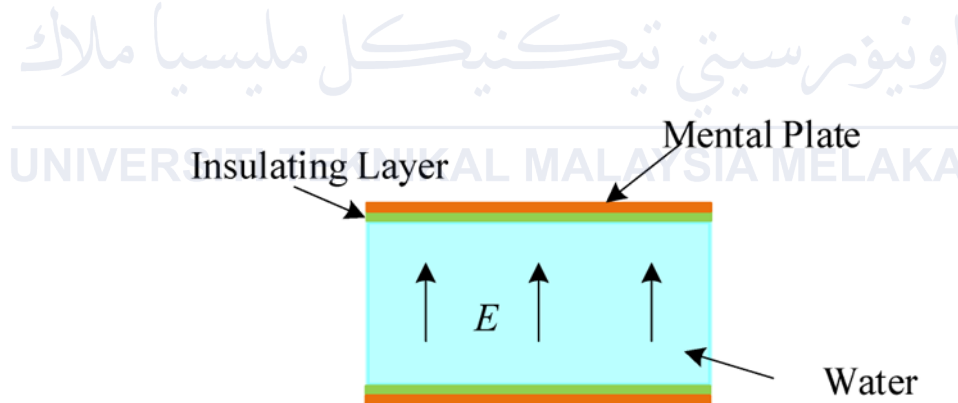


Figure 2.11 The structure of a single pair of metal plates in water medium [4].

The single pair of metal plates in the illustration can be compared to the structure that symbolizes the capacitance that would be created by a single insulating layer when the water medium functions as a dielectric whereas C_{water} stands for the capacitance that the water medium similarly forms. The capacitances C_{water} can be calculated using the following formulas:

$$C = \frac{A\epsilon_0\epsilon_r}{d} \quad (2.1)$$

[21]

C – Capacitance value

A – area of the plates

ϵ_0 - the permittivity of free space (8.854×10^{-12} F/m)

ϵ_r (water) - the relative permittivity of water

d - distance between the plates

2.4 Capacitive coupler structure

Represents the way conventional capacitive coupler structures are classified. The power transfer between metal plates is the coupler main purpose which generates electric fields [4], [11].

2.4.1 Two-plate couplers

The construction of a typical capacitor which consists of two plates with one plate connected to the transmitter and the other to the receiver is very similar to that of a two-plate capacitive plate structure as illustrated in the Figure 2.12. Instead of using a wireless CPT configuration, a conductive path serves as the return channel for the current to close the circuit [34], [35].

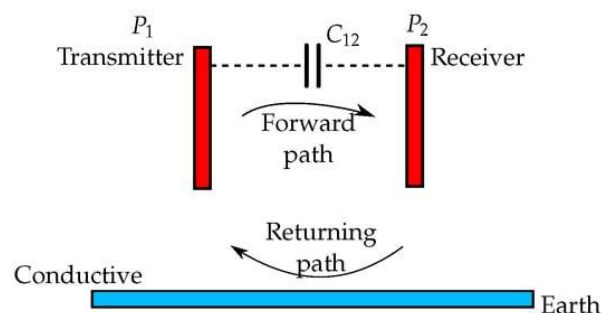
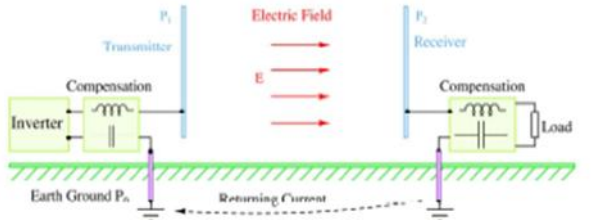
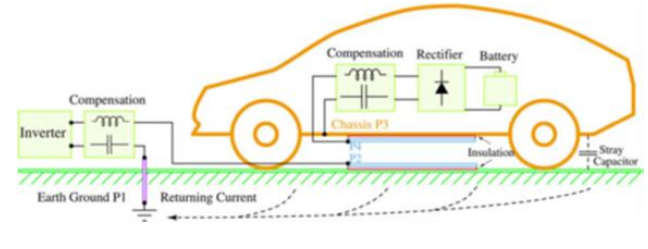
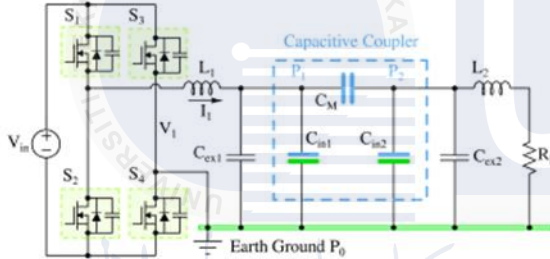
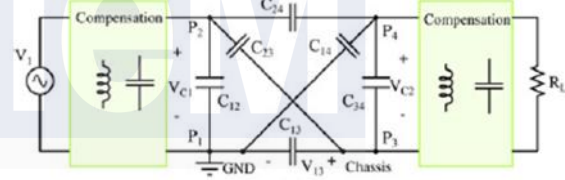


Figure 2.12 The two-plate structure [36]

Table 2.3 The two-plate CPT method structure for long-distance quasi-wireless and electric car charging applications.

Quasi-wireless	Electric vehicle
	
<p>Figure 2.13 Example of a two-plate long-distance quasi-wireless CPT system structure [34]</p>	<p>Figure 2.14 The structure of a two-plate compact CPT system use for electric vehicle charging (EV). [35]</p>
	
<p>Figure 2.15 The double-sided LC-compensated two-plate quasi-wireless CPT system [34]</p>	<p>Figure 2.16 The equivalent concept of a ground and chassis two-plate CPT system.[35]</p>

Hardware simplicity is the main benefit of a two-plate CPT system. The two-plate structures may reduce the contact voltage between the chassis and earth potential in electric vehicle applications, however this plate structure poses hazards [36].

2.4.2 Four-plate couplers

The most common plate structure of CPT is the four-plate structure. The transmitter consists of a positive and a negative plate as well as the receiver. The four-plate structure comprises of two main coupling capacitances and four leakage capacitances and can be configured either stacked or in parallel as shown in Figure 2.17 and 2.18 while the model

of the coupling capacitor in seawater conditions is illustrated alongside the four-plate CPT system topology in figure 2.19 [14], [37], [38].

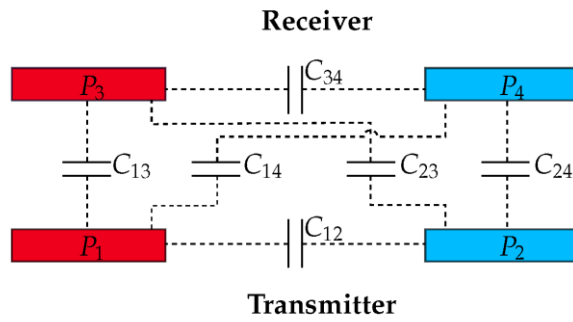


Figure 2.17 The four-plate parallel structure [36]

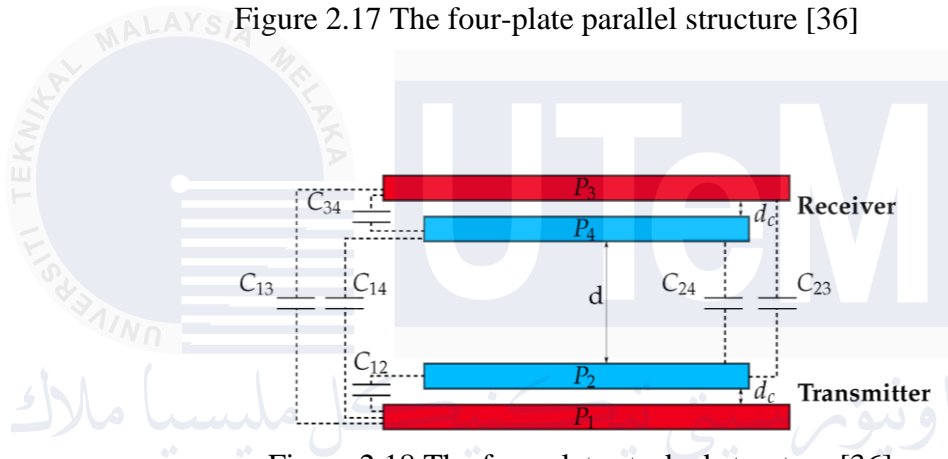


Figure 2.18 The four-plate stacked structure [36]

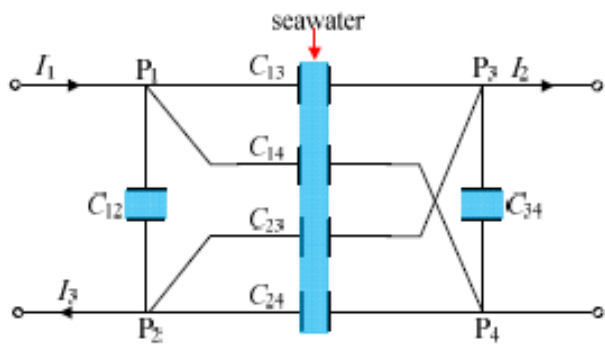


Figure 2.19 The model of coupling capacitor in seawater conditions [14].

Two parallel pairs of two plates form each of the four plates in this system. In a well-aligned and close-packed arrangement of the plates, the main connection will dominate the resulting capacity. On the other hand, if any of these requirements is not fulfilled [14] such as significant misalignment or a large distance between the plates, a larger parasitic coupling develops which lowers the capacitive coupling quality.

2.4.3 Six-plate couplers

The six-plate or shielding coupling structure shown in Figure 2.20 is actually an extension of a four-plate parallel coupling system with two big plates operating as a shield. The four plates with the numbers P1P1, P2P2, P3P3 and P4P4 that are directly connected to the compensating circuits enable the power transmission between the primary and secondary. The two extra shielding plates are large enough to cover the inner four-plate coupling structure even though they are not directly connected to the system. They are simply connected by parasitic capacitances and do not participate in the power transfer which is why they are floating. The extra shielding component main objective is to lower the electric field emissions [39], [40], [41]. As seen in Figure 2.21 and Figure 2.22 is the circuit topology of a six-plate CPT system with LCL compensation and the process of simplifying the capacitor model when $V_2 = V_3 = 0$

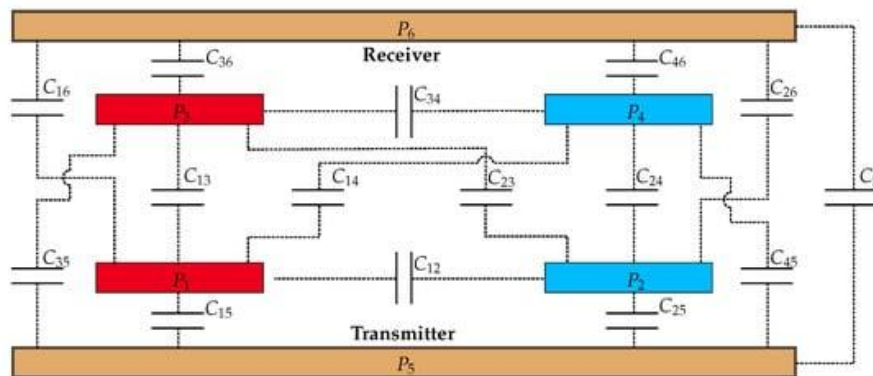


Figure 2.20 The six-plate structure of CPT system [32]

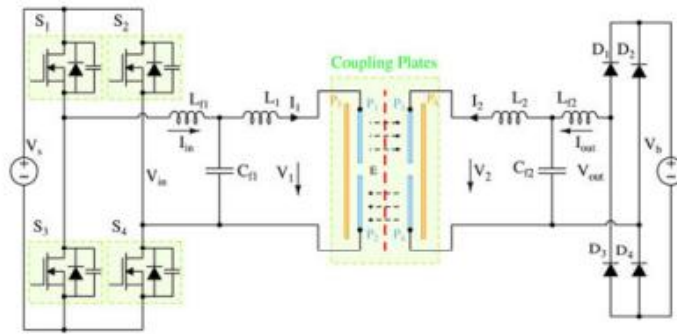


Figure 2.21 The circuit topology of a six-plate CPT system with LCL compensation [32]

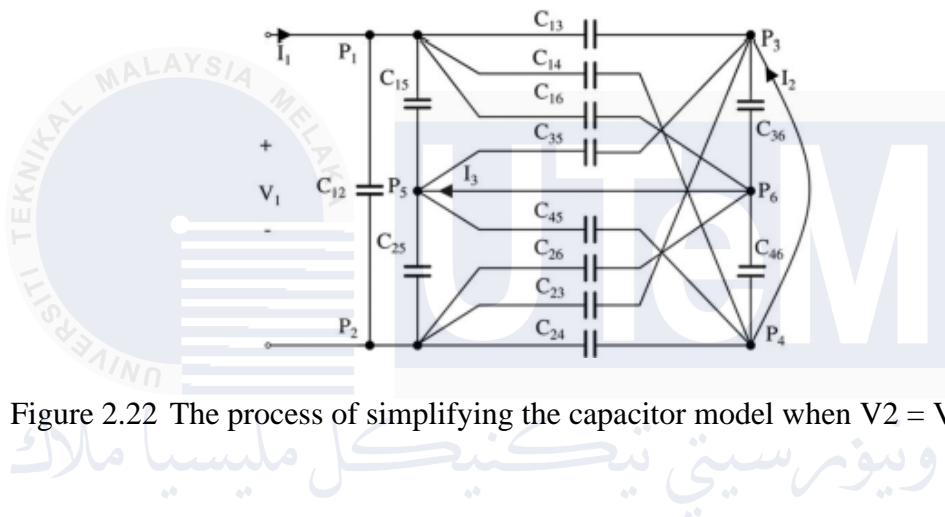


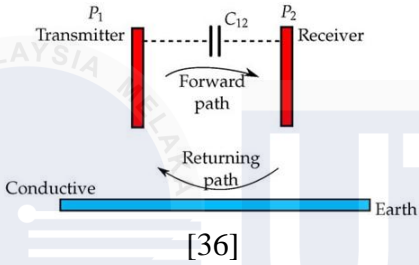
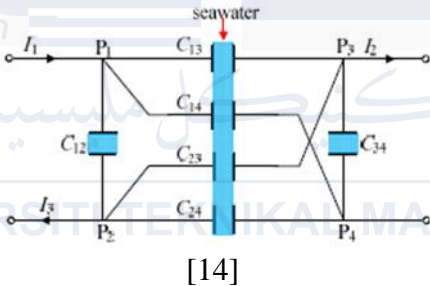
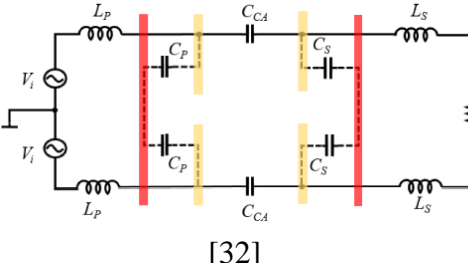
Figure 2.22 The process of simplifying the capacitor model when $V_2 = V_3 = 0$ [39]

The efficiency and safety of the system can be enhanced by the six-plate structure. The coupling model of the six-plate construction has fifteen capacitances because there are two additional plates, which complicates the coupling analysis [32], [40], [41].

In conclusion, there are benefits of using the two-plate structure despite consuming lesser metal plates. Among the four-plate coupler structures, the four-plate vertical construction is the most compact and it has a higher self-capacitance which can withstand rotational misalignment in CPT applications. However, the four-plate horizontal configuration is usually used because the equivalent circuit may be produced with simplicity. The six-plate coupler is a common coupler structure in the safety concept among conventional coupler configurations. However, the disadvantage of implementing

such couplers are the higher number of coupling capacitors. Long-distance wireless power transfer can be achieved with the electric field transmitter. On the other hand, the coupler negative side is the greater number of plates [21], [36], [42].

Table 2.4 The comparison between plate structure and their equation.

Coupler Structure	Plate structure	Equation
Two-plate		$C = \frac{A\epsilon_0\epsilon_r}{d}$ <p>[36]</p>
Four-plate		$\begin{bmatrix} V_{1A} \\ I_{1A} \end{bmatrix} = \begin{bmatrix} A & B \\ C & D \end{bmatrix} \begin{bmatrix} V_{2B} \\ I_{2B} \end{bmatrix}$ $C_1 = C_{12} + \frac{(C_{13} + C_{14})(C_{23} + C_{24})}{C_{13} + C_{14} + C_{23} + C_{24}}$ $C_2 = C_{34} + \frac{(C_{13} + C_{23})(C_{14} + C_{24})}{C_{13} + C_{14} + C_{23} + C_{24}}$ $C_M = \frac{C_{13}C_{24} - C_{14}C_{23}}{C_{13} + C_{14} + C_{23} + C_{24}}$ <p>[14]</p>
Six-plate		$\begin{bmatrix} V_{1A} \\ I_{1A} \end{bmatrix} = \begin{bmatrix} A & B \\ C & D \end{bmatrix} \begin{bmatrix} V_{2B} \\ I_{2B} \end{bmatrix}$ $C_C = \frac{C_{CA}}{2}$ $C_1 = \frac{C_P}{2}$ $C_2 = \frac{C_S}{2}$ <p>[32]</p>

2.5 Application of CPT system

Because of its straightforward design, low weight, and affordability, research teams from all over the world have been paying close attention to the CPT system ongoing development. Research groups have thoroughly investigated the application possibilities using the benefits of CPT technology in addition to concentrating on transmission power and distance. This section will outline the state of research on CPT technology as it relates to biomedical implants, transportation applications, and underwater applications [43].

2.5.1 Electronic application

Capacitive Power Transfer (CPT) is widely used in electronic applications for its efficient and contactless energy transfer capabilities. It is commonly employed in wireless charging systems for consumer electronics, such as smartphones and tablets, providing a convenient and cable-free charging experience [10], [44], [45].

Applications for charging portable devices are divided into two categories which is laptop and mobile phone charging. A step-up and step-down transformer-equipped power amplifier topology is suggested in order to increase coupling capacitance and lower the quality factor [44]. A design for a position-independent capacitive coupler shaped like a cell is suggested. To provide stable functioning during coupling and load fluctuations, the frequency and duty cycle control approach is implemented [44]. The lower cost highlights the air-core inductor structure. In conclusion, space-saving wireless charging for portable device applications requires multi-MHz technology. In order to achieve improved efficiency, converter topologies focus on the WBG semiconductor devices. L compensation is widely used in situations involving the charging of portable devices when compensation

topologies are taken into into consideration. [10], [44], [45] As seen in Figure 2.23 and Figure 2.24

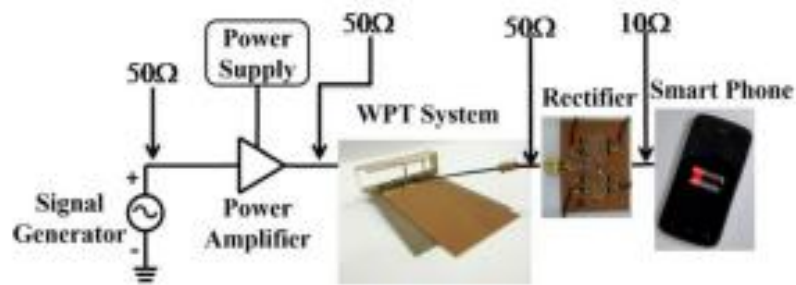


Figure 2.23 Display strategy for the suggested WPT system with near field capacitively coupling [44].

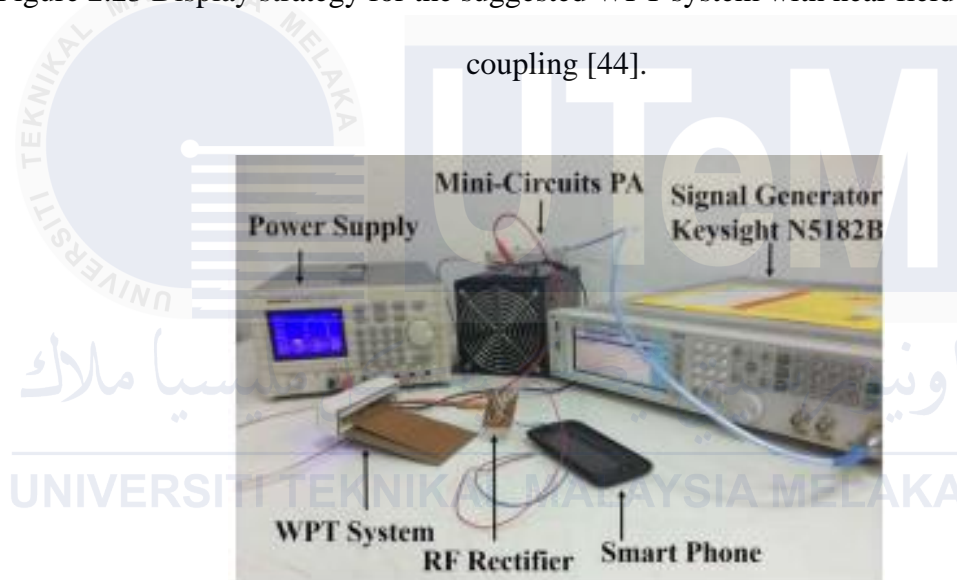


Figure 2.24 Demonstrate the proposed near-field capacitively connected WPT system's experimental setup [44].

2.5.2 Transportation application

Transport applications come up in three categories electric car charging, underwater and drone [18], [31], [46]

Electric vehicles (EVs) have become gaining popularity in recent years as a result of the slow the decreasing supply of conventional fossil fuels. EV charging is challenging. The use of wireless power transfer in EV charging has attracted a lot of interest. The IPT system for EV charging has gradually advanced. On the other hand, disadvantages of IPT include high levels of electromagnetic radiation, significant eddy current loss, and the absence of metal barriers in the distance of the coupling area. CPT uses electric field coupling opposed to IPT magnetic field coupling, which helps address some of IPT limitations. [47], [48], [49] To provide some example can be seen in Figure 2.25, Figure 2.26 and Figure 2.27

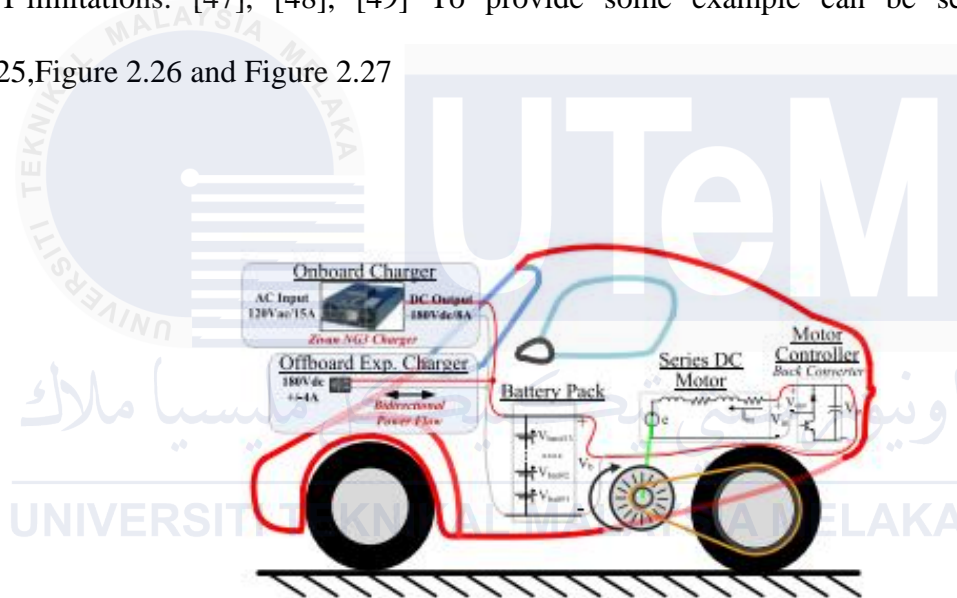


Figure 2.25 The Corbin Sparrow equipped with an onboard battery charger and an offboard experimental charger's DC charging port [47].

The foam-based charging station used to charge Corbin Sparrows is shown in



Figure 2.26 a) show conformal bumper charging station that has transmitter foil strips attached to a foam rubber [47].

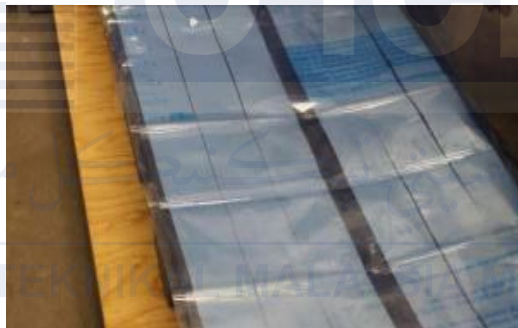


Figure 2.27 b) show conformal bumper for charging stations that has transmitter foil strips attached to a foam rubber pad [47].

Underwater charging is a solution for powering electric vehicles (EV) in marine environments. Applications involving underwater charging benefit greatly from the use of capacitive WPT technology. This is because metal plates are inexpensive and can withstand the intense pressure of an underwater environment. Furthermore, the high permittivity of seawater may enhance the coupling capacitance, hence increasing the power transmission capacity. Wireless underwater charging is an approach to the challenges of underwater device charging taking a long time, limited range, and higher system maintenance cost [41], [50]. As seen in Figure 2.28 and Figure 2.29

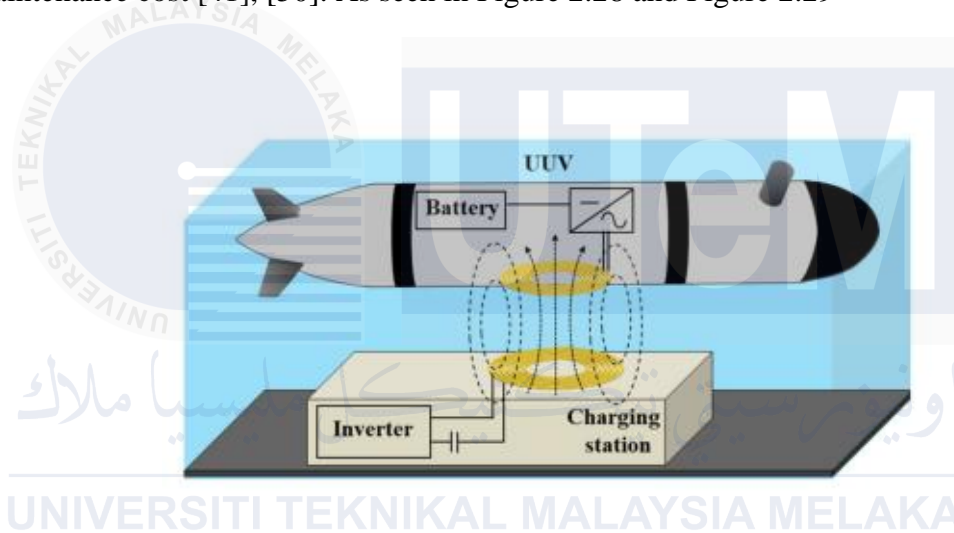


Figure 2.28 The overview of underwater wireless charging system [12].

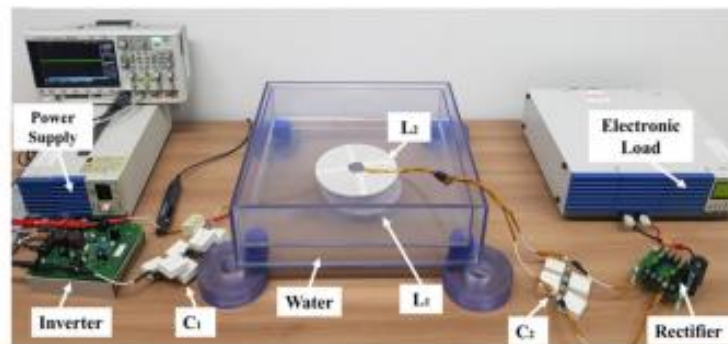


Figure 2.29 The experimental setup for the UWPT system [41].

Unmanned Aerial Vehicles (UAV) commonly known as drones, have revolutionized numerous industries with their versatility and capabilities. Numerous methods are proposed to extend the flight range of drones including the use of high voltage power headlines and battery dampening techniques [51]. Applications for drone charging evaluate limitations and difficulties. It states that the two biggest drawbacks of electric UAV are their small battery capacity and lack of durability. Technologies for inductive and capacitive power transfer are currently being investigated for drone charging application [51], [52]. As seen in Figure 2.30 and Figure 2.31 displayed a charging system illustration for a drone

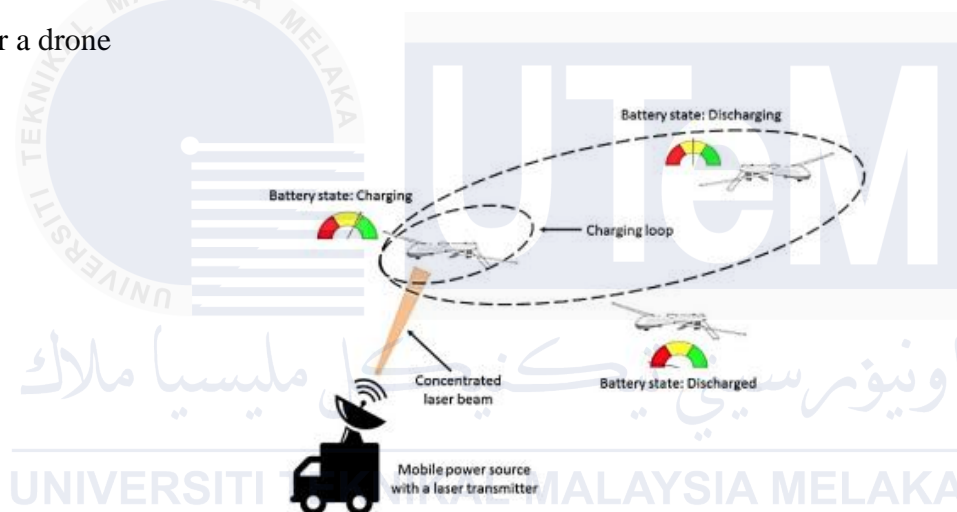


Figure 2.30 The illustration The drone recharge process using laser beaming [51]

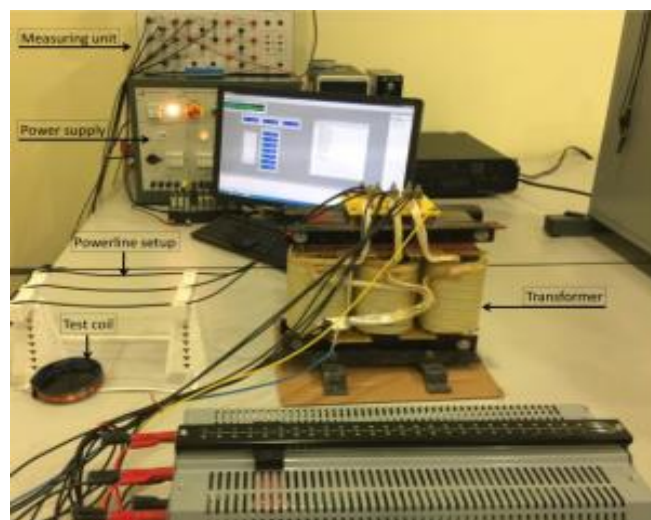


Figure 2.31 Power line emulation setup, side view [51]

2.5.3 Biomedical

The benefits of the CPT system over the IPT system are low electromagnetic radiation, low eddy current loss and a simple coupling structure. It widely used in implanted biomedical devices. [53], [54]. As seen in Figure 2.32

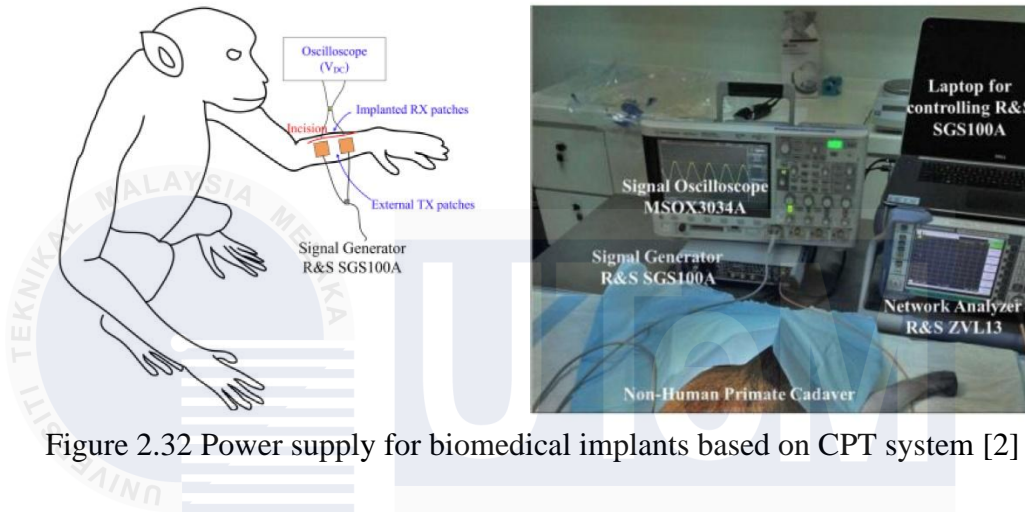


Figure 2.32 Power supply for biomedical implants based on CPT system [2]

Table 2.5 Review various applications using CPT system

Application types	Output power (W)	Frequency (Hz)	Efficiency (%)	Transfer distance (mm)	Coupler types
Portable device	5W	790MHz	88.2%	9.4mm	Two-plate [44]
Electrical vehicle (EV)	1kW	100MHz	90%	Not stated	Metal foil [47]
Underwater (AUV)	226.9 W	6.78MHz	60.2%.	500mm	Two-plate [31]
Drone (UAV)	45W	6.78MHz	78.2%	2mm	Four-plate [51]
Biomedical	214-319mW	120kHz	58-61%	5mm	Not mentioned [2]

2.6 Research, Ideology and Concept of Previous Project

In one research by Yang et al., 2019 introduced Underwater Bidirectional Capacitive Power Transfer (UB-CPT) system developed for autonomous underwater vehicles (AUVs) [29]. This system uses two H-Bridge circuits, based on GaN devices, to enable bidirectional power flow with high switching frequency and low power loss. LCLC compensation networks are employed on both the transmitter and receiver sides. Simulations were conducted using Ansys Maxwell, PSIM, and MATLAB, and experiments were performed using seawater bags to simulate underwater conditions between metal plates. A 100W prototype, featuring two H-Bridges, LCLC networks, a load resistor, and a filter capacitor, was tested at a resonant frequency of 625kHz, achieving an efficiency of 80.15% with a distance between couplers of 180mm. The results demonstrated stable and efficient bidirectional power transfer, affirming the system's suitability for AUVs and other underwater applications[29]



Figure 2.33 The BD-UCWPT experimental prototype [29]

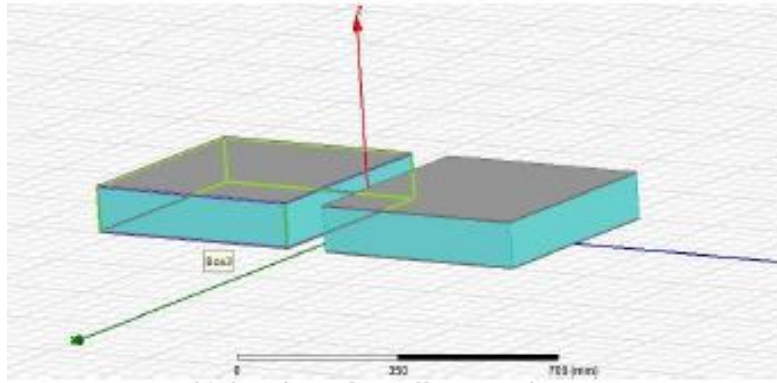


Figure 2.34 The 3-dimensional coupling capacitance [29]

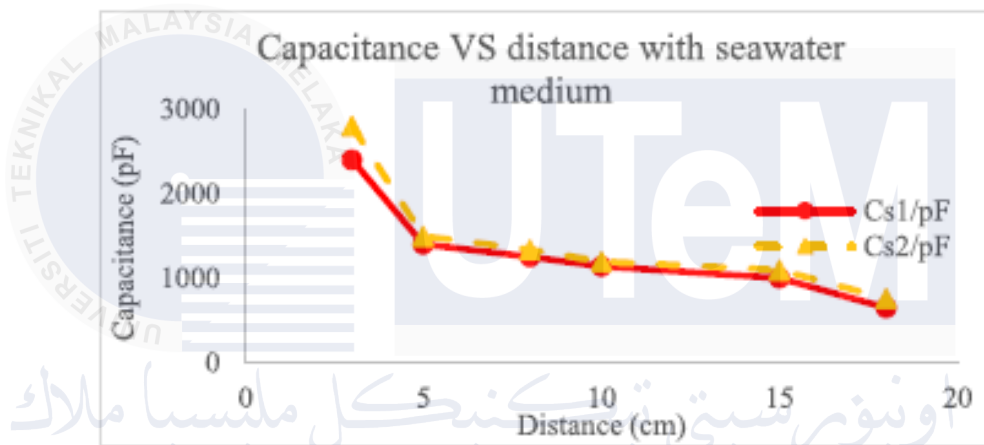


Figure 2.35 The connecting CS1 and CS2 capacitance to a flexible distance in a seawater medium [29]

In one research paper by Yang et al., 2021 introduced a four-plate undersea capacitive wireless power transfer (CPT) system. This system is specifically designed for underwater applications like autonomous underwater vehicles (AUVs) [14]. To explain the operation of the CPT system, in which electrons move forward and then backward during a single switching cycle, they brought out a theory of virtual electrons periodic repeating flow. This research designed and analyzed an undersea four-plate CPT system includes coupling capacitors forming a closed-loop path and utilizes a small inductor for resonant compensation. With a single-phase full-bridge inverter and diode rectifier, DC voltage is converted to AC and vice versa. A 100W CPT system was built to validate the theoretical

analysis. experimental testing, conducted using seawater, PSIM, and ANSYS Maxwell, revealed that despite the careful system design, experiments revealed that despite the system's design, its efficiency was limited, reaching only about 50% at a power level of 100W and a distance of 400mm between the transmitter and receiver [14].

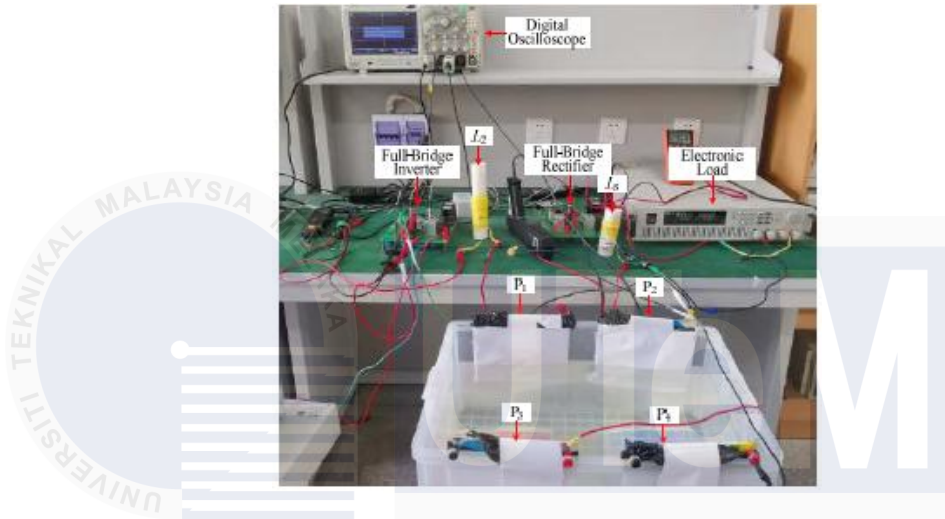


Figure 2.36 The Experimental setup for the four-plate CPT system undergoing testing. [14]

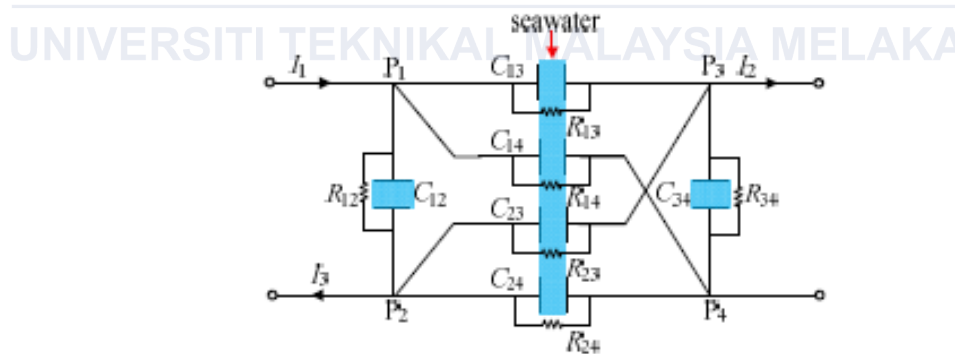


Figure 2.37 The coupling capacitor structure in the seawater condition. [14]

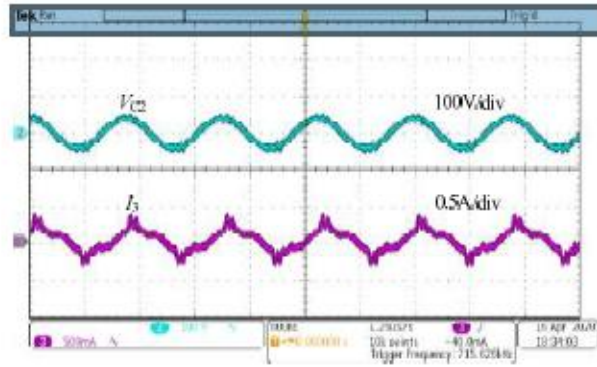


Figure 2.38 Waveforms of experimental voltage and current in coupling capacitors [14]

In one research paper by Mahdi et al., 2022 into capacitive coupling in a system of capacitive power transfer (CPT) designed mainly for charging purposes [16]. It provides mathematical formulas for calculating air-gapped and underwater capacitance using conformal transformation, as well as validating these formulas using research and COMSOL Multiphysics simulations. By immersing capacitors in seawater, research findings demonstrate that it is possible to achieve nano-farad capacitance ranges with minor capacitance fluctuations while modifying gap distance or operating frequency. However, the study also highlights the adverse impact of cross-coupling effects on system power transfer capability and efficiency. By addressing these effects, the system achieves a notable output power of 129W with an efficiency of 81.2%. To validate their findings, experiments involved constructing capacitors to assess fringing effects and conducting tests on a series-compensated CPT system in seawater to evaluate cross-coupling effects on power transferability and efficiency [16].

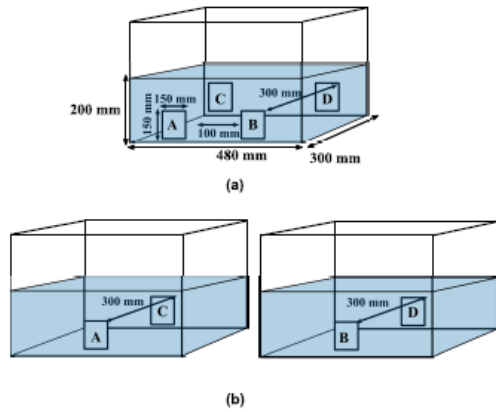


Figure 2.39 a) The experimental configuration incorporating the cross-coupling effect.

b) With no cross coupling [16]

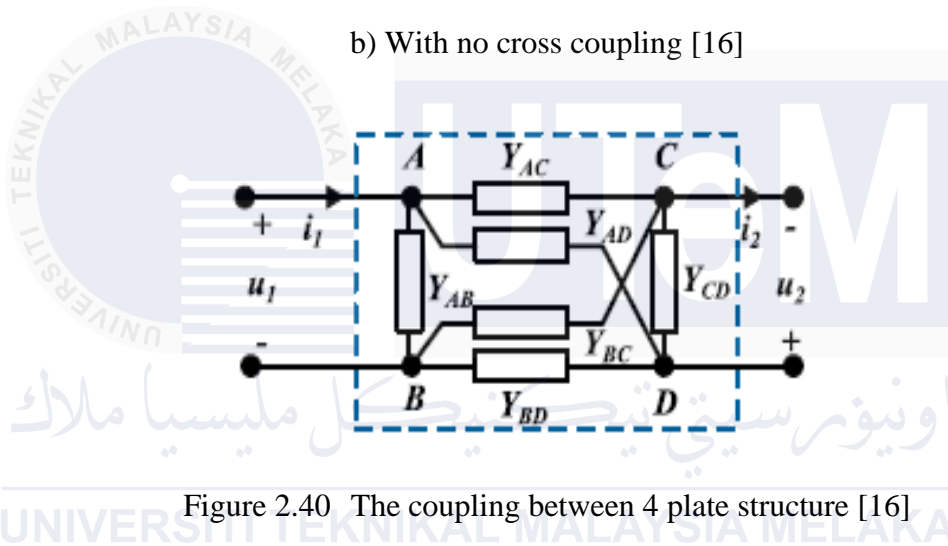


Figure 2.40 The coupling between 4 plate structure [16]

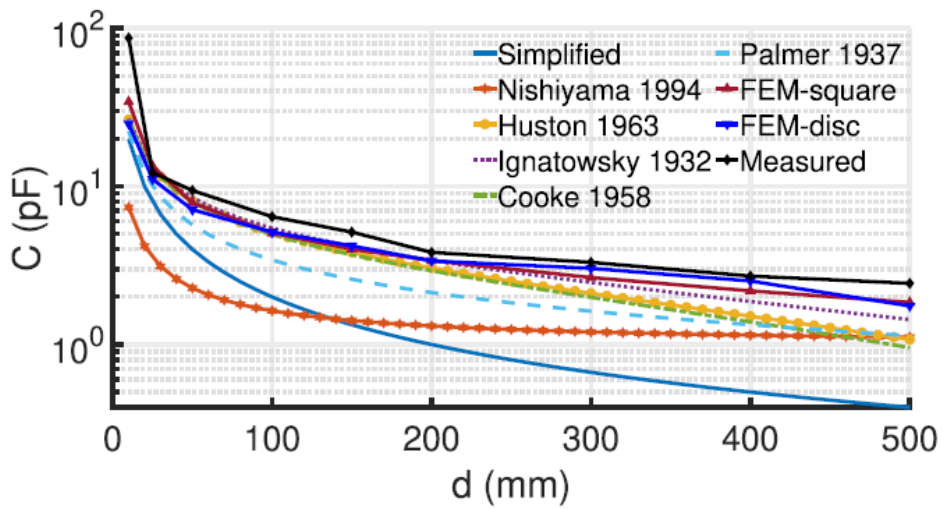


Figure 2.41 Compare the observed capacitance of separation distance in air with the analytical and numerical approaches [16]

In one research by (Hua Zhang et al,2019) explore underwater capacitive wireless power transfer technology for electric ship charging applications [13]. To figure out the power transfer capabilities of an underwater system, firstly develop a theoretical coupling model for the underwater capacitive coupler and then outline a typical charging system topology. It gives a prototype of the system to demonstrate that it is feasible in a freshwater setting. developing using HFSS software to do finite element analysis (FEM), the demonstration for the underwater coupler is capable of handling high power levels up to the megawatt (MW) range, allowing electric ships to be charged quickly. Developers create a smaller prototype and test it out in a lab environment in order to validate their suggested system. The testing results show that hundreds of watts of power can be successfully transferred over 500 mm. They accomplish efficient power transfer by incorporating high-frequency thin-film capacitances and external capacitors into the prototype. Experiments demonstrate a 60.2% efficient power transfer of 226.9W over a 500mm distance [13].

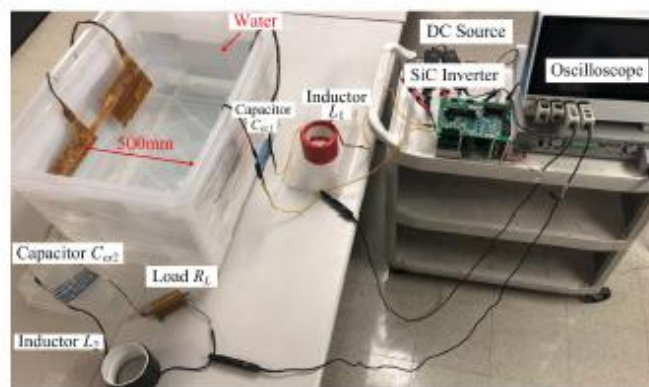


Figure 2.42 A scaled-down prototype of the capacitive coupler-equipped LC compensated CPT system prototype [13]

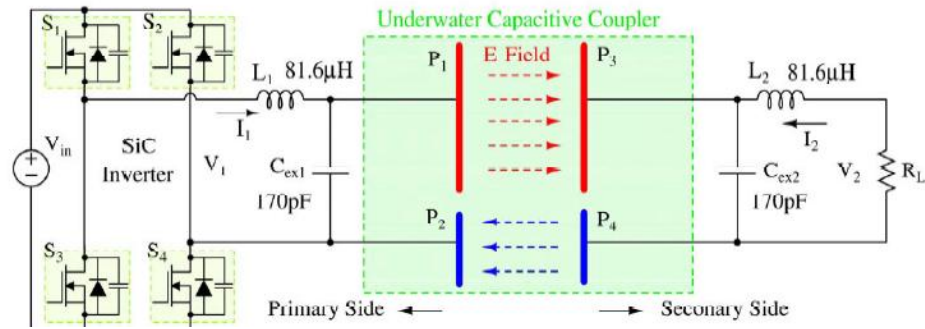


Figure 2.43 The component requirements and circuit topology of the underwater CPT system with LC compensation [13].

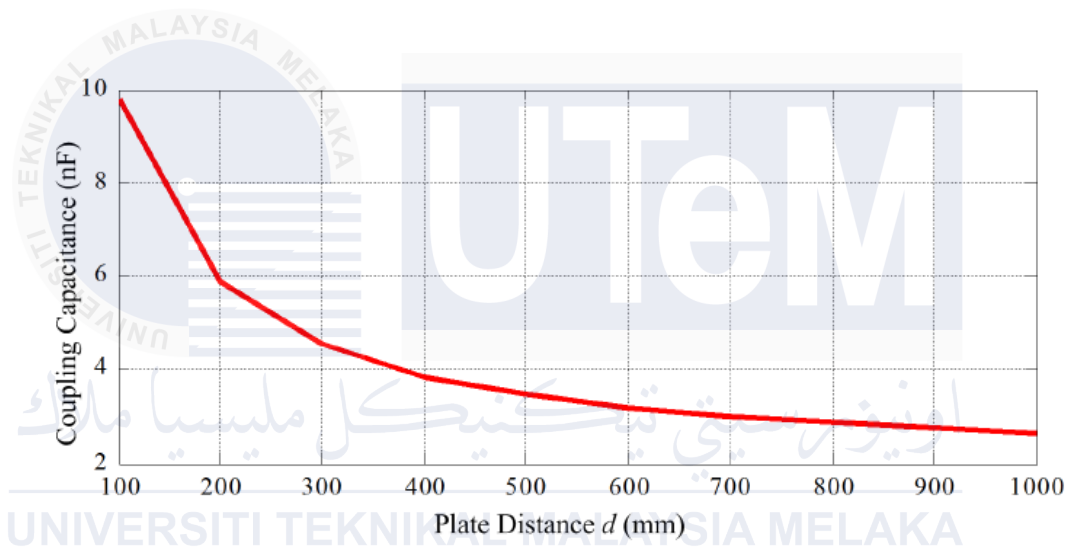


Figure 2.44 HFSS-simulated coupling capacitance between the two plates within a wide range of relative distances d [13]

In one research by Masaya Tamura et al, 2018 focus on developing a capacitive coupler specifically designed for underwater wireless power transmission (U-WPT) [55], with a focus on optimizing the kQ product. It discovers that the unloaded Q -factor of water and the coupling coefficient (k) of the coupler are the two key factors influencing the system's power transfer efficiency. It demonstrates that the capacitive coupling achieves a transfer efficiency of 80.9% by choosing the design parameters that optimize the kQ product. It demonstrates this using measured tap water Q -factors and computed coupling

coefficients comparable to conventional magnetic coupling techniques. For testing purposes and inspecting the coupler's functionality, immerse the device in a tank of tap water. Its effectiveness is confirmed by two-port measurements made using a Vector Network Analyzer (VNA). Comparing simulation and measurement results reveals strong agreement, with maximum efficiencies recorded at 85.1% and 80.9% for simulated and measured results, respectively, particularly at specific frequencies. These tests were conducted using freshwater at a distance of 70mm [55]

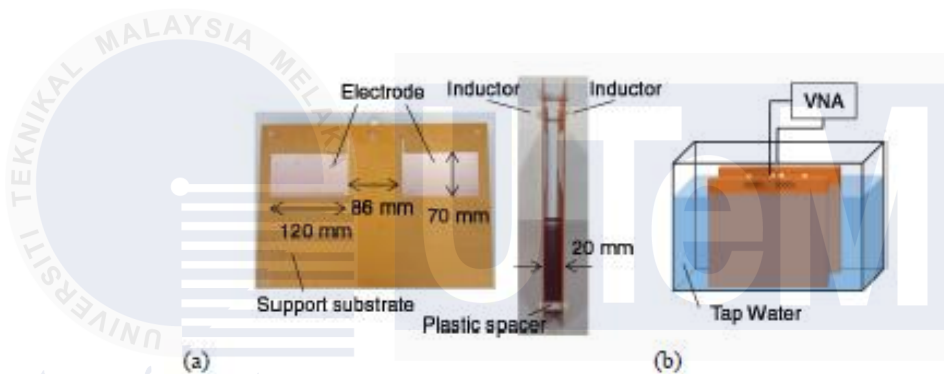


Figure 2.45 a)prototype b)measurement setup[55]

UNIVERSITI TEKNIKAL MALAYSIA MELAKA

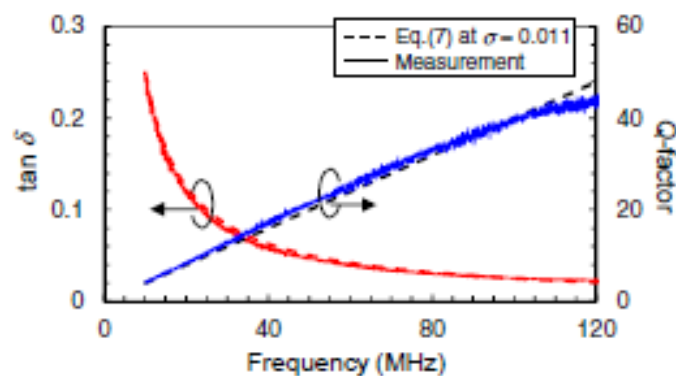


Figure 2.46 Measurements of the Q-factor and $\tan \delta$ of the frequency characteristics of tap water [55]

2.7 Comparisons of existing WPT underwater in air, fresh water, and seawater

Based on previous studies, Table 2.6 compares current wireless power transfer (WPT) systems operating in air, fresh water, and seawater. These comparisons highlight variations in efficiency, distance and power level capabilities due to differing dielectric properties and conductivity of the mediums. The table provides a clear overview of how environmental conditions impact the performance of WPT systems.



Table 2.6 Comparisons of existing WPT underwater in air, fresh water, and seawater

	Frequency (Hz)	Power Level (W)	Efficiency (%)	Distance (mm)	Medium	Experiment Setup/Application
[45]	85kHz	2kW	N/A	N/A	Air	Battery charging
[44]	790MHz	N/A	88.2%	9.4mm	Air	Charging smart phone
[54]	6.78MHz	5W	41.49%	20mm	Air	Biomedical implant
[53]	6.78MHz	2.2W	56.18%	14mm	Air	Biomedical implant
[2]	115kHz	10MHz	N/A	20mm	Air	Biomedical implant
[52]	50Hz	N/A	40%	20mm	Air	Drone, UAV
[51]	50-60Hz	N/A	50%	10mm	Air	Drone, UAV
[10]	85kHz	1.5kW	95.6%	120mm	Air	EV battery charging System
[25]	1MHz	6.06kW	92.3%	60mm	Air	Electric Vehicle wireless charging
[56]	N/A	10W	85%	30mm	Air	Electric Vehicle wireless charging
[38]	1MHz	226.9W	60.2%	500mm	Freshwater	Electric ship charging application
[12]	N/A	3.3kW	75.9%	50mm	Freshwater	Electric ship charging application
[28]	35.4kHz	3kW	92%	5mm	Air, freshwater and seawater	Autonomous underwater vehicle (AUV)
[57]	32kHz	300W	88%	5mm	Salt water	Autonomous underwater vehicle (AUV)
[41]	1MHz	5kW	81.4%	50mm	Freshwater	Underwater application
[55]	25.7MHz	N/A	80.9%	70 mm	Freshwater	Underwater application
[16]	1.1MHz.	129.2 W	81.2%.	300 mm	Seawater	Underwater application
[14]	500 kHz	100W	50%	60mm	Seawater	Underwater application
[29]	625 kHz.	100 W	80.15%.	180 mm	Seawater	Underwater application
[13]	6.78MHz	226.9 W	60.2%.	500 mm.	Freshwater	Underwater application

Table 2.7 Application of wireless power transfer (WPT)

	Application	Objective	Method
[1]	Near-field (NFWPT)	Experiment on WPT using inductive coupling, aiming to achieve high efficiency	MATLAB
[44]	Mobile phone wireless charging	To verify a near-field capacitively coupled wireless charging system's effectiveness and compactness.	HFSS electromagnetic wave simulator
[48]	EV charging	Allows charging multiple EVs at once using a single charging station magnetic coupling used to transfer energy wirelessly	MATLAB
[58]	Electric vehicles (EVs)	Develop a new design for the CPT system that can increased efficiency in transferring power wirelessly	ANSYS Maxwell
[59]	Mini electric vehicles (EVs).	To achieve high efficiency and minimize electromagnetic interference (EMI) during wireless charging	LTSpiceTM
[49]	Electric vehicles (EV)	To create an indirect load estimation WPT system for EVs	MATLAB
[60]	Ship Charging Application	To develop a system for high-power underwater wireless charging of electric ships	FEM analysis
[26]	Ship Charging Application	To standardized and ideal method for creating a fuel cell (FC) system, a lithium-ion battery (LB) system, or an electrical system for a UCS	DC/DC converter topology

[12]	Charging electric ships	To suggest ideal approaches for achieving maximum power maximum efficiency in undersea CPT systems	six-plate coupler and a four-plate coupler
[29]	Autonomous underwater vehicle (AUV)	To develop a CPT system that operates specifically underwater and is both safe and effective.	MATLAB
[14]	Autonomous underwater vehicles (AUVs).	The wireless charging technology (CPT) for underwater vehicles, such as AUVs	PSIM
[41]	Autonomous underwater vehicles (AUVs).	High efficiency in submerged situations	Six-plate horizontal coupler design
[61]	Wireless charging system for underwater vehicles (AUVs).	Design underwater wireless charging system with capacitive coupling	Calculate the freshwater and seawater
[28]	Autonomous underwater vehicles (AUVs)	Inductive power transfer in submerged situations and create an AUV charging system that is more dependable and efficient.	Proposed self-latching coupling structure
[52]	Drone, Unmanned Air Vehicles (UAVs)	To research WPT potential and limitation for recharging UAVs while they are in use, in order to get around the range and endurance restrictions imposed by battery capacity	EMF test setup

[51]	Drone, Unmanned aerial vehicles (UAVs)	To improve the drones' mission time and travel distance	wireless charging technique drone mission duration
[2]	Biomedical implants	To model and experimentally validate a capacitive link for efficient power transfer to biomedical implants	Pairs of coated parallel plates
[54]	Implantable sensors and remote health monitoring	To enhance power transfer efficiency (PTE) and enable data communication for neural implants using a resonant capacitive-coupling (RCC) approach	RCC
[53]	Implanted biomedical devices (DIBDs).	To enable safe and efficient power transfer to DIBDs while minimizing implant size and patient tissue heating.	COMSOL simulations
[43]	Medical devices wearables or implants	This paper aims to provide a comprehensive overview of Capacitive Power Transfer (CPT) systems.	CPT systems

Table 2.8 Wireless power transfer (WPT)

	Application	Objective	Method
[62]	Capacitive power transfer (CPT)	To create a technique for a dual-Tx CPT system that can keep efficiency high even if the receiver and transmitters are not exactly aligned.	Dual transmitter capacitive coupler
[16]	Capacitive power transfer (CPT)	Analyze the impact of seawater on capacitance and potential benefits for underwater charging. Calculate the capacitance of the CPT system in both air and underwater environments.	COMSOL Multiphysics simulation software
[63]	Capacitive power transfer (CPT)	Review of the current state-of-the-art in CPT technology for wireless battery charging	CPT wireless battery charging
[64]	Capacitive power transfer (CPT)	estimating coupler power transfer efficiency in underwater situations	CST Microwave Studio
[65]	Capacitive power transfer (CPT)	To create a capacitive coupler that can transfer power wirelessly in seawater with great efficiency by utilizing the electric double layer (EDL) effect.	Electric double layer (EDL)
[66]	Capacitive power transfer (CPT)	capacitive couplers used for wireless power transfer underwater.	Electric Double Layer (EDL)
[64]	Capacitive power transfer (CPT)	estimating coupler power transfer efficiency in underwater situations	CST Microwave Studio
[50]	Capacitive power transfer (CPT)	Review the most recent advancements in underwater WPT technology and its potential	WPT underwater applications.

[10]	Inductive wireless power transfer (IPT)	Minimize resistance in the transmitter and receiver coils to boost the IWPT system's overall efficiency.	MATLAB
[45]	Inductive power transfer (IPT)	To create an electric vehicle (EV) 2-kW wireless charger	MATLAB
[18]	Inductive power transfer (IPT)	Reviews the development of IPT systems and implementing IPT for roadway applications.	FA IPT system
[24]	Capacitive power transfer (CPT)	Performance of two varieties of insulated couplers for CPT parallel and stacked in submerged conditions.	3D RLCG extraction tool (Q3D)
[8]	Inductive power transfer (IPT)	To understand how marine environmental parameters temperature and salinity affect the performance of UCWPT systems.	Maxwell software

2.8 Summary

Previous research on capacitive wireless power transfer (CPT) in freshwater, seawater, and air revealed that the dielectric characteristics of the medium affect CPT efficiency, with seawater show the best efficiency because of its larger dielectric constant. These results demonstrate that highly efficient CPT systems can be used in a variety of applications including underwater environments whereby can be runs for underwater sensors, charging electric cars (EVs), and enable for autonomous underwater vehicles (AUVs)

CHAPTER 3

METHODOLOGY

3.1 Introduction

This chapter will go over the procedures and approaches used in the development of capacitive wireless power transfer couplers for underwater EV charging applications. The list of the hardware and software requirements necessary for completing this project. The main focus of this discussion will be on achieving high efficiency in wireless power transfer underwater using capacitive couplers. By combining design analysis, simulation, prototyping, testing, and software integration, to achieve reliable and efficient wireless power transfer in underwater environments. LTspice will be used to model and analyze the performance of the capacitive coupler design. This step is crucial for optimizing the design parameters and predicting the behavior of the system under various underwater conditions. The simulation results will guide the refinement of the prototype design. The LTspice software will be utilized in this project to ensure its success.

3.2 Flowchart of overall system

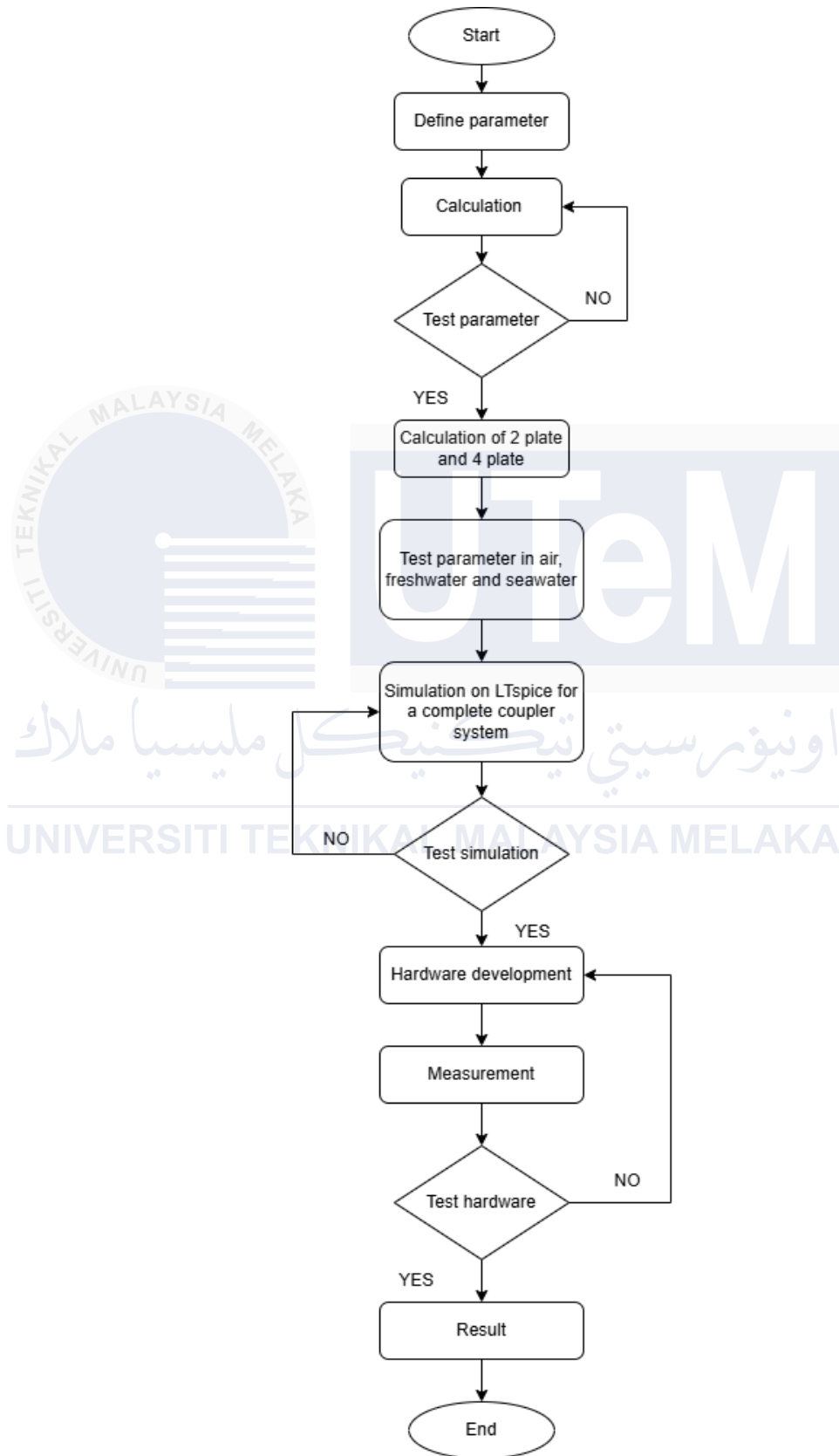


Figure 3.1 Flowchart of overall project

The process of developing a specific Capacitive Power Transfer (CPT) system starts with defining important variables such as the distance between plates, the area of the plates, and the dielectric constants of each medium freshwater, seawater, and air. When designing the system and considering performance into consideration, these parameters are important. by Using a theoretical formula for a single-plate capacitor to calculate initial estimations, theoretical analysis and simulations must be carried out before setting up an experiment measuring capacitance. The stability of these capacitance values is analyzed afterwards to make sure they meet the requirements of design, including variables that may have an impact on capacitance. The simulation results are arranged in tables for a comprehensive analysis and include various types of capacitance situations. Proceeding on, LTspice is used to simulate the entire coupler system. Further adjustments and simulations are performed in LTspice if the simulation results do not match the theoretical calculations. Hardware development continues after the simulation findings prove sufficient understanding. The hardware apparatus is measured, and the findings are placed forward for test. The system development process concludes following the collection of results. Finally, the compiled results mark the end of the system development.

3.3 Block diagram

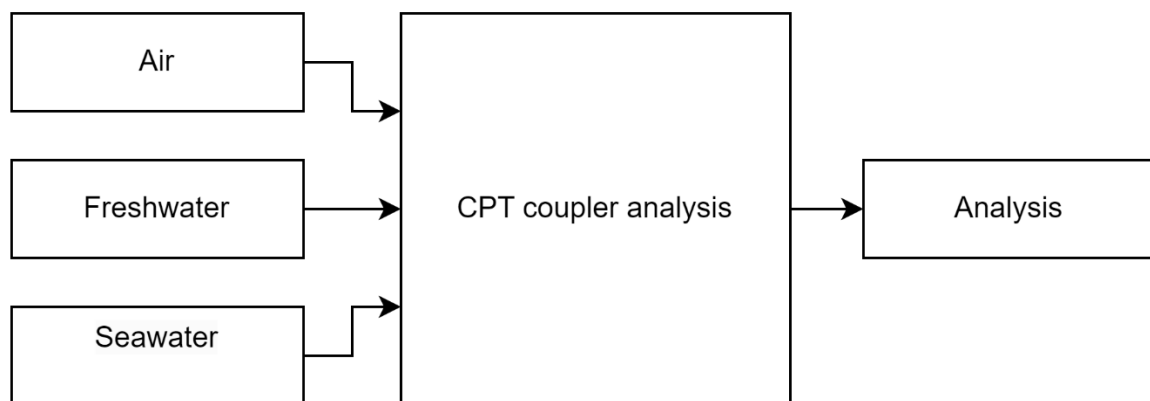


Figure 3.2 Block diagram

The block diagram outlines the process for studying the relationship between capacitance, plate area, and distance in a single-plate capacitor setup, considering different mediums in air, freshwater, seawater. The blocks represent the different stages involved in the process. The process starts with defining the parameters to be investigated, including the range of plate areas, plate distances, and permittivity values for the three mediums. The next block uses theoretical formula to calculate capacitance in different mediums then simulation tool like MATLAB is used to design model of the system and calculate capacitance values under various conditions defined by the parameters. The final block focuses on setting up a single-plate capacitor using both theoretical calculations and simulations to explore and validate the relationship between capacitance, plate area, and distance in different mediums.

3.4 Circuit Modelling

Circuit modeling involves creating a mathematical representation of an electrical circuit to analyze its behavior and evaluate its performance. This process helps to predict how a circuit will function under different conditions. By utilizing circuit modeling, various design options can be assessed and compared without the need to physically construct the circuit, making it an efficient and effective tool for evaluation and optimization. this report evaluates various design options using circuit modelling.

3.4.1 Analysis of sheilded CPT circuit model

Figure 3.3 illustrates the circuit model for analyzing the coupling interface of the proposed shielded-CPT system. The system is designed with symmetrical primary and secondary side components to ensure balanced power transfer. The input voltage source (V_0) provides a sinusoidal AC voltage applied at terminals a and b of the primary side.

On the primary side, the series-resonant inductor (L_R) and coupling capacitance (C_R) work together to tune the system to its resonant frequency, compensating for reactance and maintaining efficient energy transfer. The primary and secondary sides are coupled through the coupling capacitance (C_C) and shielded by parasitic capacitances (C_P), which result from the physical design of the plates and the surrounding environment. On the secondary side, an identical configuration with L_R and C_R ensures resonance tuning, while the load resistance (R_{Load}) is connected through the resonant inductor to enable effective power delivery. The mutual inductance (L_m) and mutual capacitance (C_m) represent the coupling effect between the primary and secondary sides, modeling energy transfer through the electric field created by the coupling plates. The system's symmetrical design and parameter tuning on both sides minimize power losses and optimize efficiency, even with the influence of shielding and parasitic effects. The simplified model of the shielded CPT coupling structure as shown in Figure 3.4 is used to represent the essential components and interactions within the system.

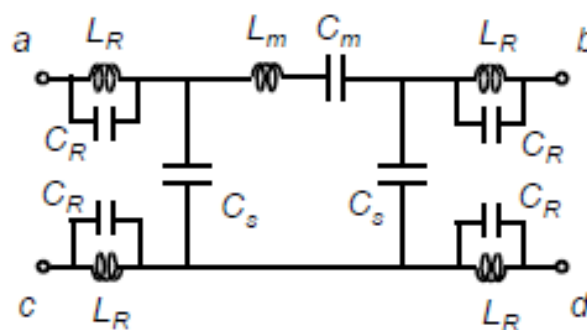


Figure 3.3 Circuit model for S-CPT coupling capacitance circuit analysis [67]

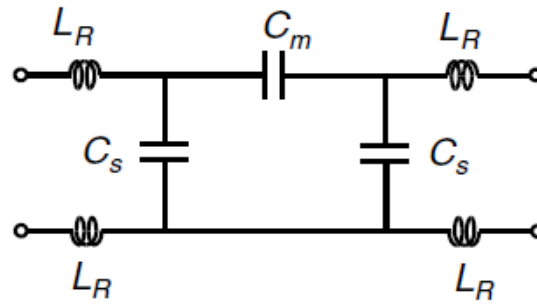


Figure 3.4 Simplified model of shielded-CPT coupling structure [68]

3.4.2 LTspice

LTspice, used to simulate electronic circuit as shown in Figure 3.5, LTspice by Linear Technology is a widely used simulation tool for electronic circuit design and analysis. It allows engineers and electronics enthusiasts to simulate and evaluate the behavior of analog, digital, and mixed-signal circuits before creating physical prototypes. With a user-friendly graphical interface and support for netlist-based design, LTspice enables users to construct and edit circuit schematics efficiently. The software offers a comprehensive library of components, including transistors, operational amplifiers, resistors, capacitors, inductors, and digital logic gates. Frequently employed in the electronics industry, LTspice is instrumental in circuit design and verification, selecting component values, analyzing circuit behavior under various conditions and troubleshooting. Its practical and it is an effective tool that gives engineers of all levels a practical and affordable way to iterate and improve circuit designs.



Figure 3.5 LTspice Illustration

3.4.3 MATLAB

MATLAB is a high-performance software from MathWorks it is extensively utilized in the design and analysis of circuits for capacitive power transfer (CPT) in underwater applications. MATLAB's comprehensive suite of tools allows engineers to model complex electrical systems and simulate their behavior under various conditions. MATLAB are used to develop mathematical models of the capacitive coupling and simulate power transfer efficiency, considering the unique challenges posed by the underwater environment, such as signal attenuation and variable conductivity. The software's powerful computational capabilities facilitate the optimization of circuit parameters and the analysis of system performance, enabling the identification and mitigation of potential issues before physical prototyping. MATLAB's Simulink, a block diagram environment for multidomain simulation, further enhances the design process by allowing for the integration of control algorithms and real-time data processing. This holistic approach ensures that the CPT system is both efficient and reliable, aligning with the rigorous requirements of underwater applications.



Figure 3.6 MATLAB illustration

3.5 Simulation in MATLAB

Throughout the simulation process, simulation tools are used to validate proposed solutions for accurate and efficient data. MATLAB is one of the important simulation tools

used to validate the proposed solutions ensuring accurate and efficient data analysis. MATLAB is utilized in this project to calculate and analyze the performance of capacitive configurations involving two, four, and six plates. These calculations are performed with the objective of simulating theoretical models which allowing for precise predictions of their behavior under different conditions.

3.5.1 Calculations on CPT structure

Table 3.1 Comparisons of existing WPT underwater in air, fresh water, and seawater

Medium	Conductivity (S/m)	Relative permeability	Relative permittivity (ϵ_r)
Air	0	1	1.0006
Fresh water	0.01	0.99	78.50
Seawater	4	0.99	81.50

$$C = \frac{A\epsilon_0\epsilon_r}{d} \quad (3.1)$$

C – Capacitance value

A – area of the plates

ϵ_0 - the permittivity of free space (8.854×10^{-12} F/m)

ϵ_r (water) - the relative permittivity of water

d - distance between the plates.

The parameters are set as in Table 3.2. The table sets a constant area of 100 square meters and varies the distance between 1 mm and 50 mm in several increments. By using formula in (3.1) [21], these values will be used to analyze the impact of distance on the performance of the capacitive power transfer system. This estimation can be performed in different mediums, such as air, freshwater, and seawater.

Table 3.2 Parameter are set for calculation.

Area (m ²)	Distance (mm)
100	1
100	5
100	10
100	15
100	20
100	30
100	50

The parameters are set as in Table 3.3 shows the relative permittivity (ϵ_r') values for three mediums which is in air, freshwater, and seawater used for MATLAB simulations. The conductivity value of 0.011 S/m was applied uniformly for all three mediums during the simulations.

Table 3.3 Parameter are set for calculation.

Medium	Relative permittivity, ϵ_r'
Air	1.0006
Freshwater	79
Seawater	81.50

3.5.2 Case of WPT under fresh water

The parameters listed in Table 3.4 are critical for the design and analysis of the wireless power transfer (WPT) system in freshwater. Each parameter represents an electrical property of the circuit: These parameters are incorporated into circuit simulations to evaluate the system's performance under freshwater conditions.

Table 3.4 Parameter for calculation in freshwater

Symbol	Description	Value	Unit
L_m	Parasitic Inductance	60	nH
C_m	Mutual coupling	180	pF
C_s	Self-coupling	72	pF
L_R	Feeding line	122	nH
C_R	Parasitic Capacitance	5.5	pF

The circuit depicted in Figure 3.7 represents the electrical model used for analyzing the wireless power transfer (WPT) system in freshwater conditions. It incorporates essential parameters such as parasitic inductance (L_m), mutual capacitance (C_m), self-capacitance (C_s), feeding line inductance (L_R), and parasitic capacitance (C_R), as shown in the configuration. This circuit serves as the foundation for calculating key performance metrics of the capacitive coupler in a freshwater environment. The interactions between these components are modeled to evaluate the system's impedance, resonance frequencies, and coupling efficiency.

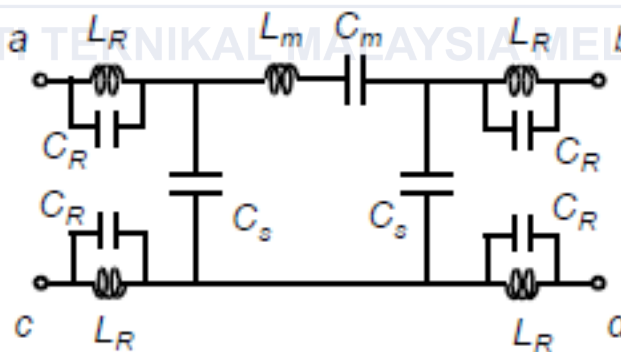


Figure 3.7 Calculation based on circuit in freshwater [67]

3.5.3 Freshwater Adaptation , K

The freshwater adaptation factor (K) is defined by using the formula in (3.2) [68]. This factor quantifies the relationship between mutual capacitance (C_m) and self-capacitance (C_s) in the circuit. In the freshwater environment, high relative permittivity

($\epsilon r'$) significantly affects the coupling efficiency. K helps assess the effectiveness of power transfer under these conditions by balancing the contribution of mutual and self-coupling to the overall system behavior. By using this formula, the project evaluates the circuit's adaptability to freshwater, enabling fine-tuning of design parameters to achieve optimal performance in such a medium

$$K = \frac{C_m}{2C_s + C_m} \quad (3.2)$$

3.5.4 Quality factor , Q

The quality factor (Q) is defined by using the formula in (3.3) [67]. This formula defines the quality factor (Q) of the coupler in relation to frequency (ω), relative permittivity ($\epsilon r'$), and conductivity (σ) of the medium. It is used to assess the losses due to the medium and ensure that the design minimizes energy dissipation while maximizing power transfer efficiency.

$$Q_{factor} = \frac{\omega \epsilon r' \epsilon_0}{\sigma} \quad (3.3)$$

ϵ_0 - the permittivity of the vacuum (8.854×10^{-12} F/m)

$\epsilon r'$ - the relative permittivity of water

σ - electric conductivity

3.5.5 Pseudo-coupling coefficient , k_p

The pseudo-coupling coefficient (k_p) is crucial in this project to evaluate and optimize the power transfer efficiency between the transmitter and receiver in the capacitive wireless power transfer (WPT) system. It measures the strength of electromagnetic coupling between plates and helps analyze configurations like 2-plate and

4-plate setups under air, freshwater and seawater conditions. By using the formula in (3.4) [67], (3.4) [67] and (3.5) [67], k_p ensures sufficient coupling for efficient power transfer while minimizing losses. It is particularly useful for assessing performance in underwater environments where dielectric properties affect coupling.

$$k_p = \left| \frac{V_2}{V_1} \right| = \left| \frac{Cm(1 - \omega^2 CRLR)}{A\omega^4 - B\omega^2 + 2Cs + Cm} \right| \quad (3.6)$$

$$A = (CR + 2Cs)CmLmCsLR \quad (3.7)$$

$$B = \{(2Cs + Cm)CR + 4Cs(Cs + Cm)\}LR + CmCsLm \quad (3.8)$$

3.5.6 $k_p Q$ product, kQ

The parameter kQ is essential for evaluating the power transfer efficiency in the capacitive wireless power transfer (WPT) system. It combines the coupling coefficient (k_p) and the quality factor (Q) to assess the system's ability to transfer power efficiently. By using formula in (3.7) [67], kQ represents system losses.

$$k_p Q = kQ = \frac{V_2}{V_1} = \left| \frac{Cm(1 - \omega^2 CRLR)}{A\omega^4 - B\omega^2 + 2Cs + Cm} \right| \cdot \left| \frac{\omega \epsilon r' \epsilon_0}{\sigma} \right| \quad (3.9)$$

3.5.7 Maximum power transfer efficiency, η_{max}

The formula shows in (3.8) [67] is crucial for determining the maximum power transfer efficiency (η_{max}) of the system. It evaluates how effectively energy is transferred through the coupler. By incorporating the coupling coefficient (k) and the quality factor (Q), it provides insights into the performance of capacitive configurations and helps identify optimal conditions for efficient power transfer.

$$\eta_{max} = 1 - \frac{2}{1 + \sqrt{1 + (kQ)^2}} \quad (3.10)$$

3.5.8 Frequency characteristics, f_k

The equation shown in (3.9) [67], (3.10) [67] and (3.11) [67] determines the resonance frequencies of the system which are critical for achieving maximum power transfer and minimum frequency. It is used to validate the system's theoretical performance through simulations and ensures that the capacitive configurations are tuned to the desired frequency range. The frequency characteristics of the coupler underwater are determined by k_p which obtained from equivalent circuit.

Maximum frequency (f_{k1} and f_{k3});

$$f_{k1}, f_{k3} = \frac{1}{2\pi} \sqrt{\frac{B \pm \sqrt{B^2 - 4A(2C_s + C_m)}}{2A}} \quad (3.11)$$

Minimum frequency (f_{k0}), k formula is 0;

$$f_{k0} = \frac{1}{2\pi\sqrt{CRLR}} \quad (3.12)$$

Very high frequency (f_{k2} and f_{k4});

$$f_{k2}, f_{k4} = \frac{1}{2\pi} \sqrt{\frac{1}{CRLR} \mp \sqrt{\frac{1}{CR^2CL^2} - \frac{B}{CRLRA} + \frac{2C_s + C_m}{A}}} \quad (3.13)$$

These frequencies would be tested experimentally to determine which provides the best power transfer efficiency especially when the plates are submerged in water which presents a unique challenge due to its dielectric properties. The frequencies would also be used to analyze how capacitive coupling behaves in different conditions and configurations.

3.5.9 Case of WPT under seawater

The parameters listed in Table 3.5 are critical for the design and analysis of the wireless power transfer (WPT) system in seawater. Each parameter represents an electrical property of the circuit: These parameters are incorporated into circuit simulations to evaluate the system's performance under seawater conditions.

Table 3.5 Parameter for calculation in seawater

Symbol	Description	Value	Unit
Lp	Parasitic Inductance	15.8	nH
Gp	Parasitic Conductance	1.97	mS
Cp	Parasitic Capacitance	2.73	pF
Cm	Mutual coupling	198	pF
Gm	Mutual Conductance	0.689	S
Cs	Self-coupling capacitance	3.62	pF
Gs	Self-Coupling Conductance	20.7	mS
CR	Parasitic Capacitance	5.5	pF

The circuit depicted in Figure 3.8 represents the electrical model used for analyzing the wireless power transfer (WPT) system in seawater condition. It incorporates essential parameters such as parasitic inductance (Lp), mutual conductance (Gm), self capacitance (Cs), self coupling conductance (Gs) and parasitic capacitance (Cp and CR) as shown in the configuration. This circuit serves as the foundation for calculating key performance metrics of the capacitive coupler in seawater environment. The interactions between these components are modeled to evaluate the system's impedance, resonance frequencies and coupling efficiency while also accounting for the conductive losses introduced by the seawater medium.

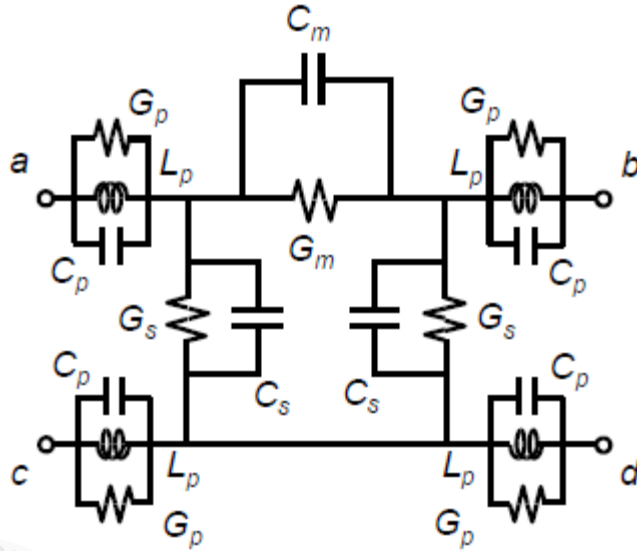


Figure 3.8 Calculation based on circuit for seawater [67]

3.5.10 Maximum power transfer efficiency, η_{max}

The equation in (3.13) [67] calculates the maximum power transfer efficiency (η_{max}) of the wireless power transfer system. It shows how the coupling coefficient (K) directly impacts the efficiency providing insight into the optimal design for minimizing power losses in underwater applications.

$$\eta_{max} = 1 - \frac{2}{1 + \sqrt{1 + (K)^2}} \quad (3.14)$$

3.5.11 Coupling coefficient, K

The equation in (3.12) [67] defines the coupling coefficient (K) of the system. It measures how effectively power is transferred between the transmitter and receiver circuits in the presence of mutual and self-conductances. A higher value of K indicates better coupling efficiency which is critical in seawater environments due to conductive losses.

$$K = \frac{G_m}{\sqrt{(G_s + G_m)^2 - G_m^2}} \quad (3.15)$$

3.5.12 Refined Coupling coefficient, K

The formula in (3.14) [67] is refined version of the coupling coefficient (K) includes additional system parameters an advanced coupling coefficient calculation, incorporating parasitic parameters (L_p , C_p) and operating frequency (ω), crucial for optimizing underwater WPT systems.

$$K = \frac{Gm}{\sqrt{[(Gp + Gs)GpLp - 2Cp] GsLp\omega^2 + Gs}F} \quad (3.16)$$

There are differences between equation in (3.13) [67] and equation in (3.14) [67] by their level of detail and parameter inclusion used to calculate the coupling coefficient (K) in the wireless power transfer (WPT) system under seawater conditions. Equation in 3.13 gives a general estimate of the coupling coefficient while equation in 3.14 provide a more realistic and accurate representation by including parasitic and frequency dependent parameters.

3.5.13 Frequency dependent transfer function , F

The equation in (3.15) [67] represents the frequency dependent transfer function (F) of the system. It incorporates inductance, capacitance and conductance terms, showing how these factors determine the system's resonance and stability. Fine-tuning these parameters helps achieve maximum power transfer efficiency.

$$F = Lp (2Gm + Gs)\{(4Gm + Gp + 2Gs)GpLp - 2Cp\}\omega^2 + Gs + 2Gm \quad (3.17)$$

3.6 Simulation LTspice

Throughout the simulation process, simulation tools are used to validate proposed solutions for accurate and efficient data. LTspice is one of the essential simulation tools utilized to validate the proposed solutions ensuring reliable and precise circuit analysis. LTspice is employed in this project to model and analyze the performance of capacitive circuits involving two and four plates. These simulations are conducted with the aim of examining the theoretical models allowing for accurate predictions of their electrical behavior under various conditions.

3.6.1 Freshwater

The development of the schematic circuit for the capacitive coupler simulation in LTspice involves several key steps to accurately model and analyze the system's performance. The process begins with defining the fundamental components of the capacitive coupler including the capacitive plates, the power source and the load. Each component is carefully selected and configured to represent the theoretical design parameters. For instance, capacitors are used to stimulate the behavior of the capacitive plates with their values reflecting the estimated capacitance for two and four plate. The design of schematic capacitive coupler in freshwater designed as shown in Figure 3.9.

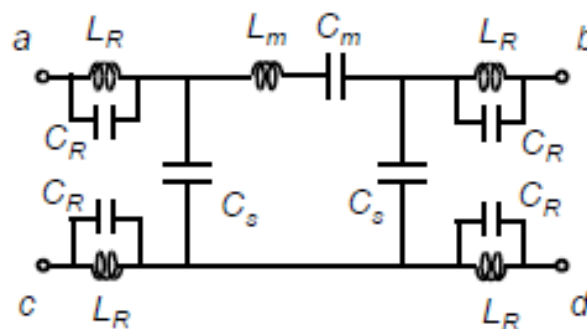


Figure 3.9 Schematic of capacitive coupler in freshwater [67]

By using the parameters listed in Table 3.6 is design and analysis of the wireless power transfer (WPT) system in freshwater. These parameters are essential inputs that define the circuit's operational conditions and influence its overall performance during simulation in LTspice. Each parameter is carefully chosen based on theoretical calculations and experimental measurements to ensure the circuit accurately reflects real-world scenarios.

Table 3.6 Parameter for calculation in freshwater

Symbol	Description	Value	Unit
Lm	Parasitic Inductance	60	nH
Cm	Mutual coupling	180	pF
Cs	Self-coupling	72	pF
LR	Feeding line	122	nH
CR	Parasitic Capacitance	5.5	pF

To simulate real-world conditions, the medium of operation in air and freshwater is modeled by adding resistors that represent its dielectric properties and conductivity. These resistors are placed in parallel with the capacitors to study the medium's impact on the coupler's performance.

Then, an AC voltage source is included to provide input power with its frequency and amplitude set to match the system's operating conditions. A load resistor is added to measure output behavior while voltage probes and current markers are placed strategically to collect data during the simulations.

The circuit is logically designed with proper grounding and labeling to ensure clarity. Simulations are performed air and freshwater conditions such as different frequencies or medium properties to observe voltage, current and power transfer efficiency. This process helps validate theoretical models and refine the design by ensuring the

simulation accurately reflects the capacitive coupler's behavior and its feasibility for wireless power transfer. The designed implemented in LTspice as shown in Figure 3.10.

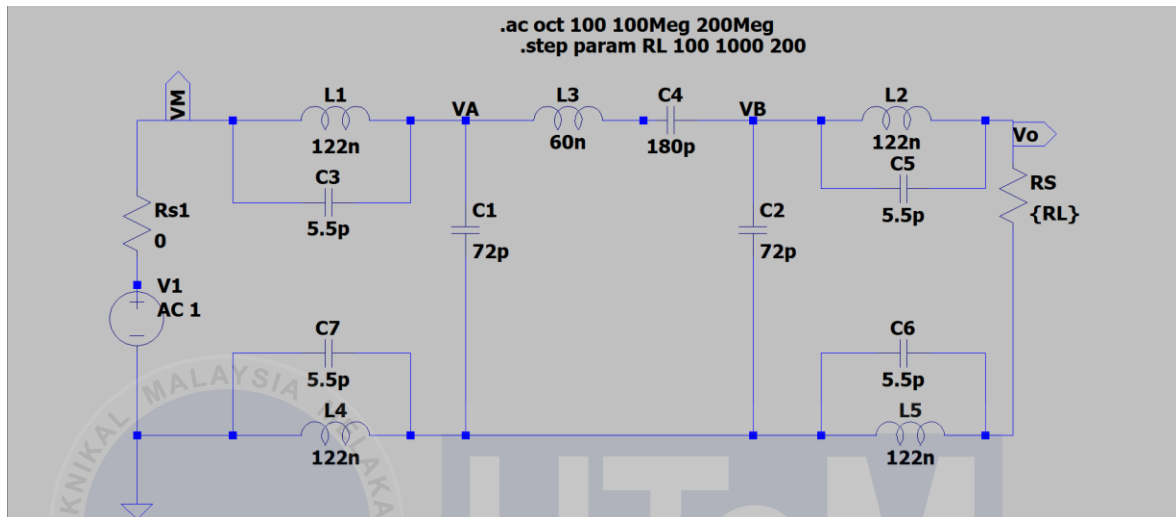


Figure 3.10 Schematic of capacitive coupler in freshwater designed in LTspice

3.6.2 Seawater

The development of the schematic circuit for the capacitive coupler simulation in LTspice involves several key steps to accurately model and analyze the system's performance. The process begins with defining the fundamental components of the capacitive coupler including the capacitive plates, the power source and the load. Each component is carefully selected and configured to represent the theoretical design parameters. For instance, capacitors are used to simulate the behavior of the capacitive plates, with their values reflecting the estimated capacitance for two and four plates. The schematic design of the capacitive coupler in seawater is illustrated in Figure 3.11.

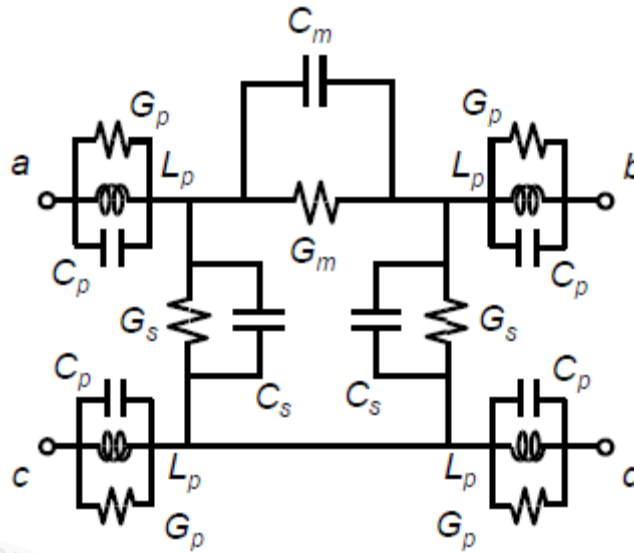


Figure 3.11 Schematic of capacitive coupler in seawater [67]

By using the parameters listed in Table 3.7 is critical for the design and analysis of the wireless power transfer (WPT) system in seawater. These parameters are essential inputs that define the circuit's operating conditions and impact its overall performance during LTspice simulations. Each parameter is carefully selected based on theoretical calculations and experimental data to ensure the circuit accurately represents real-world scenarios in seawater environments.

Table 3.7 Parameter for calculation in seawater

Symbol	Description	Value	Unit
L_p	Parasitic Inductance	15.8	nH
G_p	Parasitic Conductance	1.97	mS
C_p	Parasitic Capacitance	2.73	pF
C_m	Mutual coupling	198	pF
G_m	Mutual Conductance	0.689	S
C_s	Self-coupling capacitance	3.62	pF
G_s	Self-Coupling Conductance	20.7	mS
CR	Parasitic Capacitance	5.5	pF

To simulate real-world conditions, the medium of operation in seawater is modeled by adding resistors that represent its dielectric properties and conductivity. These resistors are placed in parallel with the capacitors to analyze how the medium affects the coupler's performance.

An AC voltage source is included to provide input power, with its frequency and amplitude adjusted to match the system's operating conditions. A load resistor is added to evaluate the output while voltage probes and current markers are strategically placed to collect data during the simulations.

The circuit is designed with proper grounding and labeling for clarity. Simulations are performed under seawater conditions, including variations in frequency and medium properties to study voltage, current and power transfer efficiency. This process helps validate theoretical models and refine the design to ensure the simulation accurately reflects the capacitive coupler's behavior and its suitability for wireless power transfer. The design is implemented in LTspice as shown in Figure 3. 12.

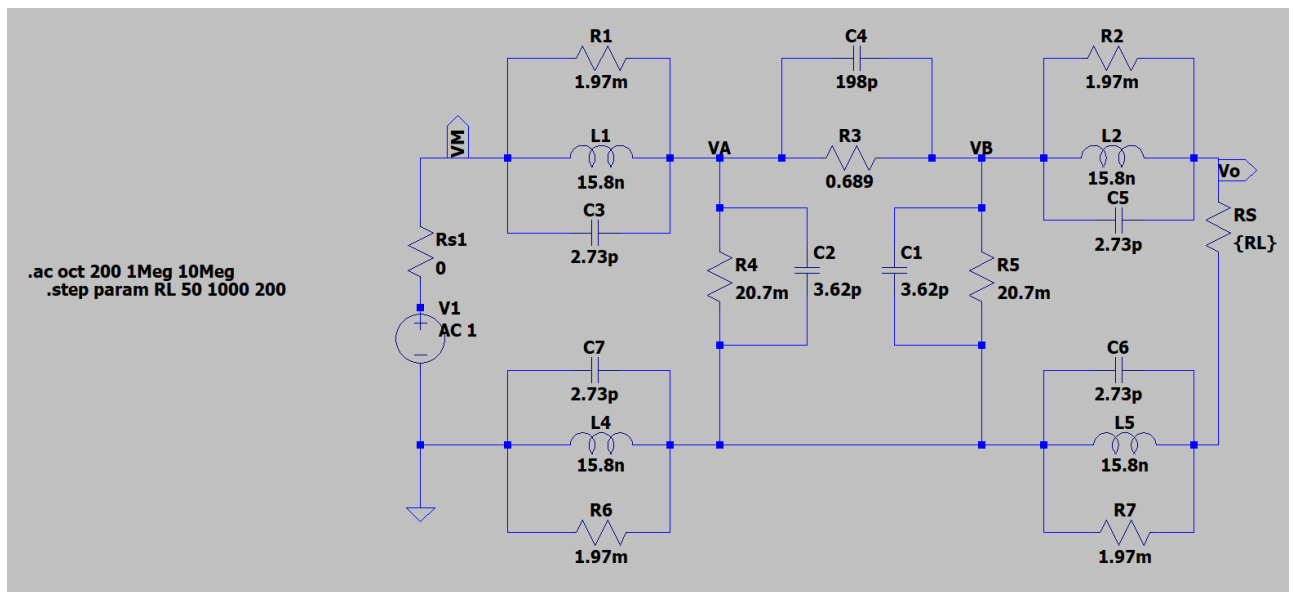


Figure 3.12 Schematic of capacitive coupler in seawater designed in LTspice

3.7 Hardware development

Hardware development is essential for ensuring the validity of results as software simulations often fail to capture real-world complexities. Simulations rely on predefined parameters which can lead to inaccurate outcomes and frequently overlook environmental factors such as temperature, humidity and external forces that significantly impact performance. By developing hardware, will provide a real-world data more accurate representation of the system performance and a comprehensive understanding of the interaction between hardware and software. This process can enhances design and modeling skills enabling to translate theoretical models into practical implementations. In this project, the development of specific hardware components facilitates the collection of accurate data accounts for environmental influences and achieves a holistic understanding of the system. This comprehensive approach validates the findings and strengthens the overall design and development capabilities.

3.7.1 System of project

The system of this project focuses on analyzing the performance of a wireless power transfer (WPT) coupler in underwater conditions. The analysis begins with theoretical calculations of the coupler's performance for 2-plate and 4-plate configurations. These calculations are carried out using MATLAB to simulate the theoretical models and predict the coupler's behavior under specific conditions. MATLAB plays a critical role in providing a detailed understanding of the expected performance of the capacitive.

To confirm the theoretical findings, LTspice is used to perform circuit simulations. The circuit models are designed to replicate the theoretical parameters and simulate the coupler's behavior under similar conditions. This step ensures that the theoretical

calculations and circuit simulations are aligned by providing greater confidence in the accuracy of the predictions. Once the theoretical and simulated results are verified, real-time experiments are conducted to further validate the system's performance.

In the experimental phase, the capacitive plates are immersed in different medium which freshwater and seawater include in air to test their efficiency in transmitting power. This step also examines the dielectric properties and conductivity of the medium which significantly influence the coupler's performance. Advanced tools such as NanoVNA Saver and NanoVNA Vector Network Analyzer are utilized to measure the key parameters during the experiments. These tools provide precise data on impedance and resonance allowing for a comprehensive analysis of the system's behavior.

The data collected from the real-time experiments are analyzed and compared with the theoretical and simulated results to ensure consistency and reliability. This multi-step process ensures a thorough understanding of the capacitive coupler's efficiency and its potential for wireless power transfer in underwater environments which can contributing to advancements in this field.

3.7.2 Experimental setup

The experimental setup for this project is designed to validate the findings from LTspice simulations and assess the real-world performance of the wireless power transfer (WPT) system. The setup involves immersing capacitive plates in three different medium such as air, freshwater and seawater to replicate the conditions modeled in the simulations. The setup consists of two parallel plates, each dimensions of 7 cm × 10 cm. The distance between the electrodes on each plate is 2 cm while the separation between the parallel plates is maintained at 5 cm as shown in Figure 3.13. The capacitive plates are arranged in

configurations of 4-plates as defined in the LTspice circuit designs to analyze their power transfer efficiency and dielectric behavior. The experimental setup connection in real time experiment are as shown in Figure 3.14.

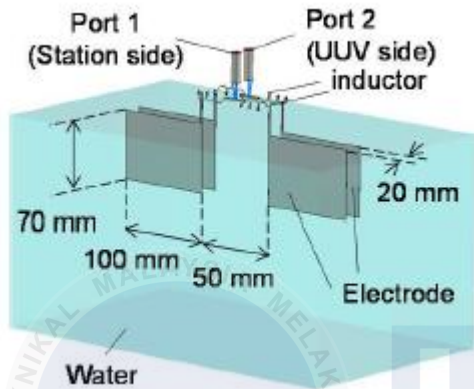


Figure 3.13 The simulation model based on research paper

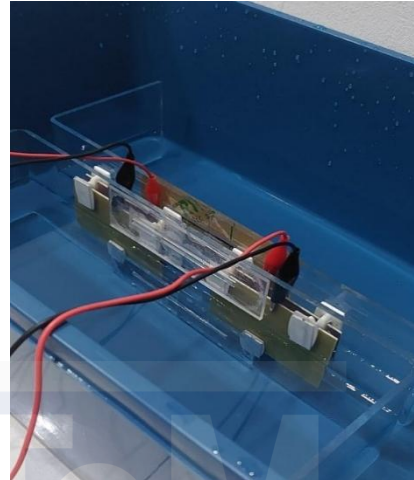


Figure 3.14 The setup circuit connection in freshwater by referring to research paper

Each inductor coil in the capacitive wireless power transfer coupler has a specific inductance value essential for the system's performance. The inductance is determined using an online calculator or calculated manually with formulas considering coil geometry, number of turns and surrounding material. These values ensure resonance which is critical for efficient power transfer in different mediums like air, freshwater, and seawater

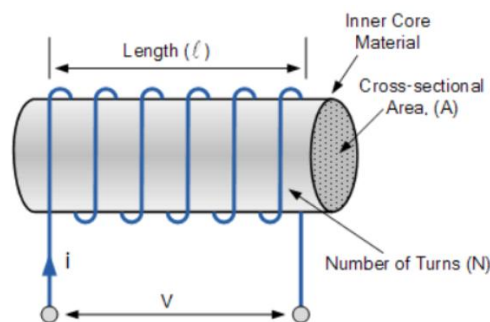


Figure 3.15 Calculation of inductor coil

$$L_{coil} = \frac{\mu_r \mu_0 N^2 A}{l} \quad (3.18)$$

L_{coil} - Inductor of the coil in Henries (H)

μ_r - the relative permeability of the core (dimensionless)

μ_0 - the permeability of free space ($4\pi \times 10^{-7} \text{H/m}$)

N - number of turns

A - cross-sectional area of the coil ($A = \pi r^2$), where r is the radius of the coil

l - length of the coil

The experimental setup for this project is designed to assess the performance of the capacitive wireless power transfer system under varying conditions. The NanoVNA is connected to the circuit which includes inductor coils, RF antenna cables and probes. These components are systematically integrated to form the measurement circuit. The inductor coils play a critical role in the wireless power transfer system acting as a key part of the resonance between the capacitive plates while the RF antenna cable and probes are essential for collecting data related to the system's impedance and frequency response. The setup allows for testing the coupling efficiency and power transfer characteristics between the capacitive plates which is essential in evaluating the performance of the wireless power transfer system. The NanoVNA is used to perform frequency sweeps and provide detailed measurements on parameters such as impedance, reflection coefficient and power transfer efficiency at different frequencies. By analyzing the NanoVNA output, data can be gathered that reflects how well the system operates in air and under other mediums such as freshwater and seawater. Each step of the setup process is performed with careful calibration and verification to guarantee that the data collected accurately represents the system's behavior. By using this experimental setup, the performance of the capacitive wireless power transfer system can be thoroughly analyzed and compared across different mediums providing insights into its efficiency and feasibility for real-world applications.

3.7.3 Experimental setup in Air

The experimental setup in Figure 3.16 shows the inductor coils connected in the circuit with the necessary wiring and probes attached to the NanoVNA.

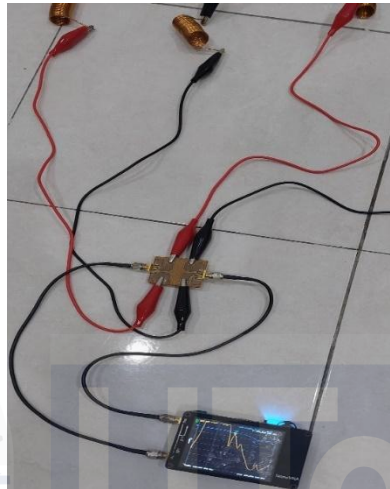


Figure 3.16 The setup connection for NanoVNA in air

The experimental setup in Figure 3.17 shows for circuit conducted in air to test the performance of the shielded CPT system. The circuit consists of various components including capacitors, inductors and connectors that arranged according to the designed schematic. The connections are made using standard electrical cables with alligator clips to ensure secure and stable contacts between the components.

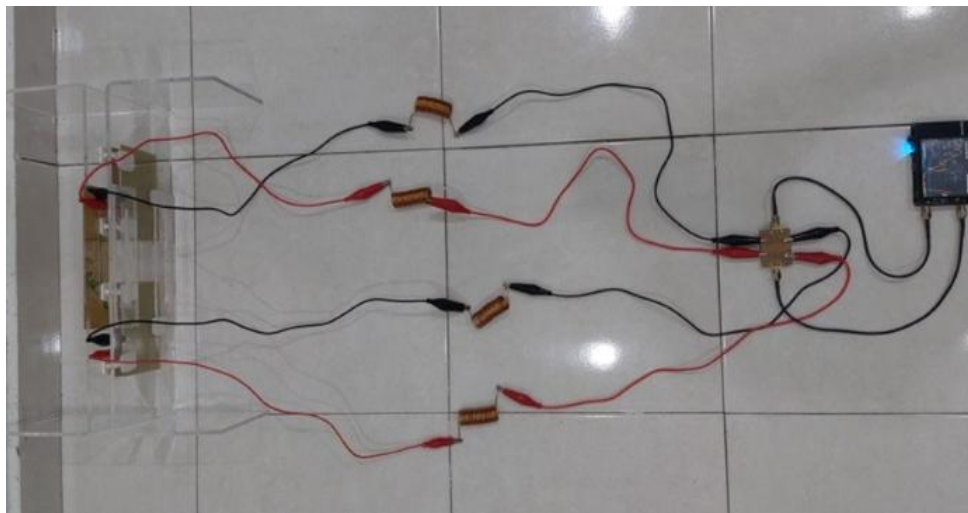


Figure 3.17 The setup connection circuit in air

3.7.4 Experimental setup in Freshwater

The experiment was conducted using a parallel plate setup submerged in freshwater as shown in Figure 3.18. The parallel plates were securely positioned inside a water tank to ensure stability and accurate measurements. Electrical wires were connected to the plates, allowing a controlled voltage to be applied across them. The water level in the tank was maintained at a consistent height of 6 cm as indicated in Figure 3.19. A ruler was placed vertically to ensure precise measurement of the water height.

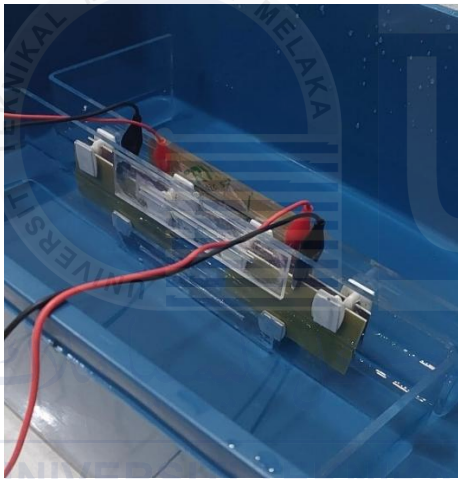


Figure 3.18 The condition of parallel plate in freshwater



Figure 3.19 The water level with height of 6cm

In Figure 3.20 displays the experimental setup where the circuit is immersed in freshwater. The parallel plate system is carefully submerged in a water tank with a maintained water level of 6 cm. Electrical connections are made using insulated cables to prevent short circuits and the plates are securely positioned to ensure consistent spacing and alignment throughout the experiment

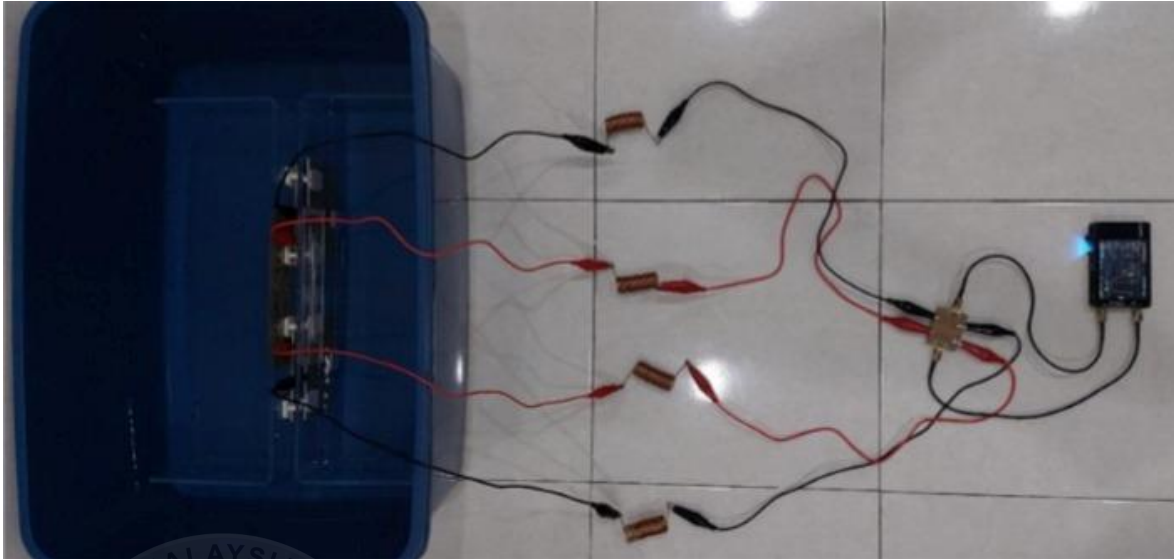


Figure 3.20 The setup connection circuit in freshwater

3.7.5 Experimental setup in Seawater

The experimental setup shown in Figure 3.21 illustrates the condition of the parallel plate system submerged in seawater. The plates are carefully positioned in a water tank filled with seawater ensuring consistent spacing and alignment for accurate measurements while in Figure 3.22 displays the connection of the NanoVNA device which is used for analyzing the circuit's performance in seawater. The NanoVNA is connected to the parallel plates via standard electrical cables allowing impedance and frequency response measurements to be accurately recorded.



Figure 3.21 The condition of parallel plate in seawater



Figure 3.22 The setup connection of NanoVNA for seawater

The complete circuit setup in seawater shown in Figure 3.23, where all electrical components including capacitor plate, inductors and connectors are securely arranged and connected using insulated cables to prevent short circuits. The circuit connections are carefully made to ensure stable contact and the system is monitored throughout the experiment.

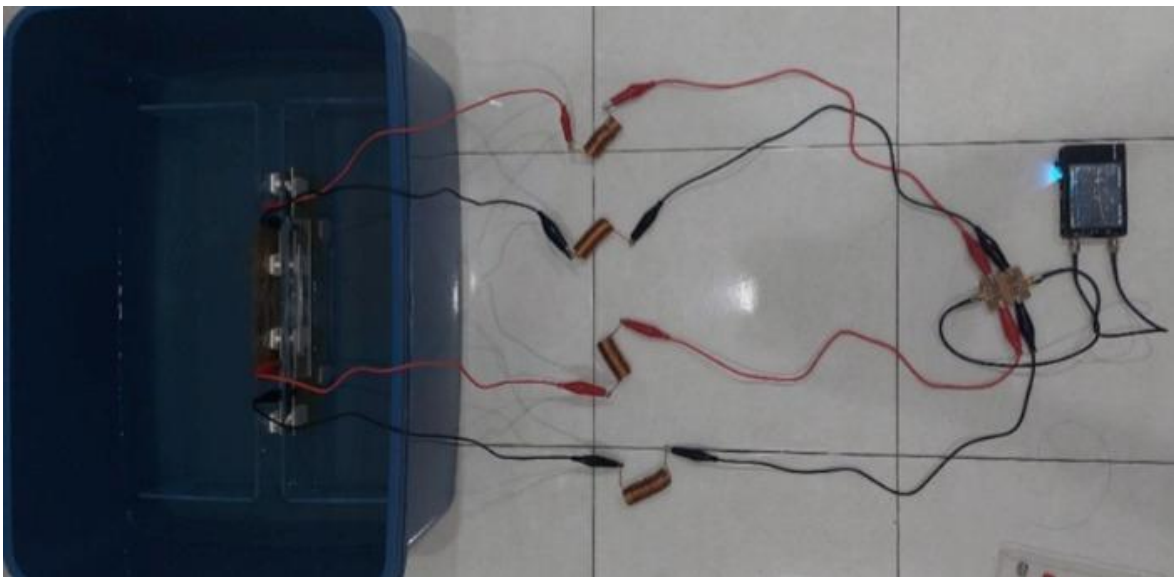


Figure 3.23 The setup connection circuit in seawater

The experimental setup is structured to align closely with the LTspice circuit model to ensure consistency between simulated and real-world conditions. By comparing the experimental results with the simulated data, the accuracy of the theoretical models is validated and the system's feasibility for underwater wireless power transfer is thoroughly assessed. This approach connect between simulation and practical implementation to ensuring a comprehensive evaluation of the WPT system.

3.7.6 NanoVNA saver

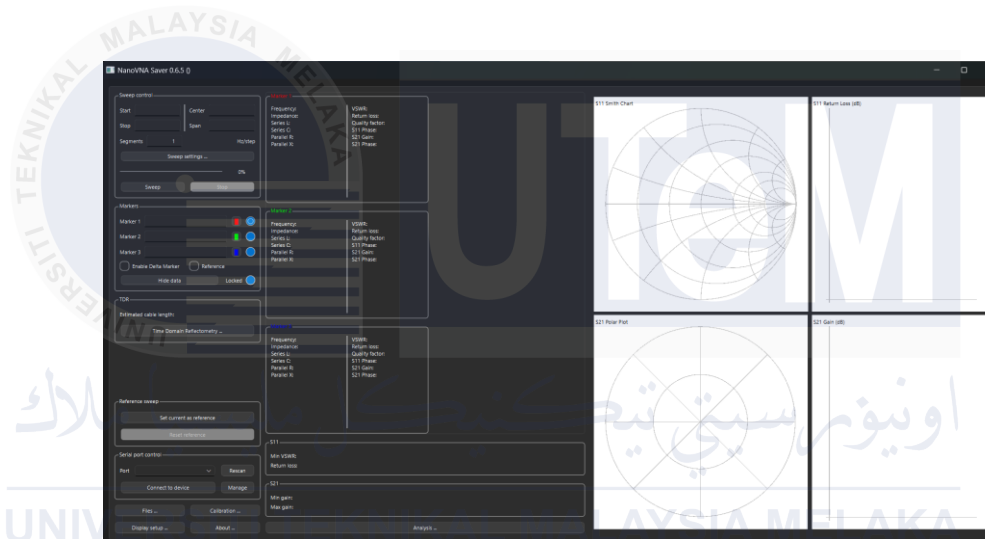


Figure 3.24 NanoVNA saver

NanoVNA Saver as shown in Figure 3.24 is a powerful software tool used in this project to enhance the analysis and visualization of data captured from the NanoVNA. After the NanoVNA captures a waveform during real-time experiments, the data is transferred to a computer via USB and processed using NanoVNA Saver. This software enables the extraction and detailed examination of key parameters such as log magnitude (logmag) and standing wave ratio (SWR), which are essential for evaluating the performance of capacitive configurations under different conditions. One of the significant advantages of NanoVNA Saver is its ability to capture and display data points with greater clarity, making it easier to identify trends and analyze the performance of the system. It

allows for the recording and visualization of up to 101 data points captured during real-time experiments offering a more precise and detailed view compared to the NanoVNA display alone. This enhanced clarity is invaluable for assessing the behavior of the capacitive configurations 2-plate and 4-plate setups and optimizing their design for improved power transfer efficiency. By using NanoVNA Saver, the project benefits from more accurate data analysis, streamlined data management and a deeper understanding of the experimental results.

3.7.7 NanoVNA vector network analyzer

The NanoVNA (Nano Vector Network Analyzer) is a compact and versatile tool that plays a crucial role in this project by enabling real-time analysis of the electrical properties of the capacitive configurations being studied. It is particularly useful for measuring impedance, reflection coefficients and transmission parameters of circuit components across a wide frequency range. In this project, the NanoVNA is utilized to evaluate the performance of capacitive configurations 2-plate and 4-plate setups under various conditions including their behavior in air, freshwater, and seawater. By providing accurate and real-time data, it facilitates the assessment of critical parameters such as resonance frequencies, capacitance and power transfer efficiency. This data is essential for validating the theoretical models and MATLAB simulations, ensuring consistency between predicted and actual behavior. Furthermore, the portability and user-friendly interface of the NanoVNA make it an ideal tool for conducting experiments in different environments allowing for efficient testing, fine-tuning of configurations and optimization of the capacitive wireless power transfer system. Its real-time feedback accelerates the iterative process of design, experimentation and improvement in contributing significantly to the success of the project.

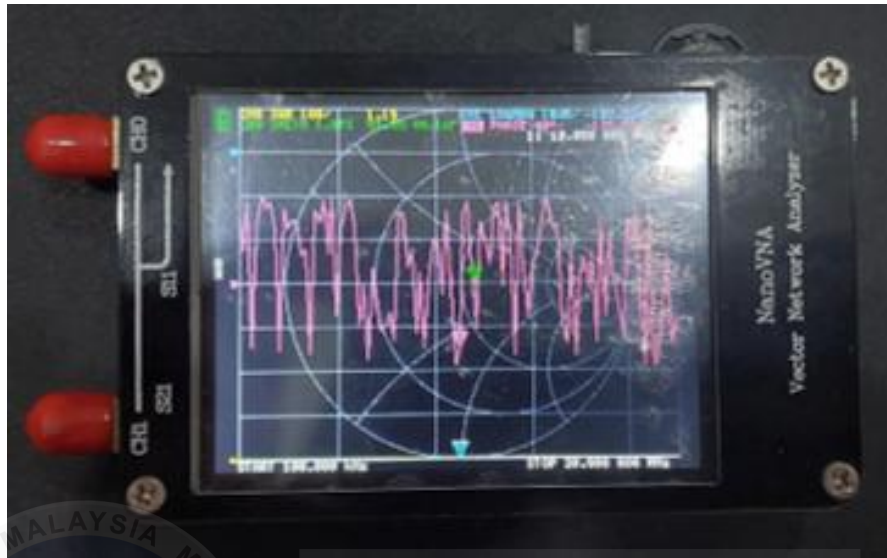


Figure 3.25 NanoVNA vector network analyzer



Figure 3.26 The NanoVNA vector network analyzer with its calibration standards for short, open and thru is used for accurate measurements.



3.8 Gantt Chart of the project

The Gantt chart ensures that the project stays on track by accurately showing the progress of the project schedule in terms of tasks and weeks. When time management is planned, it is more beneficial and efficient.

Table 3.8 The tasks or activities and duration to completed BDP 1

	WEEK						DATE						
	1	2	3	4	5	6	7	8	9	10	11	12	13
Use Mendeley													
Paper/journal download													
Problem statement													
Objective													
Abstract													
Scope													
Introduction													
Methodology													
Chapter 1 -obj, prob,													
Chapter 2- literature review													
Chapter 3 - methodology													
Chapter 4 -result													
Chapter 5 -conclusion													
hardware/simulation													
Presentation													
Presentation Progress													
Draft Report 1													
Draft report 2													
Turn it in													
Report submission to panel													
Slide Submission to SV													

Table 3.9 The tasks or activities and duration to completed BDP 2

	WEEK						DATE						
	1	2	3	4	5	6	7	8	9	10	11	12	13
Buy component/equipment		■					■						
Decide parameter		■					■						
Calculation for k_p in MATLAB		■					■						
Calculation for k_Q and its frequency		■					■						
Calculation for n_{max}			■				■						
Plot graph MATLAB			■				■						
Simulation circuit LTspice				■			■						
Simulation circuit with other parameter				■			■						
Hardware development			■	■			■						
Nanosaver and NanoVNA analyzer dsts				■	■	■	■	■					
Collect data for three mediums							■	■	■				
Finalized collected data							■			■			
Update Chapter 3 – methodology							■		■	■	■	■	
Update Chapter 4 -result							■		■	■	■	■	
Update Chapter 5 -conclusion				■			■	■					
Presentation Progress							■			■			
Report and poster discussion							■			■			
Finalized report and Turnitin							■				■		
Report submission to SV							■					■	
Report submission to panel							■						■
PSM2 presentation							■						■

3.9 Summary

The project begins with a well explained flowchart of overall system for studying the relationship between capacitance, plate area, and distance in a single-plate capacitor setup across different mediums in air, freshwater and seawater. Then followed with block system of the project system includes defining parameters, using theoretical formulas to calculate capacitance and employing simulation tools like MATLAB. Applications used such as MATLAB for modeling the system and calculating capacitance values under various conditions. LTspice is then used to simulate the circuit, comparing the results with MATLAB to ensure accuracy. The theoretical calculations, simulations and experimental conducted help in clarifying the usage and effectiveness of the CPT structure in these three different medium.

CHAPTER 4

RESULTS AND DISCUSSIONS

4.1 Introduction

The results and discussion presented in this section focus on the evaluation and analysis of capacitive power transfer CPT in air, freshwater, and seawater. The performance characteristics of the coupler have been performed through theoretical calculation, simulation and experimental investigation. The efficiency and effectiveness of CPT varies across different mediums as proven in thorough simulations and calculation.

4.2 Result simulation using MATLAB

To validate the calculation of capacitance in air, freshwater and seawater, simulations are performed in MATLAB. These simulation data were more precise than were compared with theoretical calculation. The comparison proved consistent results with the theoretical capacitance values for each medium.

Distance (mm)	Capacitance (Air), erair =1.0006	Capacitance (freshwater), erfw =78.5	Capacitance (seawater), ersea =81.5
1	$C = \frac{(100) (8.854e-12) (1.0006)}{(1.0)}$ = 8.86e-10	$C = \frac{(100) (8.854e-12) (78.5)}{(1.0)}$ = 6.95e-08	$C = \frac{(100) (8.854e-12) (81.5)}{(1.0)}$ =7.22e-08
5	$C = \frac{(100) (8.854e-12) (1.0006)}{(5.0)}$ = 1.77e-10	$C = \frac{(100) (8.854e-12) (78.5)}{(5.0)}$ =1.39e-08	$C = \frac{(100) (8.854e-12) (81.5)}{(5.0)}$ =1.44e-08
10	$C = \frac{(100) (8.854e-12) (1.0006)}{(10.0)}$ = 8.86e-11	$C = \frac{(100) (8.854e-12) (78.5)}{(10.0)}$ =6.95e-09	$C = \frac{(100) (8.854e-12) (81.5)}{(10.0)}$ =7.22e-09
15	$C = \frac{(100) (8.854e-12) (1.0006)}{(15.0)}$ = 5.91e-11	$C = \frac{(100) (8.854e-12) (78.5)}{(15.0)}$ =4.63e-09	$C = \frac{(100) (8.854e-12) (81.5)}{(15.0)}$ =4.81e-09
20	$C = \frac{(100) (8.854e-12) (1.0006)}{(20.0)}$ =4.43e-11	$C = \frac{(100) (8.854e-12) (78.5)}{(20.0)}$ =3.48e-09	$C = \frac{(100) (8.854e-12) (81.5)}{(20.0)}$ =3.61e-09
30	$C = \frac{(100) (8.854e-12) (1.0006)}{(30.0)}$ =2.95e-11	$C = \frac{(100) (8.854e-12) (78.5)}{(30.0)}$ =2.32e-09	$C = \frac{(100) (8.854e-12) (81.5)}{(30.0)}$ =2.41e-09
50	$C = \frac{(100) (8.854e-12) (1.0006)}{(50.0)}$ =1.77e-11	$C = \frac{(100) (8.854e-12) (78.5)}{(50.0)}$ =1.39e-09	$C = \frac{(100) (8.854e-12) (81.5)}{(50.0)}$ =1.44e-09

4.2.1 Result calculation of capacitance versus distance

The results observed from the MATLAB simulation based on Figure 4.1 show the capacitance values for air, freshwater, and seawater across varying distances.

```

Command Window
Air Capacitance (F)
Distance (m)    1.00    5.00    10.00    15.00    20.00    30.00    50.00
Capacitance 8.86e-10    1.77e-10    8.86e-11    5.91e-11    4.43e-11    2.95e-11    1.77e-11

Freshwater Capacitance (F)
Distance (m)    1.00    5.00    10.00    15.00    20.00    30.00    50.00
Capacitance 6.95e-08    1.39e-08    6.95e-09    4.63e-09    3.48e-09    2.32e-09    1.39e-09

Seawater Capacitance (F)
Distance (m)    1.00    5.00    10.00    15.00    20.00    30.00    50.00
Capacitance 7.22e-08    1.44e-08    7.22e-09    4.81e-09    3.61e-09    2.41e-09    1.44e-09
fx >>

```

Figure 4.1 Tabulated data from MATLAB simulation

The relationship between capacitance and distance in air can be seen in Figure 4.2, which illustrates a dramatic drop in capacitance with increasing distance. This inversely relationship shows how drastically the capacitance decreases with even a slight increase in distance. The graph shows obvious the sensitivity capacitance is to slight differences in distance in the air medium.

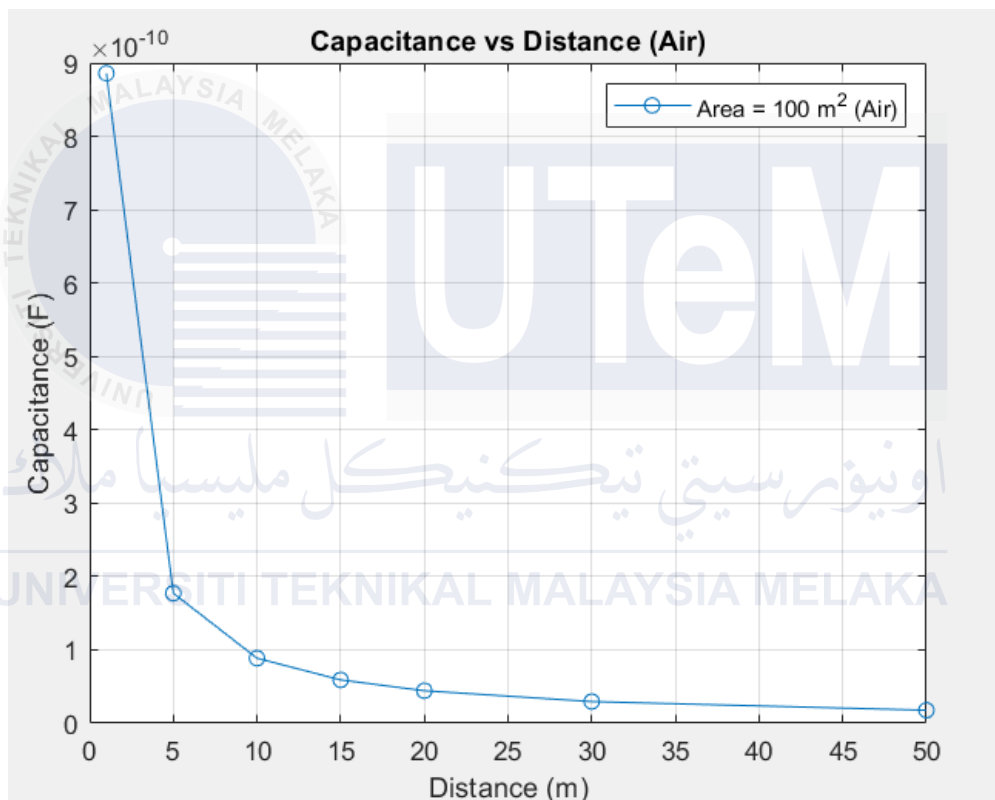


Figure 4.2 The graph of capacitance vs. distance in the air, displaying a sharp decrease in capacitance as distance increase.

The relationship between capacitance and distance in freshwater can be seen in Figure 4.3, where its decrease is more steadily than in air. It means that in freshwater, capacitance is more resistant to changes in distance. The graph illustrates how different mediums affect capacitance sensitivity.

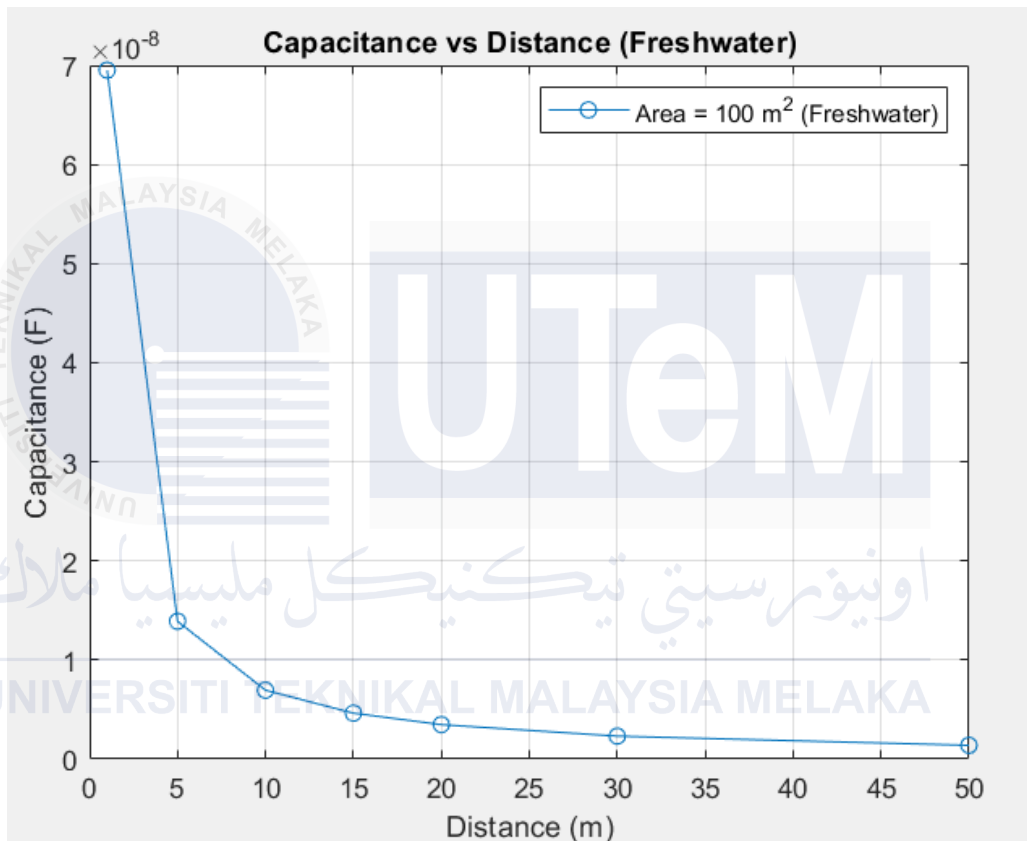


Figure 4.3 Capacitance vs. distance graph in freshwater, illustrating a more gradual drop than in air.

The capacitance vs distance in seawater is displayed in Figure 4.4 , the trend is similar to that observed in freshwater, but the values are slightly larger. This indicates that seawater maintains a larger capacitance at related distances even when it declines gradually like freshwater. The graph highlights how capacitance is affected by seawater increased conductivity.

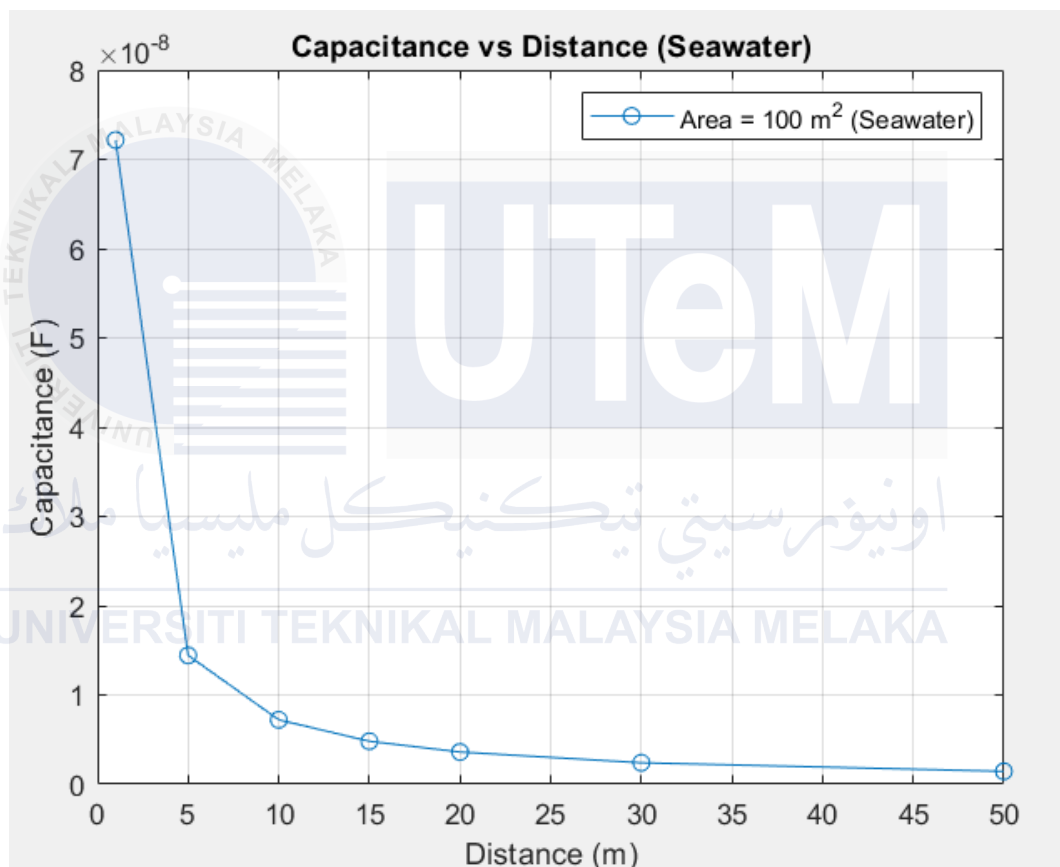


Figure 4.4 Capacitance vs. distance graph in seawater, similar in trend to freshwater but with slightly higher values

Figure 4.5 presents a combined graph of capacitance vs distance for air, freshwater, and seawater. The graph highlights the steep decline in capacitance with distance in air, contrasted by the more gradual decreases in freshwater and seawater, with seawater showing the highest capacitance values. This comprehensive comparison emphasizes the varying impacts of different media on capacitance.

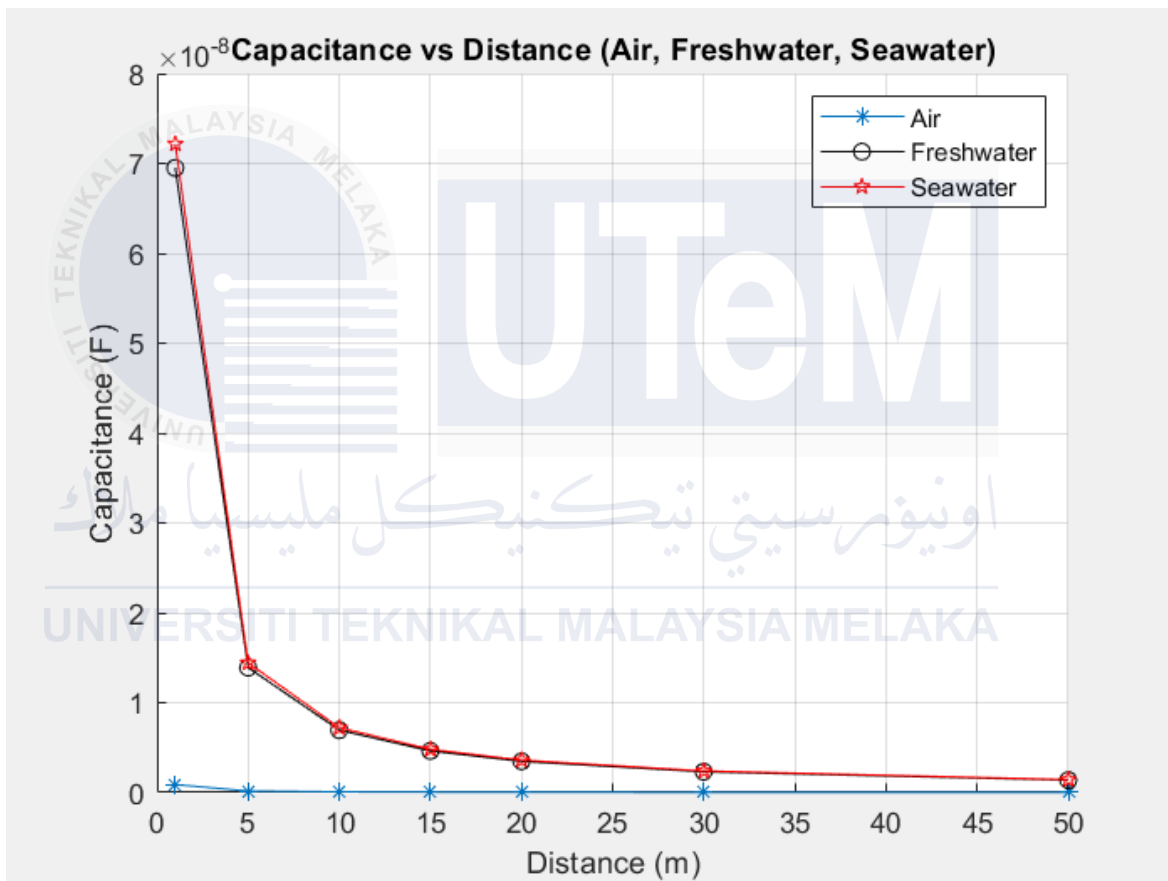


Figure 4.5 The graph of capacitance vs distance combines the data in air, freshwater and seawater

4.2.2 Result calculation of η_{max} (maximum power transfer efficiency) VS frequency

The results obtained from the MATLAB simulation, as shown in Figure 4.6 illustrate the calculation of maximum power transfer efficiency in different frequency in air.

Frequency (MHz)	Q_{air}	k_p	kQ_{air}	η_{max} (Air, %)
0 MHz	1.52	0.56	0.00	0.00
20 MHz	1.52	1.04	0.00	0.27
40 MHz	1.52	0.71	0.00	0.52
60 MHz	1.52	0.21	0.00	0.10
80 MHz	1.52	0.12	0.00	0.06
100 MHz	1.52	0.10	0.00	0.06
120 MHz	1.52	0.16	0.00	0.24
140 MHz	1.52	0.07	0.00	0.07
160 MHz	1.52	0.01	0.00	0.00
180 MHz	1.52	0.00	0.00	0.00
200 MHz	1.52	0.00	0.00	0.00
220 MHz	1.52	0.00	0.00	0.00
240 MHz	1.52	0.00	0.00	0.00
260 MHz	1.52	0.00	0.00	0.00
280 MHz	1.52	0.00	0.00	0.00
300 MHz	1.52	0.00	0.00	0.00

Figure 4.6 Tabulated data from MATLAB simulation for air medium

Figure 4.7 presents a combined graph of maximum power transfer efficiency versus frequency in air medium. The efficiency of (η_{max}) starts at 0% at 0 MHz and increases sharply reaching a peak of 0.52% at 40 MHz. The efficiency continues to fluctuate with another local maximum of 0.24% at 120 MHz. However, at 160 MHz the efficiency drops rapidly. This indicates that the air medium initially shows some improvement in efficiency at lower frequencies, it suffers a significant decline as the frequency increases.

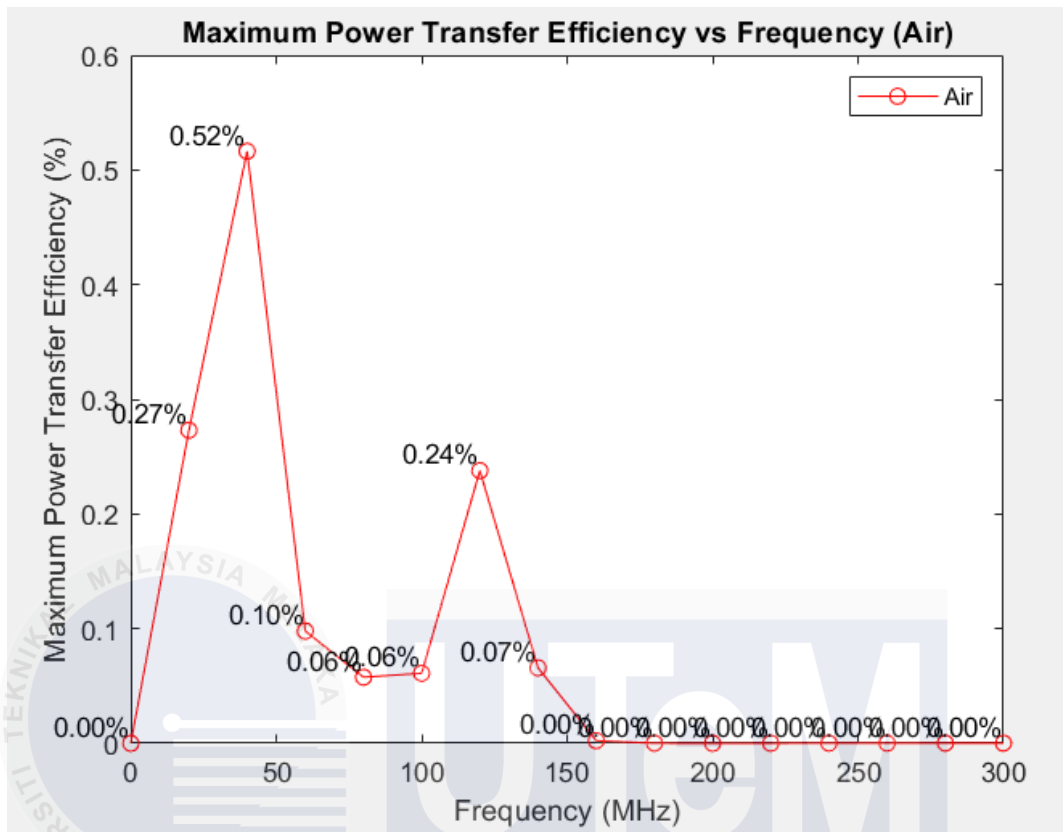


Figure 4.7 The graph maximum power transfer efficiency versus frequency in air medium

The results obtained from the MATLAB simulation, as shown in Figure 4.8 illustrate the calculation of maximum power transfer efficiency in different frequency in freshwater.

Freshwater Medium				
Frequency (MHz)	Q _{fw}	k _p	kQ _{fw}	n _{max} (Freshwater, %)
0 MHz	119.86	0.56	0.21	0.00
20 MHz	119.86	1.04	0.21	78.57
40 MHz	119.86	0.71	0.21	83.93
60 MHz	119.86	0.21	0.21	66.92
80 MHz	119.86	0.12	0.21	59.38
100 MHz	119.86	0.10	0.21	60.24
120 MHz	119.86	0.16	0.21	77.23
140 MHz	119.86	0.07	0.21	61.35
160 MHz	119.86	0.01	0.21	11.41
180 MHz	119.86	0.00	0.21	0.69
200 MHz	119.86	0.00	0.21	0.05
220 MHz	119.86	0.00	0.21	0.45
240 MHz	119.86	0.00	0.21	0.77
260 MHz	119.86	0.00	0.21	0.95
280 MHz	119.86	0.00	0.21	1.03
300 MHz	119.86	0.00	0.21	1.05

Figure 4.8 Tabulated data from MATLAB simulation for freshwater medium

Figure 4.9 presents a combined graph of maximum power transfer efficiency versus frequency in freshwater medium, the efficiency (η_{\max}) starts at 0% at 0 MHz and increases sharply reaching a peak of 83.93% at 40 MHz. After this peak, the efficiency fluctuates, with a local maximum of 77.23% around 120 MHz. However, at 160 MHz, the efficiency decreases significantly, stabilizing at around 0.69% and lower at higher frequencies. This trend indicates that freshwater maintains higher efficiency at low-to-mid frequencies but experiences a sharp decline at higher frequencies due to increased dielectric losses and reduced coupling effectiveness.

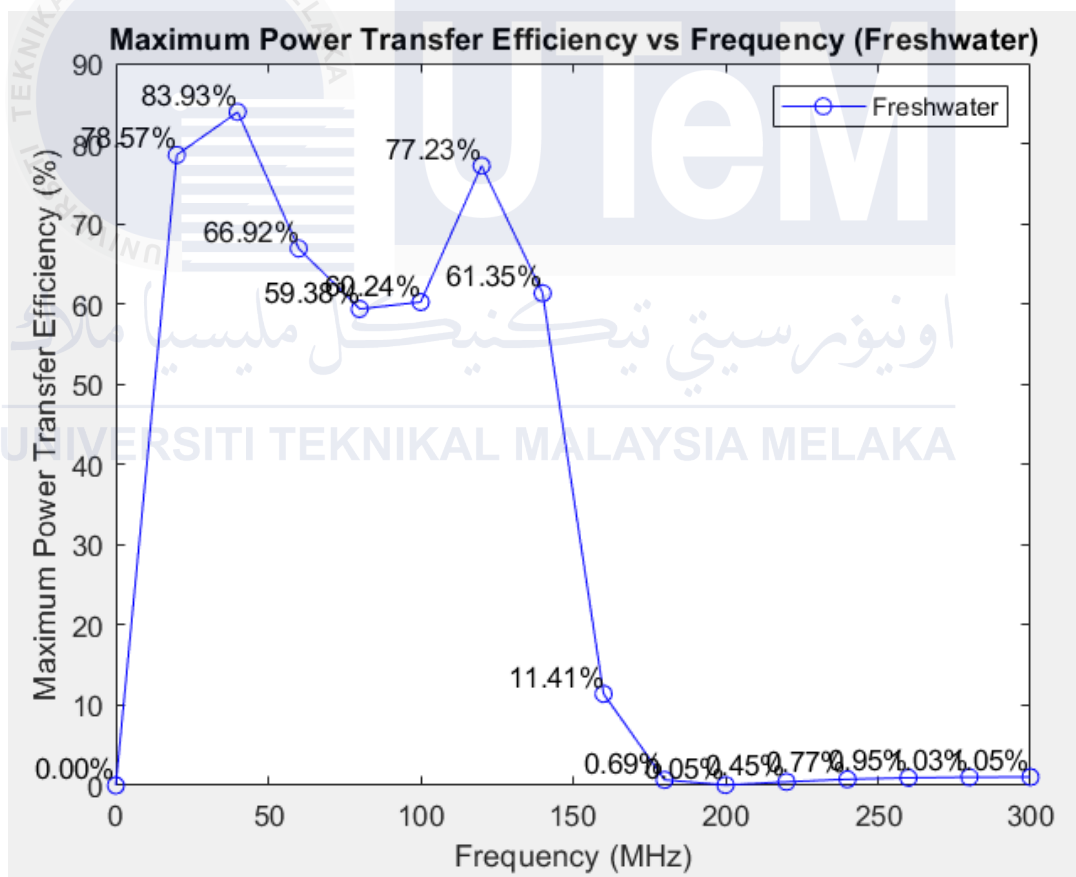


Figure 4.9 The graph maximum power transfer efficiency versus frequency in freshwater medium

The results obtained from the MATLAB simulation, as shown in Figure 4.10 illustrate the calculation of maximum power transfer efficiency in different frequency in seawater.

Seawater Medium Frequency (MHz)	Q _{sea}	k _p	kQ _{sea}	n _{max} (Seawater, %)
0 MHz	123.66	0.56	0.21	0.00
20 MHz	123.66	1.04	0.21	79.15
40 MHz	123.66	0.71	0.21	84.38
60 MHz	123.66	0.21	0.21	67.74
80 MHz	123.66	0.12	0.21	60.32
100 MHz	123.66	0.10	0.21	61.17
120 MHz	123.66	0.16	0.21	77.84
140 MHz	123.66	0.07	0.21	62.26
160 MHz	123.66	0.01	0.21	11.99
180 MHz	123.66	0.00	0.21	0.74
200 MHz	123.66	0.00	0.21	0.05
220 MHz	123.66	0.00	0.21	0.47
240 MHz	123.66	0.00	0.21	0.82
260 MHz	123.66	0.00	0.21	1.01
280 MHz	123.66	0.00	0.21	1.10
300 MHz	123.66	0.00	0.21	1.11

Figure 4.10 Tabulated data from MATLAB simulation for seawater medium

Figure 4.11 presents a combined graph of maximum power transfer efficiency versus frequency in seawater medium, the efficiency follows a similar pattern starting at 0% at 0 MHz and rising sharply to peak at 84.38% at 40 MHz. The overall pattern mirrors that of freshwater with a peak of 77.84% around 120 MHz. After 160 MHz, the efficiency drops rapidly but remains slightly higher than freshwater at very high frequencies. This suggests that seawater due to its increased conductivity and dielectric properties retains a better power transfer efficiency compared to freshwater especially at lower frequencies. At high frequencies both mediums experience a significant drop in efficiency but seawater continues to perform slightly better.

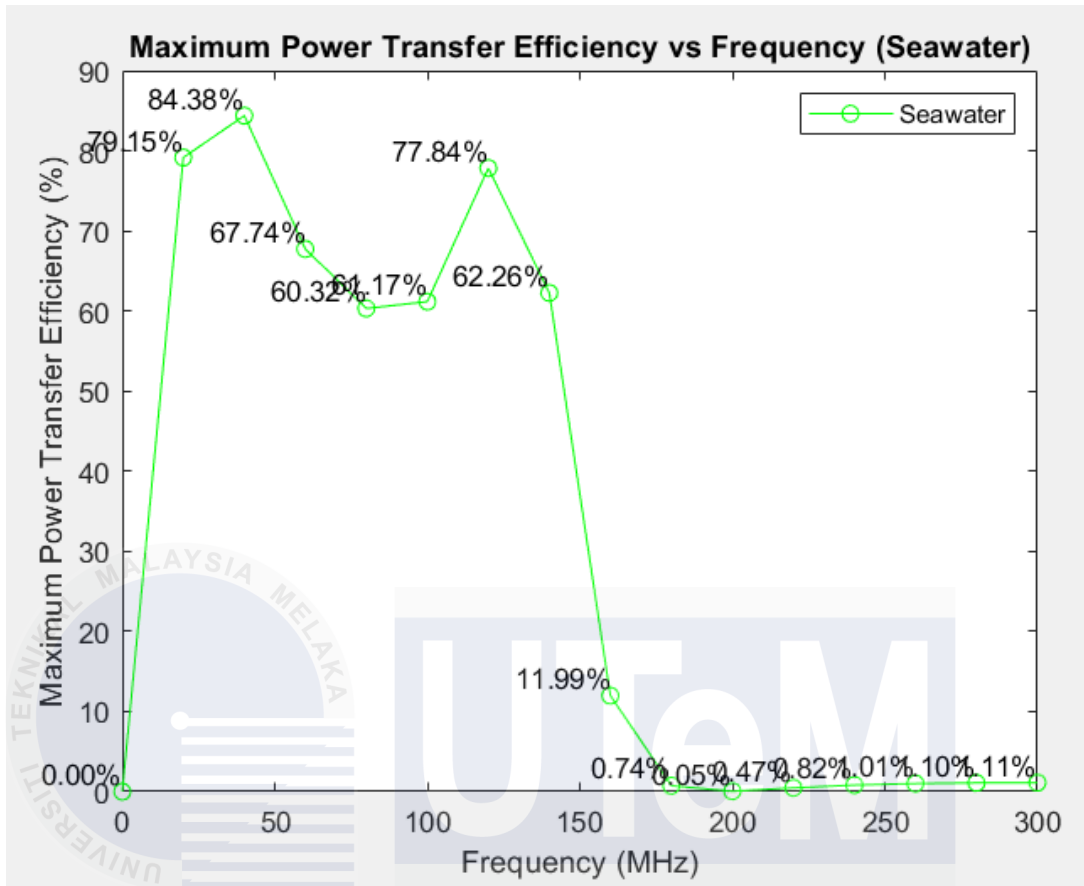


Figure 4.11 The graph maximum power transfer efficiency versus frequency in seawater medium

The results obtained from the MATLAB simulation, as shown in Figure 4.12 illustrate the calculation of maximum power transfer efficiency in different frequency in air, freshwater and seawater.

kQair	kQfw	kQsea	nmax (Air, %)	nmax (Freshwater, %)	nmax (Seawater, %)
0.56	0.00	0.00	0.00	0.00	0.00
1.04	0.10	8.27	8.54	0.27	78.57
0.71	0.14	11.40	11.77	0.52	83.93
0.21	0.06	4.95	5.10	0.10	66.92
0.12	0.05	3.79	3.91	0.06	59.38
0.10	0.05	3.90	4.03	0.06	60.24
0.16	0.10	7.72	7.96	0.24	77.23
0.07	0.05	4.05	4.18	0.07	61.35
0.01	0.01	0.76	0.79	0.00	11.41
0.00	0.00	0.17	0.17	0.00	0.69
0.00	0.00	0.04	0.04	0.00	0.05
0.00	0.00	0.13	0.14	0.00	0.45
0.00	0.00	0.18	0.18	0.00	0.77
0.00	0.00	0.20	0.20	0.00	0.95
0.00	0.00	0.21	0.21	0.00	1.03
0.00	0.00	0.21	0.21	0.00	1.05

Figure 4.12 Tabulated data from MATLAB simulation for air ,freshwater and seawater

Figure 4.13 shows the efficiency trends observed in the air, freshwater and seawater mediums follow a similar pattern with efficiency peaking at lower frequencies and declining at higher frequencies. In air, the efficiency starts at 0% and rises to a peak of at 40 MHz, followed by a sharp drop beyond 160 MHz, showing limited power transfer capabilities compared to the other two mediums. In freshwater, efficiency peaks at 83.93% at 40 MHz and declines at higher frequencies with the lowest efficiency around 0.69% at very high frequencies. Seawater demonstrates the highest efficiency peaking at 84.38% at 40 MHz and maintaining slightly better efficiency than freshwater, particularly at lower and mid frequencies. At high frequencies, both freshwater and seawater experience significant efficiency losses but seawater still performs better due to its higher conductivity and better dielectric properties, making it more effective for power transfer in comparison to both air and freshwater under high-frequency conditions.

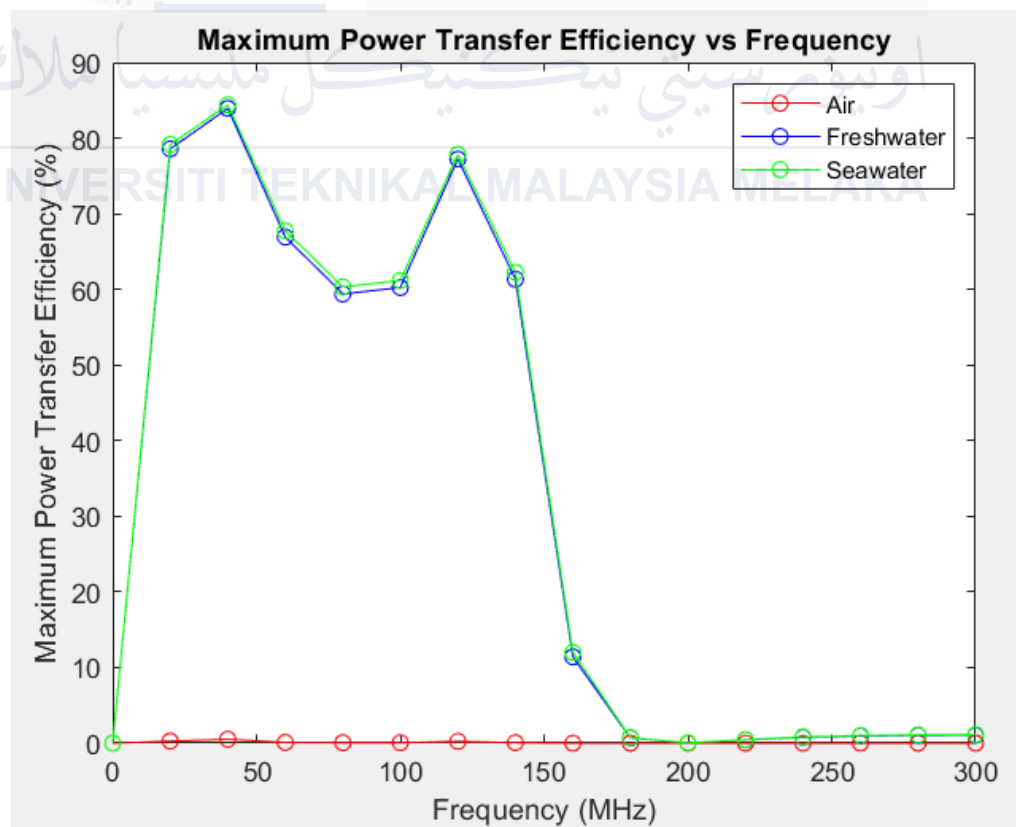


Figure 4.13 The combined graph of maximum power transfer efficiency versus frequency in air, freshwater and seawater

4.2.3 Result calculation of k_pQ VS frequency

The results obtained from the MATLAB simulation as shown in Figure 4.14, illustrate the calculation of k_pQ the ability to transfer power efficiently in different frequency in air, freshwater, and seawater .

Frequency (MHz)	Q_{air}	Q_{fw}	Q_{sea}	k_p	kQ_{air}	kQ_{fw}	kQ_{sea}
0 MHz	0.00	0.00	0.00	0.56	0.00	0.00	0.00
20 MHz	0.10	7.99	8.24	1.04	0.10	8.27	
40 MHz	0.20	15.98	16.49	0.71	0.14	11.40	
60 MHz	0.30	23.97	24.73	0.21	0.06	4.95	
80 MHz	0.40	31.96	32.97	0.12	0.05	3.79	
100 MHz	0.51	39.95	41.22	0.10	0.05	3.90	
120 MHz	0.61	47.95	49.46	0.16	0.10	7.72	
140 MHz	0.71	55.94	57.71	0.07	0.05	4.05	
160 MHz	0.81	63.93	65.95	0.01	0.01	0.76	
180 MHz	0.91	71.92	74.19	0.00	0.00	0.17	
200 MHz	1.01	79.91	82.44	0.00	0.00	0.04	
220 MHz	1.11	87.90	90.68	0.00	0.00	0.13	
240 MHz	1.21	95.89	98.92	0.00	0.00	0.18	
260 MHz	1.32	103.88	107.17	0.00	0.00	0.20	
280 MHz	1.42	111.87	115.41	0.00	0.00	0.21	
300 MHz	1.52	119.86	123.66	0.00	0.00	0.21	

Figure 4.14 Tabulated data from MATLAB simulation

Figure 4.15 presents a combined graph of kQ versus frequency in the air medium, the behavior of the kQ values shows weak coupling efficiency across the frequency range. At low frequencies (0–50 MHz), the kQ starts at zero and rises sharply, peaking at 0.14 at approximately 40 MHz. After this peak, the value declines to 0.10 at 50 MHz. This indicates that air with its minimal dielectric properties, allows only a slight improvement in coupling efficiency at these lower frequencies. At mid frequencies (50–150 MHz), a secondary peak occurs at 120 MHz, with a value of 0.10 followed by a decline to 0.05 at 150 MHz. These kQ values remain moderate compared to the peak at 40 MHz, suggesting a modest but still limited improvement in coupling efficiency. However, when it comes to high frequencies (150 MHz), the kQ values drop significantly approaching zero beyond 200 MHz, reflecting very poor coupling efficiency at higher frequencies. The rapid decline at these higher frequencies is attributed to the poor dielectric properties of air which greatly hinder energy transfer efficiency.

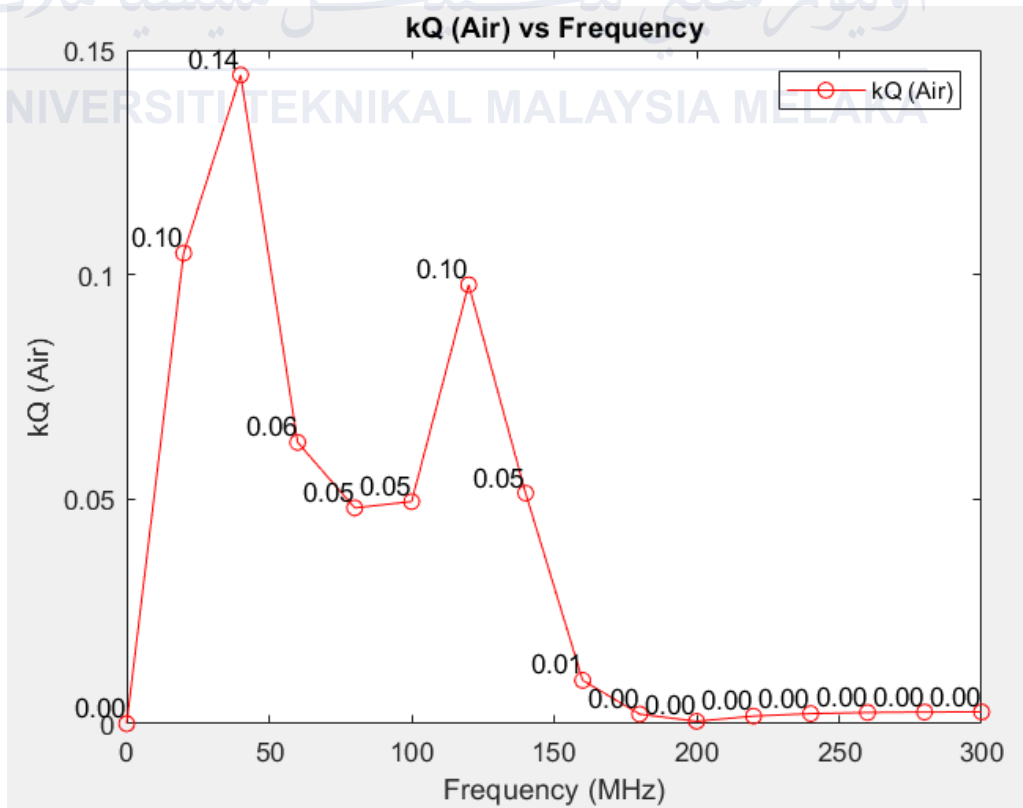


Figure 4.15 The graph of kQ versus frequency in air medium

Figure 4.16 presents a combined graph of kQ versus frequency in freshwater medium, the kQ parameter which represents the product of the coupling coefficient (k) and the quality factor (Q), shows a clear trend across frequencies. At low frequencies (0–40 MHz), kQ rises sharply peaking at 11.40 around 40 MHz, indicating efficient power transfer. In the mid-frequency range (40–160 MHz), kQ fluctuates with a notable secondary peak at 7.72 around 120 MHz and smaller peaks between these values. However, beyond 160 MHz the kQ values drop significantly and remain near zero at higher frequencies. This pattern suggests that freshwater maintains efficient power transfer at low-to-mid frequencies but dielectric losses at higher frequencies cause a sharp reduction in efficiency.

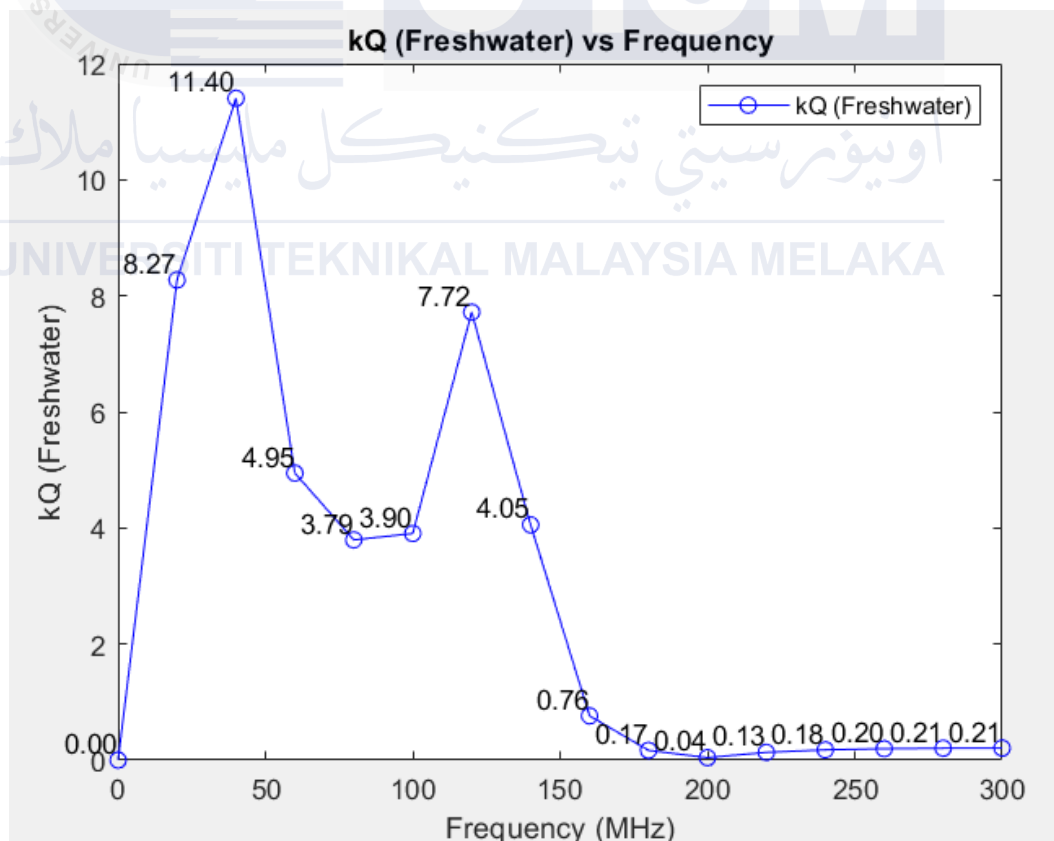


Figure 4.16 The graph of kQ versus frequency in freshwater medium

Figure 4.17 shows a combined graph of kQ versus frequency in the seawater medium, the kQ values follow a similar pattern to freshwater with a few notable differences. The first peak occurs at 11.77 around 40 MHz, slightly higher than in freshwater. In the mid-frequency range (40–160 MHz), seawater displays a peak at 7.96 around 120 MHz, mirroring the pattern seen in freshwater, but with slightly lower values. At higher frequencies (160 MHz), the kQ values decrease sharply stabilizing close to zero. Seawater shows a slightly higher kQ value at low frequencies compared to freshwater, likely due to its increased conductivity and better dielectric properties, although the overall pattern of decline at higher frequencies is similar.

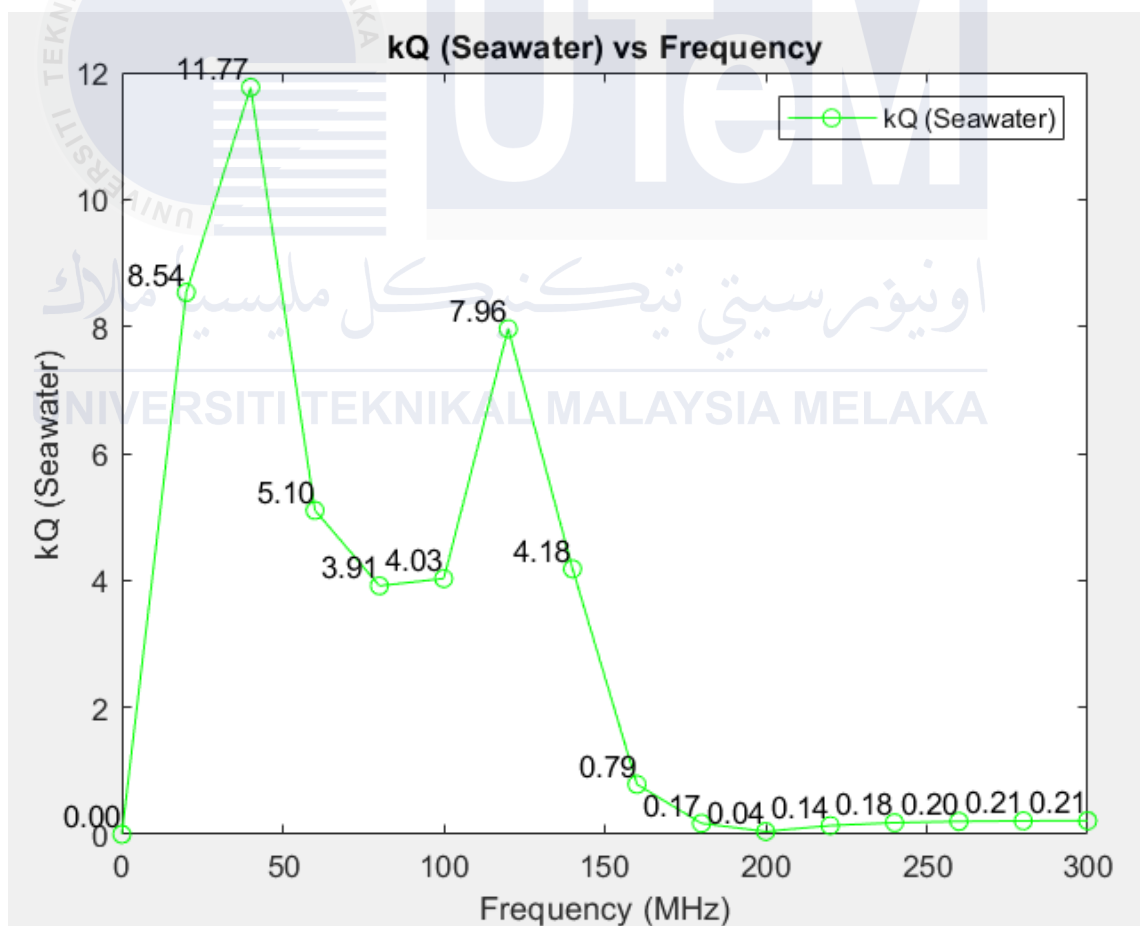


Figure 4.17 The graph of kQ versus frequency in seawater medium

Figure 4.18 shows a combined graph of kQ versus frequency for three mediums: air, freshwater, and seawater. Air shows almost negligible kQ values across all frequencies, indicating poor coupling and minimal power transfer capabilities. Both freshwater and seawater exhibit significant peaks at 40 MHz and 120 MHz, with seawater maintaining slightly higher kQ values throughout the range. At higher frequencies (160 MHz), both freshwater and seawater show sharp drops in kQ , while air remains consistently low. This comparison highlights that air is highly ineffective for wireless power transfer due to its minimal dielectric properties, while freshwater and seawater perform significantly better, with seawater showing slightly superior efficiency due to its enhanced dielectric behavior at lower frequencies.

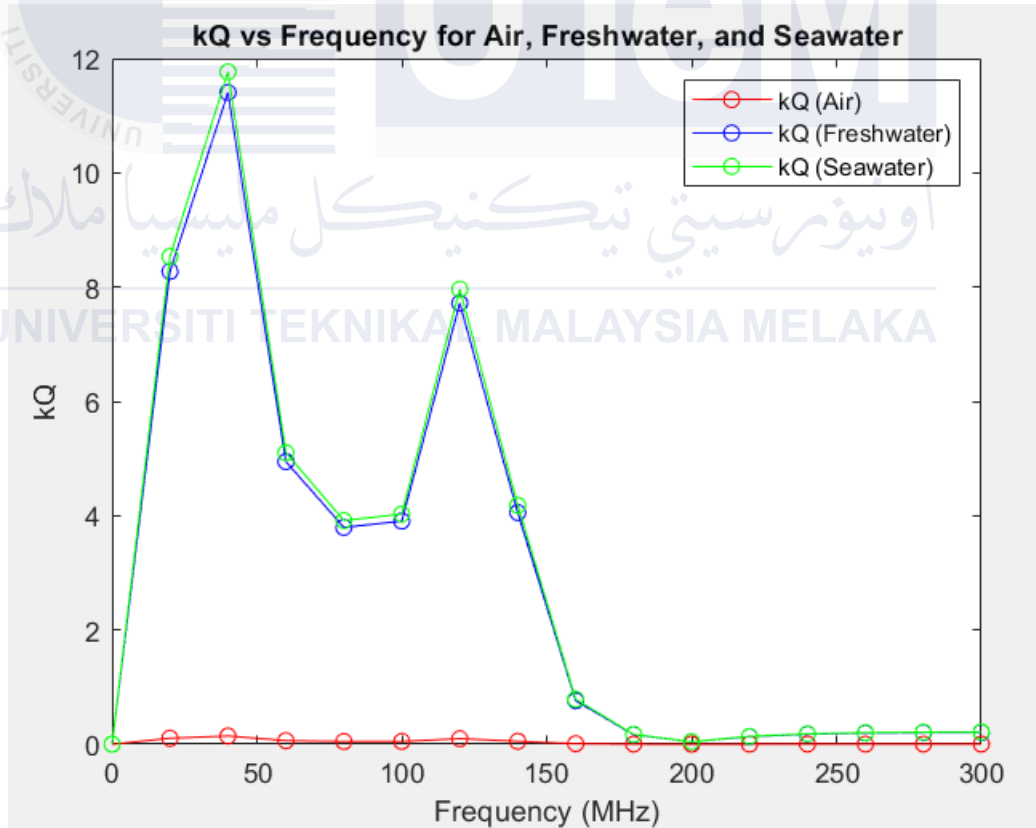


Figure 4.18 The combined graph kQ versus frequency in air, freshwater and seawater

The observed pattern indicates that air is the least effective medium for wireless power transfer compared to freshwater and seawater. Despite showing slight improvements at specific frequencies (40 MHz and 120 MHz), the kQ values in air are consistently lower than those in both liquid mediums. These peaks represent resonant conditions where coupling improves marginally but the overall coupling efficiency remains insufficient for effective wireless power transfer. Furthermore, unlike freshwater and seawater, air has a narrow range of frequencies where kQ efficiency increases with a sharp decline observed at higher frequencies. This trend underscores the limitations of air as its dielectric properties are not conducive to efficient capacitive coupling systems in wireless power transfer (WPT). The air medium shows minimal potential for wireless power transfer, emphasizing the importance of dielectric properties for effective coupling while freshwater and seawater perform significantly better due to their superior conductivity and dielectric behavior, air's limitations make it the least suitable medium for WPT.

4.2.4 Result calculation of frequency

The Figure 4.19 shows the frequencies of f_{k0} , f_{k1} , f_{k2} , f_{k3} , f_{k4} that refers to different operating frequencies for the system. These frequencies can be tuned to optimize energy transfer efficiency, minimize losses and accommodate specific characteristics of the capacitive coupling system.

Frequency Calculations:

$$f_{k1} = 29.614 \text{ MHz}$$

$$f_{k3} = 129.282 \text{ MHz}$$

$$f_{k0} = 194.294 \text{ MHz}$$

$$f_{k2} = 99.495 \text{ MHz}$$

$$f_{k4} = 256.127 \text{ MHz}$$

Figure 4.19 Value result from MATLAB of calculation for frequency

4.2.5 Result calculation of F and K

```
F =  
0.4580  
  
K =  
23.1585  
  
K_approximation =  
4.0492  
  
nmax =  
0.9173
```

Figure 4.20 Value result from MATLAB of calculation

The relationship between F and K lies in how the circuit's reactive and conductive properties influence in the coupling efficiency. F is a parameter derived from the circuit's inductance (L_p), capacitance (C_p), and conductance (G_p, G_s, G_m) at a specific frequency. It represents how these components interact to determine the system's behavior. F represents a measure of how reactive (capacitive or inductive) the system is under certain conditions. As shown in Figure 4.22 the higher values of F indicate a stronger interaction between inductance and capacitance at the given frequency. K, the coupling factor or coupling coefficient, quantifies the efficiency of power transfer or interaction between the primary and secondary components of the circuit. The coupling coefficient, K depends on F and quantifies the efficiency of power transfer between the primary and secondary sides of the circuit. Both F and K are frequency-dependent, meaning their values change as the operating frequency varies. F helps calculate K by summarizing the impact of inductive and capacitive elements, making K a measure of how effectively energy is coupled in the system and its dependence on frequency and conductance parameters.

Frequency_MHz	F
0	2.1804e-08
20	0.028502
40	0.11401
60	0.25652
80	0.45604
100	0.71256
120	1.0261
140	1.3966
160	1.8242
180	2.3087
200	2.8502
220	3.4488
240	4.1043
260	4.8169
280	5.5865
300	6.413

Figure 4.21 Tabulated data from MATLAB simulation of calculation for frequency and F

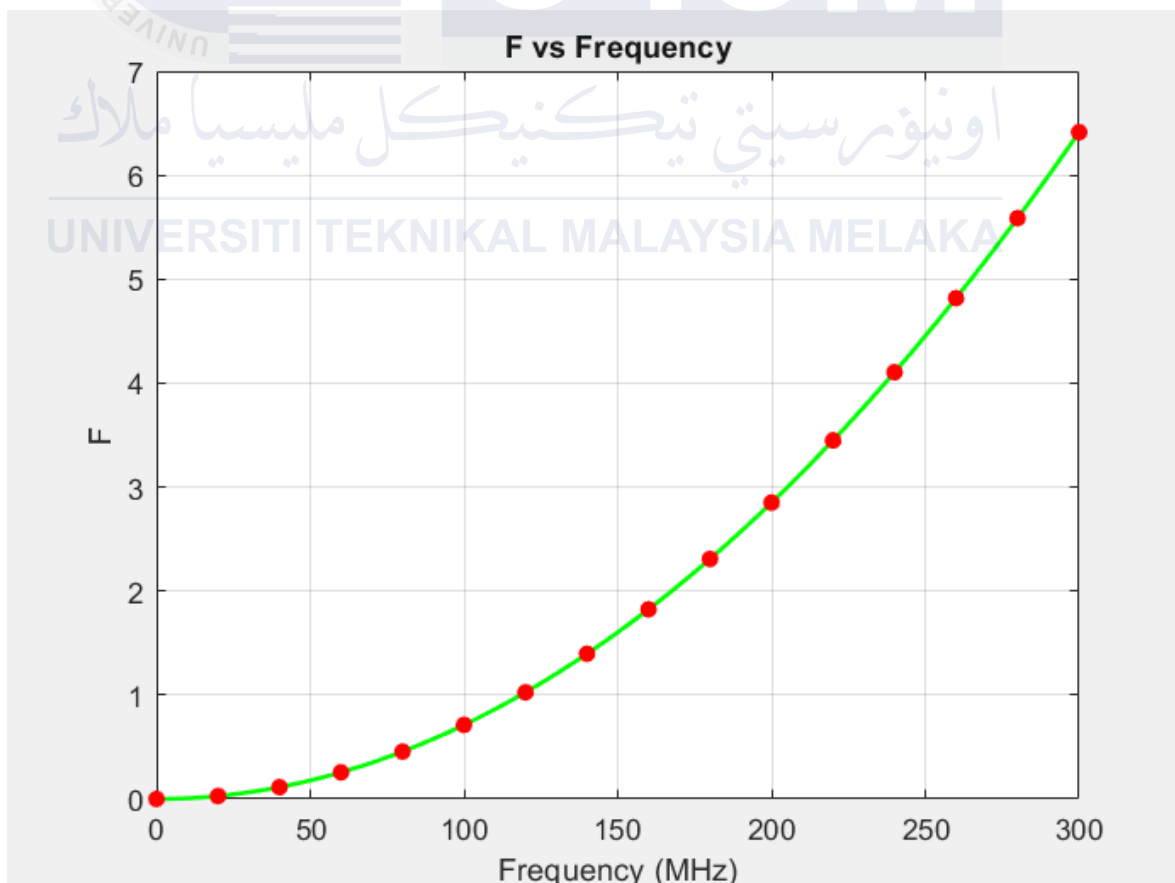


Figure 4.22 The graph of F vs frequency

4.3 Result on simulation using LTspice

The simulation of the wireless power transfer (WPT) system was conducted using LTspice, a widely recognized circuit simulation software to validate theoretical calculations and evaluate the performance of the capacitive coupler under freshwater and seawater conditions across a range of frequencies. The circuit models for both mediums were designed based on equivalent electrical parameters including parasitic inductance (L_m), mutual capacitance (C_m), self-capacitance (C_s), feeding line inductance (L_R), and parasitic capacitance (C_R). These parameters were carefully adjusted to reflect the dielectric properties of freshwater and seawater, accurately representing their permittivity and conductivity values. The simulation covered a frequency range from 0 MHz to 300 MHz, enabling an in-depth analysis of power transfer efficiency and resonant behavior.

4.3.1 LTspice in water

The simulated circuit is designed to analyze the coupling and resonance behavior of a capacitive power transfer system in water condition.

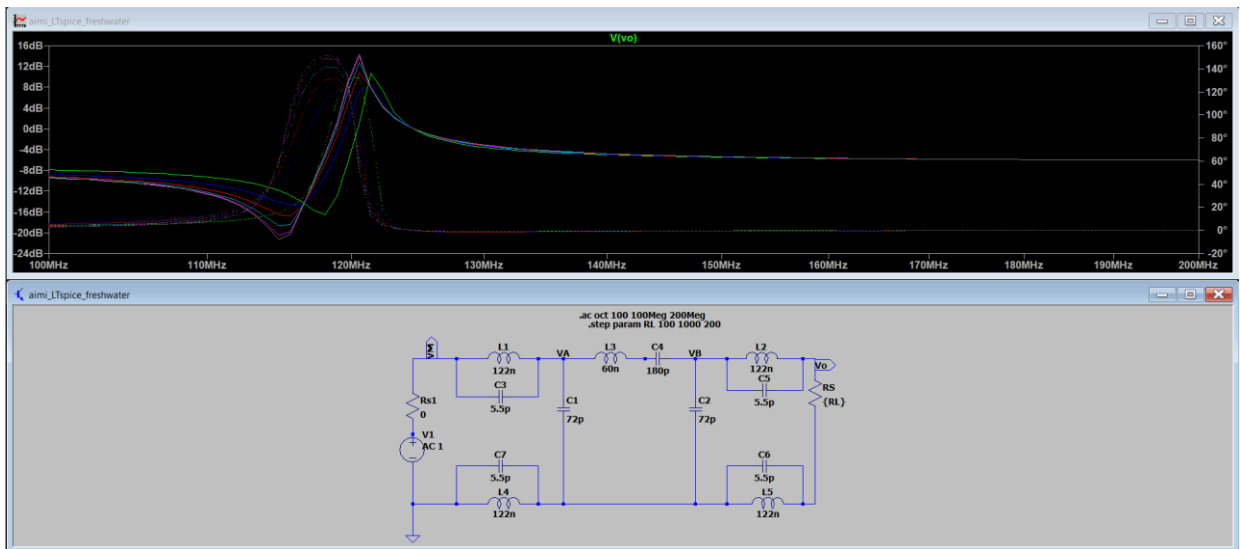


Figure 4.23 LTspice Simulation of a Resonant LC Filter Circuit in water condition

The circuit consists of inductive and capacitive components with the inductors L1, L2 and L3, along with capacitors C1, C2, and C3, forming the core reactive network. Additional capacitors and inductors represent parasitic and mutual coupling effects. The load resistance R_L is varied parametrically to study its impact on the resonance characteristics.

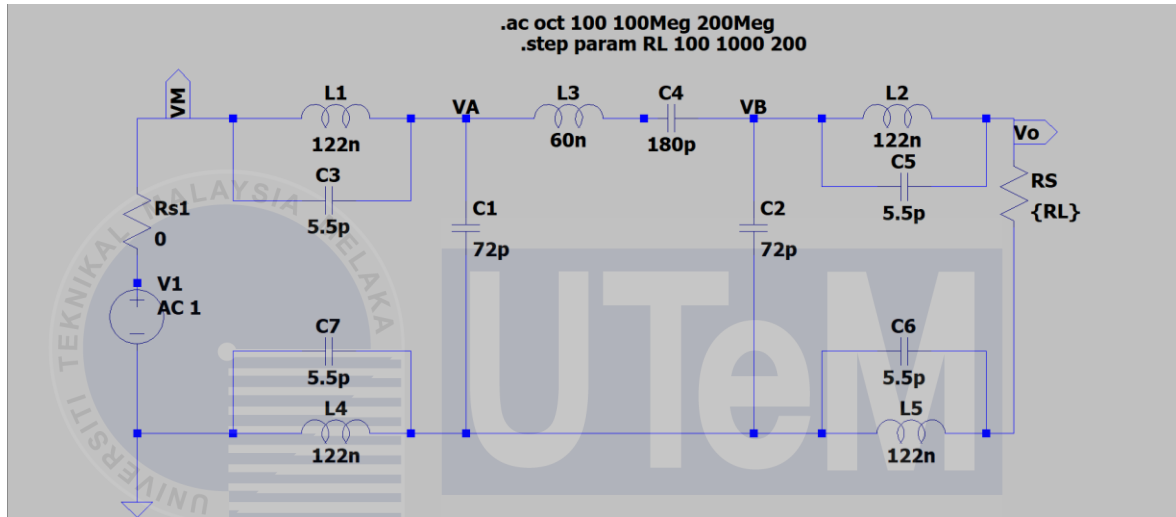


Figure 4.24 The circuit designed in LTspice in water condition

The frequency response as shown in Figure 4.25, the graph highlights the resonance peaks at specific frequencies with the most significant resonance at around 120.55 MHz, where the voltage gain reaches its peak value of approximately 14.51 dB. The behavior suggests strong coupling at this frequency which corresponds to optimal energy transfer. The variations in gain and phase across different resistance values illustrate how load resistance affects the resonance sharpness and coupling efficiency. The results validate the circuit's capability to operate effectively in water with clear resonance and energy transfer characteristics.

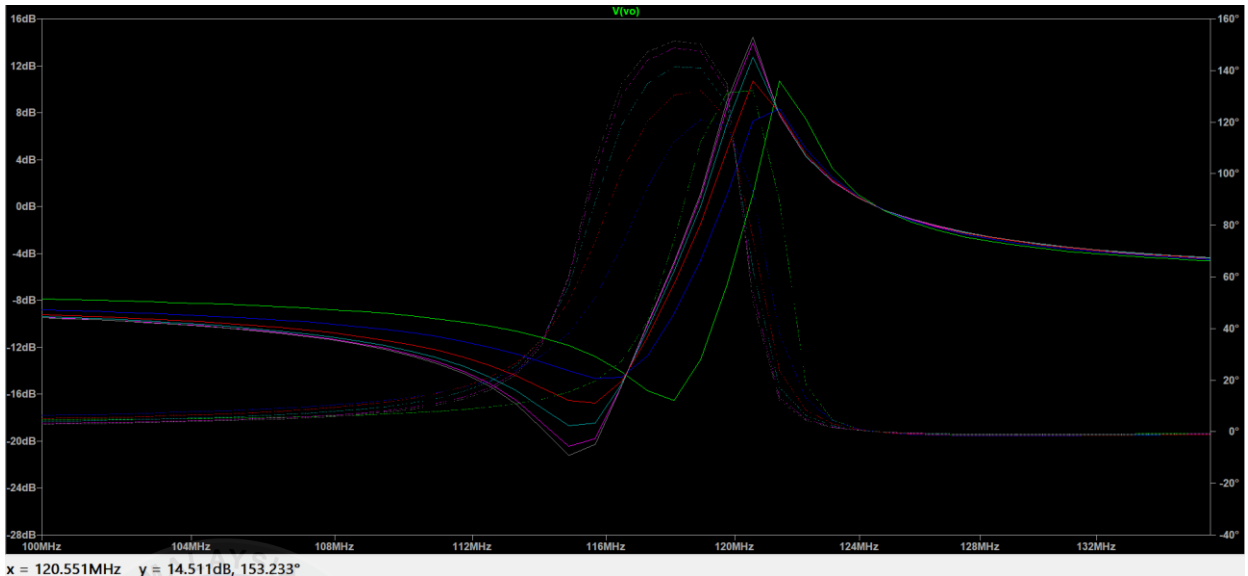


Figure 4.25 Frequency Response result gain in LTspice under water condition

4.3.2 LTspice seawater

The simulated circuit is designed to analyze the coupling and resonance behavior of a capacitive power transfer system in seawater condition.

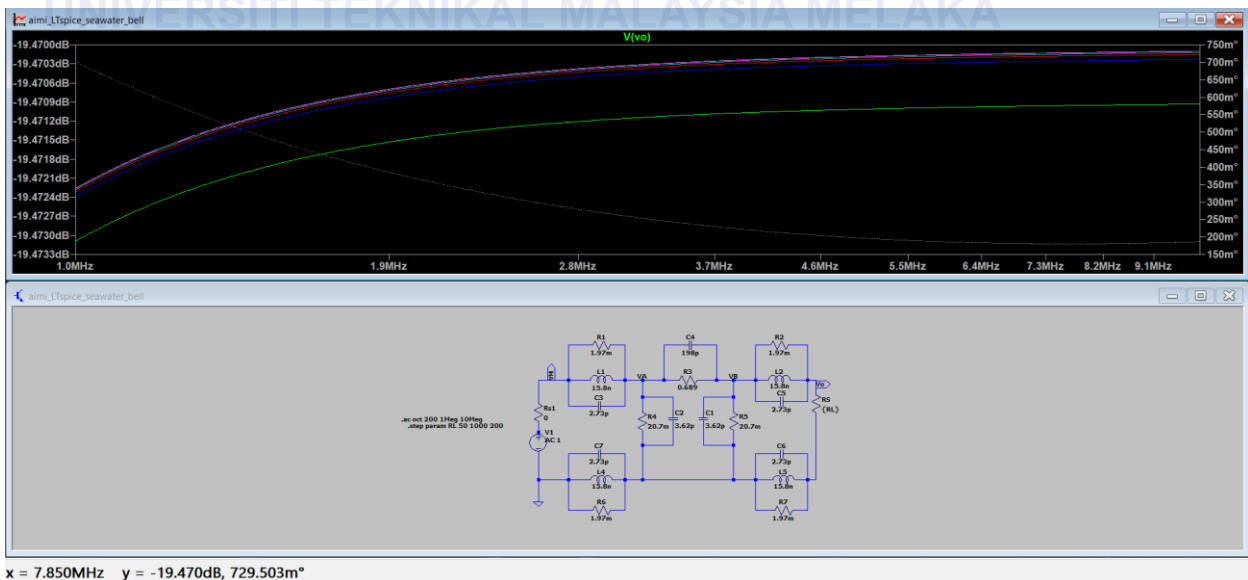


Figure 4.26 LTspice Simulation of a Resonant LC Filter Circuit under seawater condition

In Figure 4.27 illustrates the LTspice circuit model used for the seawater condition. The circuit design incorporates inductive and capacitive elements with additional parameters adjusted to reflect the dielectric and conductive properties of seawater. Key components like L1, L2, L3, and C1, C2, C3 represent the primary inductive and capacitive coupling, while the load resistance RLRL is varied to study its effect on the system's response.

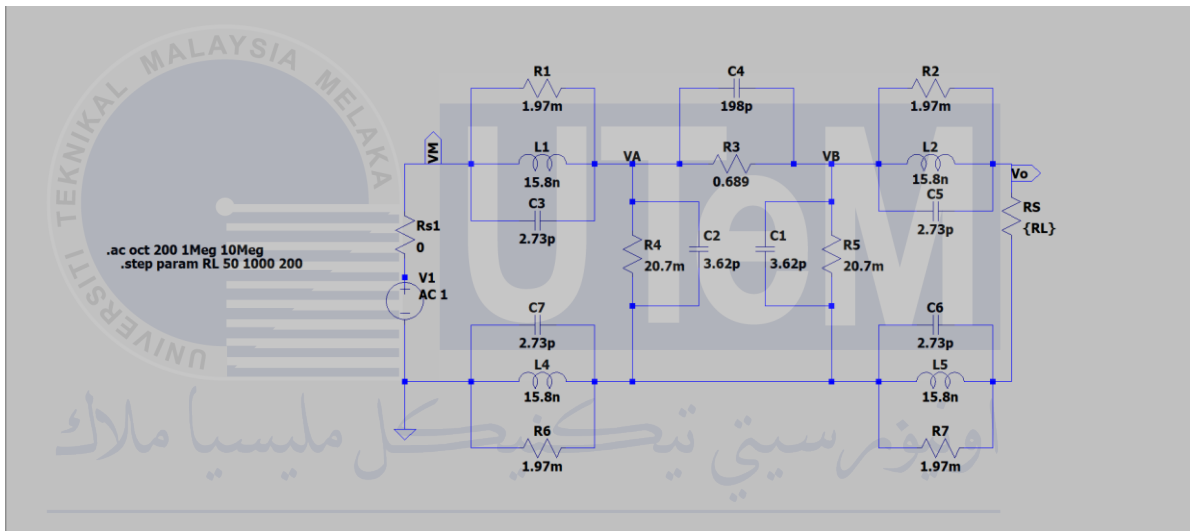


Figure 4.27 The circuit designed in LTspice in seawater condition

The frequency response as shown in Figure 4.28, the graph highlights how the gain changes across a range of frequencies. The resonance peak is observed at 7.853 MHz with a gain of 19.470 dB. However, there is a marked reduction in the overall gain compared to freshwater simulations which can be attributed to the energy losses introduced by the conductive nature of seawater. The graph also shows how the resonance peak is dampened indicating less efficient energy transfer at the resonant frequency. This dampening effect reflects the higher dielectric losses in seawater.

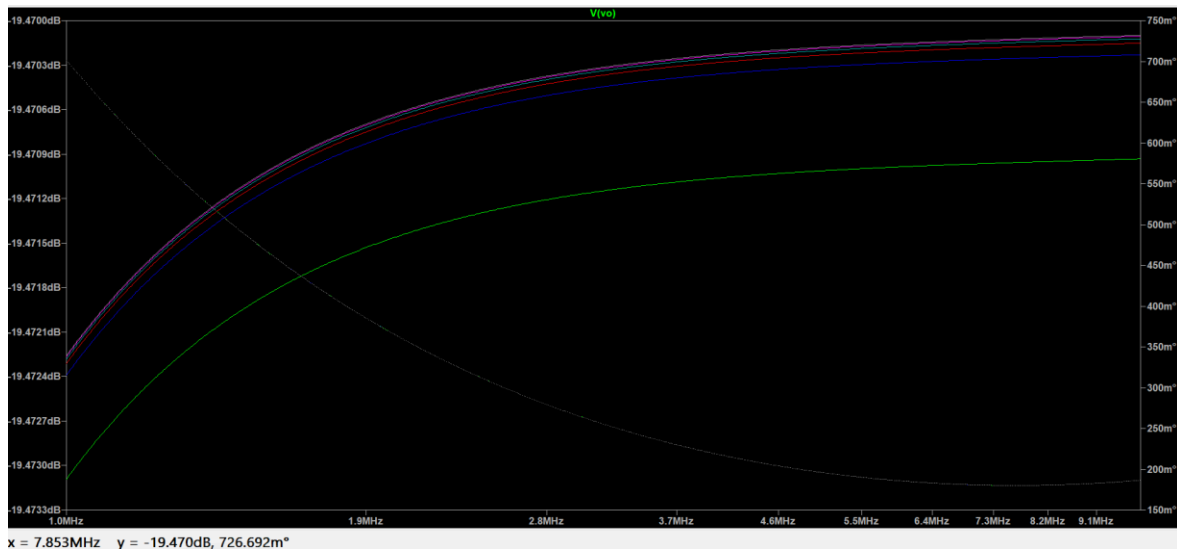


Figure 4.28 Frequency Response result gain in LTspice under seawater condition

4.4 Measurement and analysis

The validation of theoretical models and simulations is essential in developing capacitive wireless power transfer systems and hardware testing plays a key role in this process. Simulations provide useful insights into how these systems might perform but they are based on ideal conditions and assumptions. Therefore, real-world hardware tests are necessary to confirm the accuracy and reliability of the models. These tests help evaluate the system's actual performance including its efficiency, power transfer capability and other relevant parameters.

4.4.1 NanoVNA saver

The NanoVNA Saver application as shown in the Figure 4.29, captures and processes frequency sweep data from the NanoVNA analyzer in air. The device is connected to a computer via a USB cable allowing seamless data transfer.

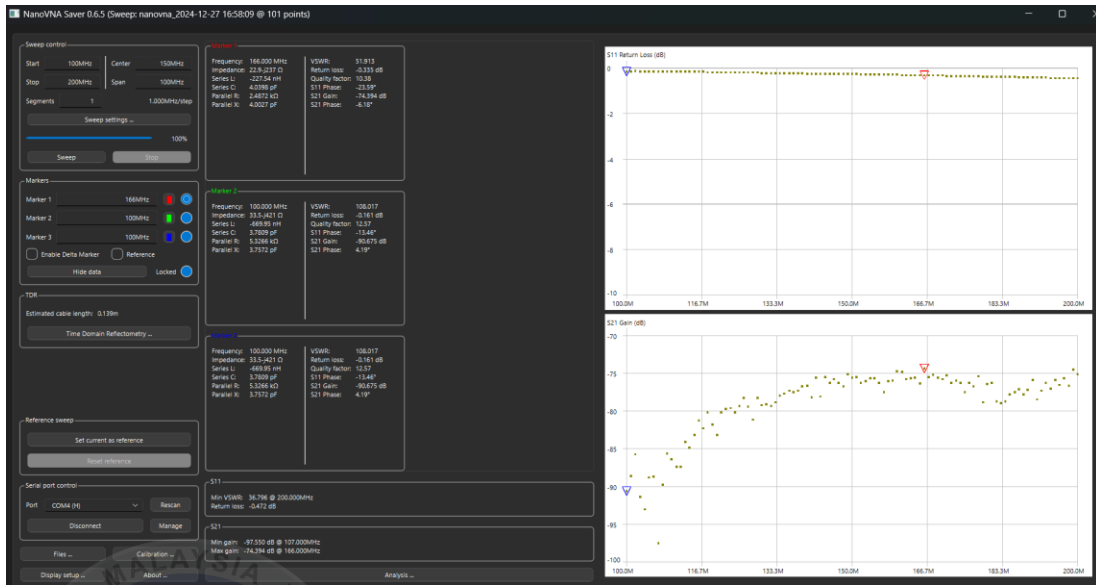


Figure 4.29 Frequency Sweep Analysis Captured Using NanoVNA Saver in air

In Figure 4.30 shows the S11 Return Loss (in dB) across a frequency range of 100 MHz to 200 MHz. Return loss measures the amount of signal reflected back towards the source due to impedance mismatches in the system. Ideally, a lower return loss (more negative dB value) indicates better impedance matching and minimal signal reflection. From the plot, it is observed that the return loss remains relatively flat and close to 0 dB across the frequency range. This suggests that the system has significant reflections indicating poor impedance matching between the source and the load.

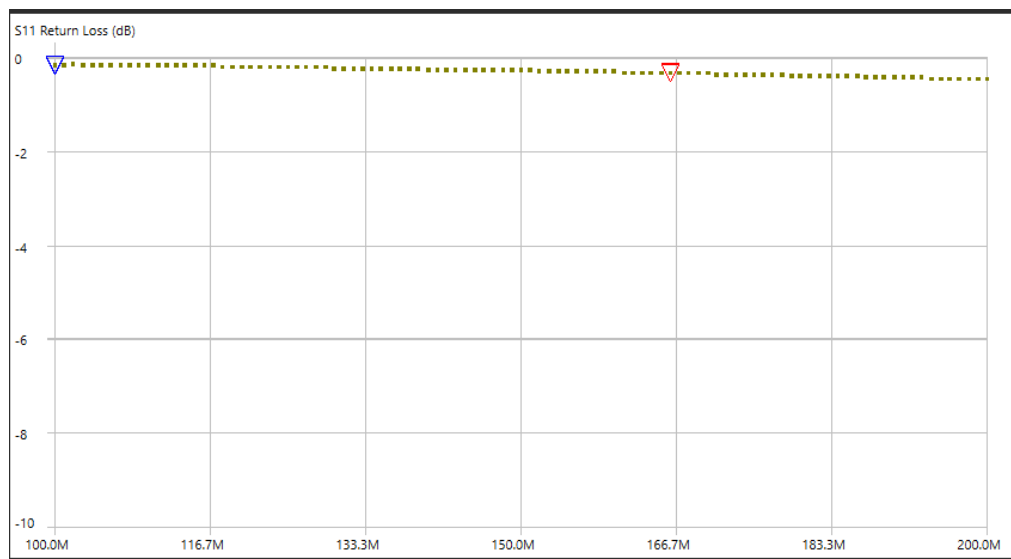


Figure 4.30 S11 Return Loss frequency response data captured by NanoVNA Saver in air

The Figure in 4.31 illustrates the S21 gain (dB) versus frequency in the range of 100 MHz to 200 MHz as short of its scale captured using the NanoVNA analyzer. The data points indicate the measured transmission coefficient (S21) which represents how effectively the signal is transmitted through the device under test (DUT). From the graph, the gain gradually increases with frequency starting at approximately -100 dB at 100 MHz and stabilizing around -75 dB at higher frequencies near 200 MHz. This shows that improved signal transmission as frequency increases due to the characteristics of the DUT or its impedance matching properties. The markers on the graph, the red and blue triangles indicate peak gain points that require further analysis. This data helps in understanding the performance and frequency response of the tested system.

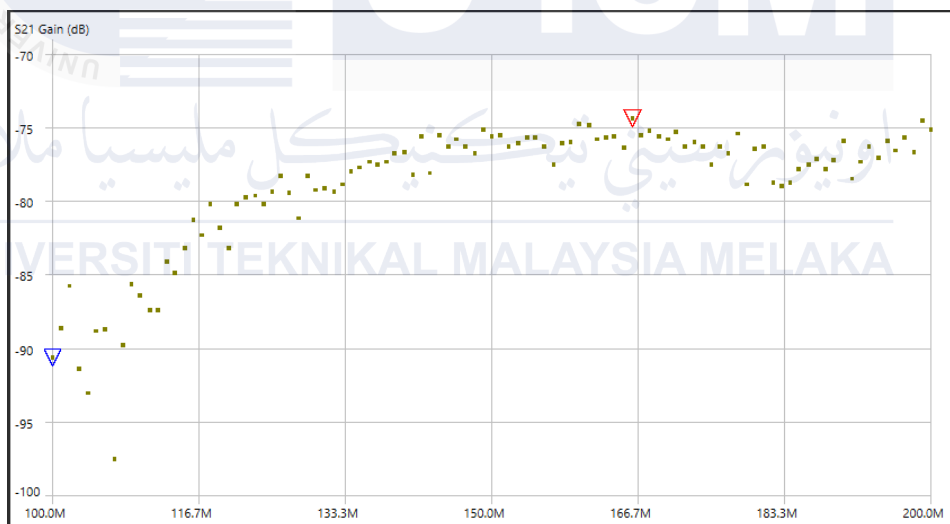


Figure 4.31 The S21 gain (dB) frequency response data captured via NanoVNA Saver in

air

The NanoVNA Saver application as shown in the Figure 4.32, captures and processes frequency sweep data from the NanoVNA analyzer in water. The device is connected to a computer via a USB cable, allowing seamless data transfer.

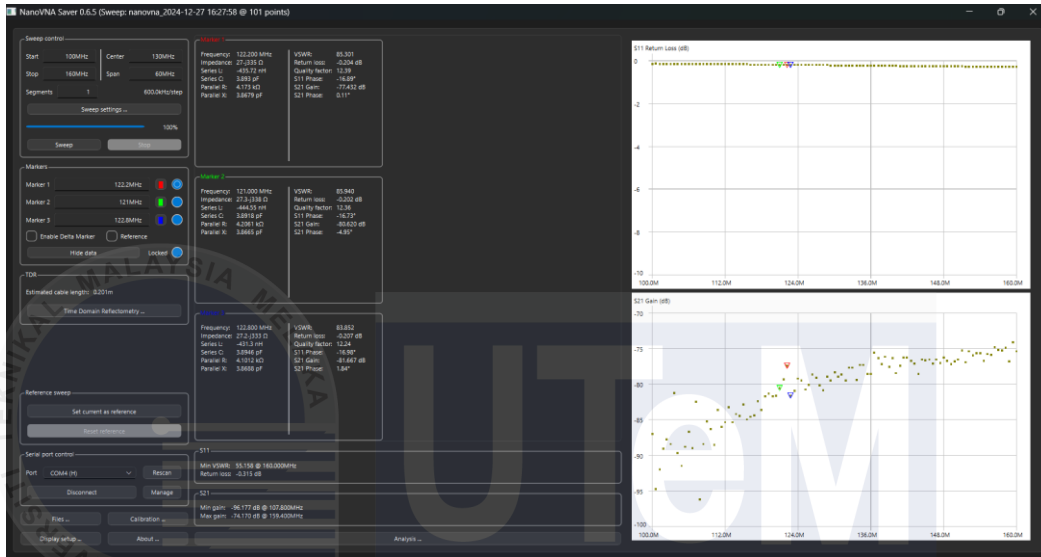


Figure 4.32 Frequency Sweep Analysis Captured Using NanoVNA Saver in water

In Figure 4.33 illustrates the S11 Return Loss (measured in dB) over a frequency range of 100 MHz to 200 MHz. The plot shows that the return loss remains relatively constant and close to 0 dB across the frequency range, indicating significant signal reflections.



Figure 4.33 S11 Return Loss frequency response data captured by NanoVNA Saver in water.

Based on Figure 4.34, the S21 gain (measured in dB) frequency response data captured using NanoVNA Saver in water is presented. The plot illustrates the gain across a frequency range of 100 MHz to 200 MHz. It is observed that the gain increases gradually with frequency indicating the frequency-dependent behavior of the system. The scattered data points suggest that the gain is not entirely smooth, possibly due to variations in the system's response to the electrical properties of water such as conductivity and its permittivity. The trend highlights the system's capability to amplify signals more effectively at higher frequencies within this range. These results provide valuable insights into the system's performance and limitations in underwater environments.

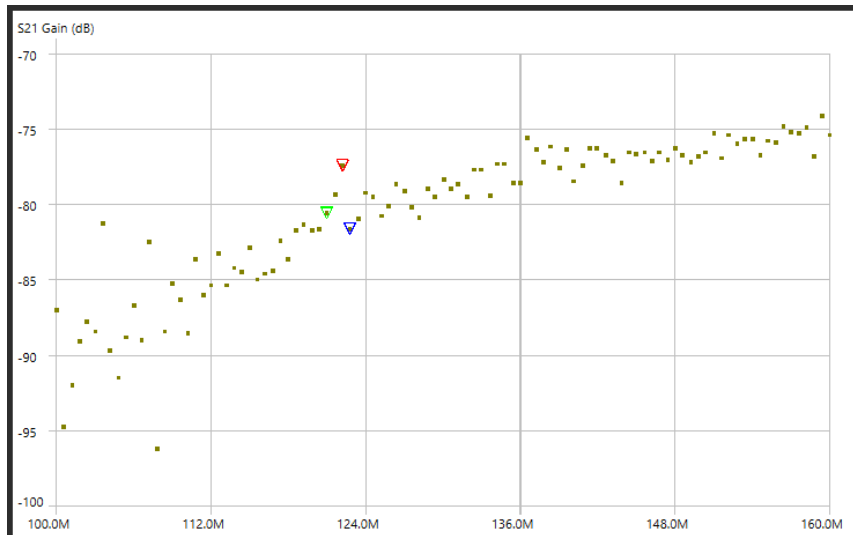


Figure 4.34 The S21 gain (dB) frequency response data captured via NanoVNA Saver in water

The NanoVNA Saver application as shown in the Figure 4.35, captures and processes frequency sweep data from the NanoVNA analyzer in seawater. The device is connected to a computer via a USB cable, allowing seamless data transfer.

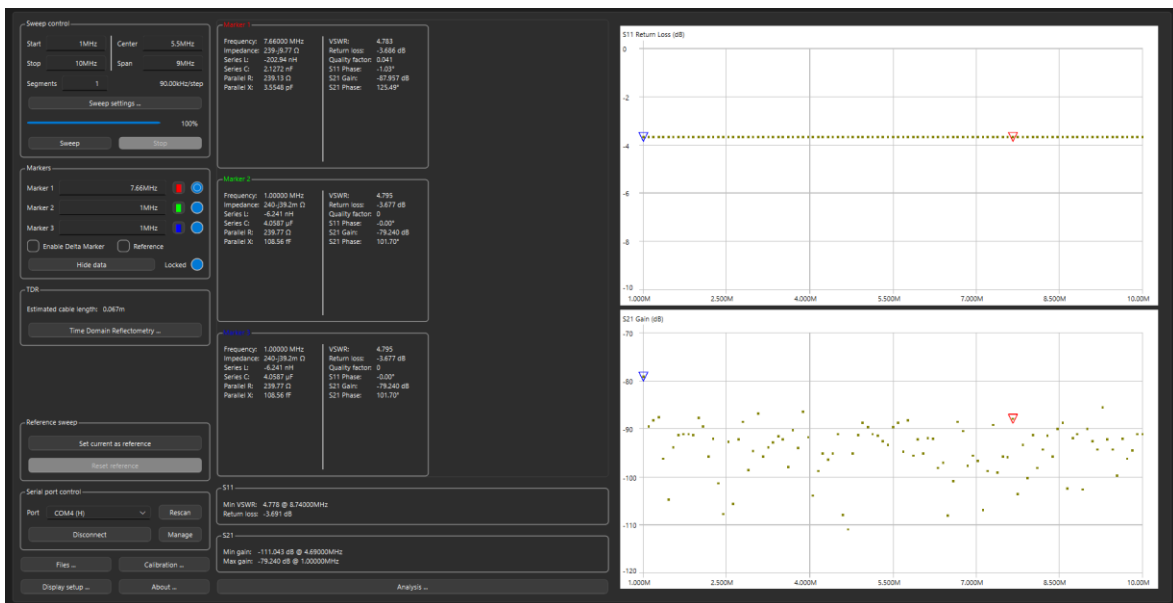


Figure 4.35 Frequency Sweep Analysis Captured Using NanoVNA Saver in seawater

In Figure 4.36 presents the S11 Return Loss frequency response data captured using NanoVNA Saver in seawater. The plot shows the return loss (measured in dB) over a frequency range of 1 GHz to 10 GHz. The return loss remains relatively stable and close to -4 dB across the frequency range, indicating consistent signal reflections throughout. The value of -4 dB suggests that a significant portion of the signal is being reflected back towards the source which implies poor impedance matching between the system components and the seawater environment. This behavior can be attributed to the complex electrical properties of seawater such as its high conductivity and permittivity which affect the impedance of the system. The results highlight the challenges in achieving effective impedance matching in seawater environments and provide important insights for optimizing the system's performance in such conditions.



Figure 4.36 S11 Return Loss frequency response data captured by NanoVNA Saver in seawater

Figure 4.37 presents the S21 gain (dB) frequency response data captured using NanoVNA Saver in a seawater environment. The S21 parameter represents the forward transmission coefficient, indicating how much signal power is transmitted from the input port to the output port of the system. From the plot, it can be observed that the gain varies significantly across the frequency range, showing noticeable fluctuations. This irregularity may indicate signal attenuation, reflections, or scattering effects caused by the conductive and lossy nature of seawater. Peaks in the gain might correspond to certain resonant frequencies where energy transfer is more efficient, while dips suggest frequencies with higher attenuation or mismatch losses.

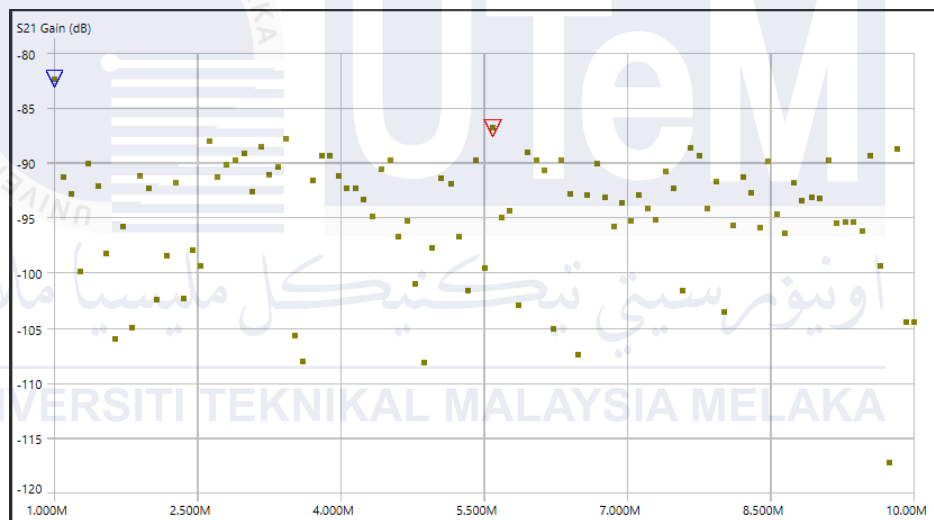


Figure 4.37 The S21 gain (dB) frequency response data captured via NanoVNA Saver in seawater

4.4.2 NanoVNA vector network analyzer

The experimental analysis using the NanoVNA vector network analyzer successfully demonstrated the resonance frequency behavior of the hardware across three distinct mediums such as air, freshwater, and seawater. The results across all three environment such as in air, freshwater, and seawater exhibit strong alignment between theoretical analysis, simulation outcomes and experimental data. This consistency validity of the methodologies employed and emphasizes the NanoVNA capability as a reliable instrument for analyzing frequency response characteristics in varying dielectric environments.

The Figure 4.38 above shows the data captured in air using the NanoVNA vector network analyzer. Based on the simulation, the hardware operating in air demonstrates a resonance frequency of 196 MHz. This result aligns with the expected values obtained from the theoretical analysis validating the accuracy of the simulation and its relevance to the hardware performance in air.



Figure 4.38 Frequency Response captured in Air using NanoVNA

The Figure 4.39 above shows the data captured in freshwater using the NanoVNA vector network analyzer. The theoretical resonance frequency was calculated to be 120.24 MHz while the LTspice simulation predicted a frequency of 120.55 MHz the hardware measurements in freshwater revealed a resonance frequency of 124 MHz, showing a 4 MHz difference from the theoretical value. Despite this slight deviation, the results align closely with the theoretical and simulated predictions validating both the accuracy of the simulation and its relevance to the hardware's real-world performance in freshwater conditions.

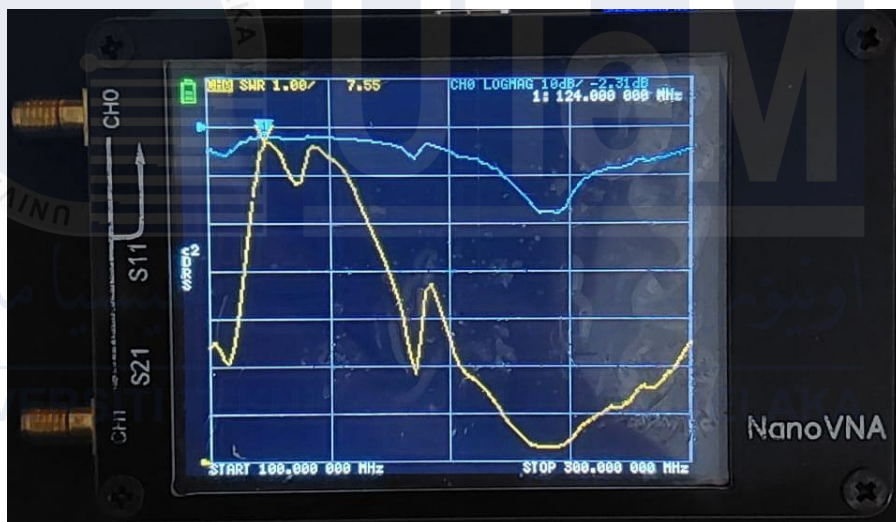


Figure 4.39 Frequency Response captured in Freshwater using NanoVNA

The Figure 4.40 presents the data captured in seawater using the NanoVNA vector network analyzer. The theoretical resonance frequency was determined through calculations to be approximately 6.78 MHz while the LTspice simulation provided a predicted resonance frequency of 7.853 MHz .Upon conducting hardware measurements in seawater, the observed resonance frequency was found to be 7.840 MHz. This measurement indicates a slight deviation from both the theoretical and simulated values, showing a difference of approximately 1.06 MHz from the theoretical calculation and 0.013 MHz from the simulation result. Despite this minor variation, the experimental results demonstrate a strong correlation with the theoretical analysis and LTspice simulation. This alignment validates the precision of the simulation model and reinforces its reliability in predicting the hardware's behavior in real-world seawater conditions. Such consistency emphasizes the effectiveness of the theoretical framework and simulation tools in guiding the design and analysis of the system's frequency response in varying environments.



Figure 4.40 Frequency Response captured in Seawater using NanoVNA

4.5 Summary

The conclusions from the simulation and experiment demonstrate that the effectiveness and efficiency of Capacitive Power Transfer (CPT) are highly dependent on the dielectric properties of the medium. Media with higher dielectric constants such as freshwater and seawater result in greater capacitance values, thereby enhancing CPT performance. Air, with its lower dielectric constant is less suitable for efficient CPT compared to freshwater and seawater. Seawater, in particular exhibits the highest capacitance indicating the greatest potential for effective CPT. However, its excellent conductivity must be considered in real-world applications to fully leverage its advantages for CPT. The conclusions from the simulation and experimental results show that the effectiveness of Capacitive Power Transfer (CPT) depends heavily on the dielectric properties of the medium. Media with higher dielectric constants like freshwater and seawater result in greater capacitance and improved power transfer efficiency. Seawater, with its high dielectric constant demonstrates the best performance especially at lower frequencies but its high conductivity introduces resistive losses that must be carefully managed. Freshwater while having a slightly lower dielectric constant offers a good balance between capacitance and manageable conductivity making it a reliable medium for CPT. In contrast, air with its low dielectric constant shows limited capacitance and reduced efficiency making it less suitable for effective CPT. Overall, seawater stands out as the most promising medium followed by freshwater while air remains more suitable for short-range or low-power applications. These findings emphasize the importance of selecting and optimizing the dielectric medium for efficient CPT performance.

CHAPTER 5

CONCLUSION AND RECOMMENDATIONS

5.1 Conclusion

This report discusses the significant developments in wireless power transfer technologies and discusses the development of a capacitive wireless power transfer coupler for underwater EV charging applications. The study methodically investigated various kinds of wireless power transmission approaches, with a focus on capacitive systems with relevant studies and examples, covering the design and analysis of CPT systems for underwater applications. A block diagram and flowchart are used to thoroughly explain the project workflow, illustrating the stages that must be followed in order to set up. The analysis begins with an introduction at a two-plate capacitor arrangement and carried on to simulations and calculations using MATLAB to calculate capacitance values in various media air, freshwater, and seawater. The simulation results were validated against theoretical calculations, showing consistent and precise capacitance values across varying distances. This consistency confirmed the achievement of the primary objective of the project, which was to calculate the parameters of a CPT coupler for underwater EV applications. The ability to effectively combine simulated and theoretical data highlights the innovative potential CPT technology is possible for underwater wireless charging devices.

5.2 Future Works

Future improvements for the Capacitive Power Transfer (CPT) system can focus on optimizing coupler design by refining plate geometry, material selection and spacing to maximize capacitance while minimizing energy losses. Adaptive frequency control can be implemented to dynamically adjust the operating frequency based on environmental variations such as salinity and temperature in seawater. Enhanced insulation techniques and advanced dielectric materials can be explored to reduce energy leakage and improve durability particularly in corrosive seawater conditions. Power electronics including inverters and rectifiers can be optimized for better efficiency and stability across varying loads. Medium-specific calibration models for freshwater, seawater and air can be developed to account for real-time environmental changes. Integrating wireless communication modules can enable remote monitoring, control and diagnostics, improving operational flexibility. Long-term experimental validation in natural environments will help assess system reliability while exploring scalability for higher power transfer will ensure broader applicability especially in industrial and underwater robotics scenarios. These advancements will collectively enhance the efficiency, adaptability and robustness of CPT technology across diverse real-world applications.

5.3 Project potential

This project demonstrates significant potential across various fields by analyzing resonance frequency behavior in air, freshwater and seawater using the NanoVNA vector network analyzer. The findings can directly contribute to advancements in wireless communication systems particularly in designing antennas and improving underwater communication technologies for applications such as autonomous underwater vehicles and remote sensing devices. Additionally, the ability to measure frequency responses in different mediums opens opportunities for environmental monitoring including water quality assessment and pollutant detection. In the biomedical field, this research can support the development of implantable sensors and non-invasive diagnostic tools where biological fluids mimic similar dielectric properties. The study also validates the accuracy of LTspice simulations, reinforcing its role as a reliable predictive tool for hardware analysis. Moving forward, this research could evolve into real-time monitoring systems, integrate machine learning models for predictive analysis and optimize hardware designs for increased precision.

REFERENCES

- [1] A. A. Bakar, A. Idris, A. R. Razali, and M. A. Zakaria, "Wireless power transfer via inductive coupling," *Journal of Telecommunication, Electronic and Computer Engineering*, vol. 10, no. 1–9, pp. 37–41, 2018, doi: 10.17993/3ctecno.2020.specialissue5.107-117.
- [2] R. Erfani, F. Marefat, A. M. Sodagar, and P. Mohseni, "Modeling and Experimental Validation of a Capacitive Link for Wireless Power Transfer to Biomedical Implants," *IEEE Transactions on Circuits and Systems II: Express Briefs*, vol. 65, no. 7, pp. 923–927, Jul. 2018, doi: 10.1109/TCSII.2017.2737140.
- [3] H. Mahdi, B. Hoff, and T. Østrem, "Optimal solutions for underwater capacitive power transfer," *Sensors*, vol. 21, no. 24, Dec. 2021, doi: 10.3390/s21248233.
- [4] X. Zhang and J. Lian, "A Novel Coupler of Capacitive Power Transfer for Enhancing Underwater Power Transfer Characteristics," *Electronics (Switzerland)*, vol. 13, no. 1, Jan. 2024, doi: 10.3390/electronics13010074.
- [5] T. Ohira, "Extended k-Q product formulas for capacitive- and inductive-coupling wireless power transfer schemes," *IEICE Electronics Express*, vol. 11, no. 9, Apr. 2014, doi: 10.1587/elex.11.20140147.
- [6] M. S. Mazli *et al.*, "Inductive Capacitive Wireless Power Transfer System," in *Proceedings of the 2018 7th International Conference on Computer and Communication Engineering, ICCCE 2018*, Institute of Electrical and Electronics Engineers Inc., Nov. 2018, pp. 307–312. doi: 10.1109/ICCCE.2018.8539263.
- [7] J. Zhou, P. Yao, Y. Chen, K. Guo, S. Hu, and H. Sun, "Design Considerations for a Self-Latching Coupling Structure of Inductive Power Transfer for Autonomous Underwater Vehicle," *IEEE Trans Ind Appl*, vol. 57, no. 1, pp. 580–587, Jan. 2021, doi: 10.1109/TIA.2020.3029020.
- [8] L. Yang *et al.*, "Coupling Capacitor Structure Model of Underwater Capacitive Wireless Power Transfer System," in *PEDG 2023 - 2023 IEEE 14th International Symposium on Power Electronics for Distributed Generation Systems*, Institute of Electrical and Electronics Engineers Inc., 2023, pp. 94–98. doi: 10.1109/PEDG56097.2023.10215202.
- [9] B. Luo, T. Long, R. Mai, R. Dai, Z. He, and W. Li, "Analysis and design of hybrid inductive and capacitive wireless power transfer for highpower applications," *IET Power Electronics*, vol. 11, no. 14, pp. 2263–2270, Nov. 2018, doi: 10.1049/iet-pel.2018.5279.
- [10] B. Bhavsingh, B. Mangu, and G. S. Babu, "Design and Analysis of a High-Efficiency dual side S-S Compensation topology of Inductive Power Transfer for EV battery charging System," in *2022 IEEE 2nd International Conference on Sustainable Energy and Future Electric Transportation, SeFeT 2022*, Institute of Electrical and Electronics Engineers Inc., 2022. doi: 10.1109/SeFeT55524.2022.9908627.
- [11] W. Zhou, M. Li, Q. Zhang, Z. Li, S. Xie, and Y. Fan, "Potential and Challenges of Capacitive Power Transfer Systems for Wireless EV Charging: A Re-view of Key Technologies," *Green Energy and Intelligent Transportation*, p. 100174, Jan. 2024, doi: 10.1016/j.geits.2024.100174.
- [12] E. Rong, P. Sun, X. Zhang, G. Yang, and X. Wu, "3.3kW Underwater Capacitive Power Transfer System for Electric Ship Charging Application," in *2023 IEEE International Conference on Power Science and Technology, ICPST 2023*, Institute

- of Electrical and Electronics Engineers Inc., 2023, pp. 1052–1057. doi: 10.1109/ICPST56889.2023.10164993.
- [13] IEEE Power & Energy Society, IEEE Power Electronics Society, and Institute of Electrical and Electronics Engineers, *ESTS 2019 : IEEE Electric Ship Technologies Symposium : Emerging Technologies for Future Electric Ships : August 14-16, 2019, Westin Crystal City Hotel, Arlington, VA*.
- [14] L. Yang *et al.*, “Analysis and Design of Four-Plate Capacitive Wireless Power Transfer System for Undersea Applications,” *CES Transactions on Electrical Machines and Systems*, vol. 5, no. 3, pp. 202–211, Sep. 2021, doi: 10.30941/CESTEMS.2021.00024.
- [15] “Design considerations for contact-less underwater power delivery a systematic review and critical analysis”.
- [16] H. Mahdi, B. Hoff, P. G. Ellingsen, and T. Ostrem, “Conformal Transformation Analysis of Capacitive Wireless Charging,” *IEEE Access*, vol. 10, pp. 105621–105630, 2022, doi: 10.1109/ACCESS.2022.3210960.
- [17] Wikipedia contributors, “Wireless_power_transfer.”
- [18] G. A. Covic and J. T. Boys, “Modern trends in inductive power transfer for transportation applications,” *IEEE J Emerg Sel Top Power Electron*, vol. 1, no. 1, pp. 28–41, 2013, doi: 10.1109/JESTPE.2013.2264473.
- [19] M. Jiang, C. Chen, H. Chen, X. Huang, and S. Jia, “A Fundamental-Harmonic Hybrid Power Transfer Strategy for Bidirectional Inductive Power Transfer,” in *Proceedings of 2021 IEEE 4th International Electrical and Energy Conference, CIEEC 2021*, Institute of Electrical and Electronics Engineers Inc., May 2021. doi: 10.1109/CIEEC50170.2021.9510888.
- [20] X. Li, C. Tang, X. Dai, P. Deng, and Y. Su, “An Inductive and Capacitive Combined Parallel Transmission of Power and Data for Wireless Power Transfer Systems,” *IEEE Trans Power Electron*, vol. 33, no. 6, pp. 4980–4991, Jun. 2018, doi: 10.1109/TPEL.2017.2725990.
- [21] Z. Wang, Y. Zhang, X. He, B. Luo, and R. Mai, “Research and Application of Capacitive Power Transfer System: A Review,” Apr. 01, 2022, *MDPI*. doi: 10.3390/electronics11071158.
- [22] L. Yang *et al.*, “Coupling Capacitor Structure Model of Underwater Capacitive Wireless Power Transfer System,” in *PEDG 2023 - 2023 IEEE 14th International Symposium on Power Electronics for Distributed Generation Systems*, Institute of Electrical and Electronics Engineers Inc., 2023, pp. 94–98. doi: 10.1109/PEDG56097.2023.10215202.
- [23] J. Zhang, S. Yao, L. Pan, Y. Liu, and C. Zhu, “A Review of Capacitive Power Transfer Technology for Electric Vehicle Applications,” Aug. 01, 2023, *Multidisciplinary Digital Publishing Institute (MDPI)*. doi: 10.3390/electronics12163534.
- [24] Z. Sun, Y. Wang, T. Li, J. Mai, M. Zeng, and D. Xu, “Performance Assessment of Capacitive Power Transfer in Water with Varied Conductivity,” in *2023 IEEE 3rd International Conference on Industrial Electronics for Sustainable Energy Systems, IESES 2023*, Institute of Electrical and Electronics Engineers Inc., 2023. doi: 10.1109/IESES53571.2023.10253747.
- [25] S. Kodeeswaran, M. Nandhini Gayathri, A. Kannabhiran, and S. S. Williamson, “Design of a Static Capacitive Power Transfer System with Six-Plate Coupler for Electric Vehicle Wireless Charging,” *IEEE Transactions on Transportation Electrification*, 2023, doi: 10.1109/TTE.2023.3316710.

- [26] Z. Zhang, J. Yang, K. Sun, Y. Zhou, Z. Hu, and Y. Wang, "Optimization Design of Electrical System for Underwater Hybrid Energy Charging Platform," Institute of Electrical and Electronics Engineers (IEEE), Mar. 2024, pp. 638–643. doi: 10.1109/acfpe59335.2023.10455307.
- [27] B. Luo, T. Long, R. Mai, R. Dai, Z. He, and W. Li, "Analysis and design of hybrid inductive and capacitive wireless power transfer for highpower applications," *IET Power Electronics*, vol. 11, no. 14, pp. 2263–2270, Nov. 2018, doi: 10.1049/iet-pel.2018.5279.
- [28] J. Zhou, P. Yao, Y. Chen, K. Guo, S. Hu, and H. Sun, "Design Considerations for a Self-Latching Coupling Structure of Inductive Power Transfer for Autonomous Underwater Vehicle," *IEEE Trans Ind Appl*, vol. 57, no. 1, pp. 580–587, Jan. 2021, doi: 10.1109/TIA.2020.3029020.
- [29] L. Yang, M. Ju, and B. Zhang, "Bidirectional Undersea Capacitive Wireless Power Transfer System," *IEEE Access*, vol. 7, pp. 121046–121054, 2019, doi: 10.1109/ACCESS.2019.2937888.
- [30] IEEE Power Electronics Society, IEEE Industry Applications Society, and Institute of Electrical and Electronics Engineers, *ECCE 2016 : IEEE Energy Conversion Congress & Expo : proceedings : Milwaukee, WI, Sept. 18-22*.
- [31] I. IEEE Transportation and Electrification Conference and Expo 2017 Chicago, Institute of Electrical and Electronics Engineers, Ill. IEEE Transportation and Electrification Conference and Expo 2017.06.22-24 Chicago, and Ill. ITEC 2017.06.22-24 Chicago, *2017 IEEE Transportation and Electrification Conference and Expo (ITEC) Chicago, Illinois, June 22-24, 2017*.
- [32] S. Ahmad, A. Muharam, R. Hattori, A. Uezu, and T. M. Mostafa, "Shielded capacitive power transfer (S-cpt) without secondary side inductors," *Energies (Basel)*, vol. 14, no. 15, Aug. 2021, doi: 10.3390/en14154590.
- [33] *2020 IEEE PELS Workshop on Emerging Technologies: Wireless Power Transfer (Wow) : Nov. 15-19, 2020, Seoul, Korea*. IEEE, 2020.
- [34] IEEE Power Electronics Society, IEEE Industry Applications Society, and Institute of Electrical and Electronics Engineers, *ECCE 2019 : IEEE Energy Conversion Congress & Expo : Baltimore MD, Sept. 29 - Oct. 3*.
- [35] F. Lu, H. Zhang, and C. Mi, "A Two-Plate Capacitive Wireless Power Transfer System for Electric Vehicle Charging Applications," *IEEE Trans Power Electron*, vol. 33, no. 2, pp. 964–969, Feb. 2018, doi: 10.1109/TPEL.2017.2735365.
- [36] C. Lecluyse, B. Minnaert, and M. Kleemann, "A review of the current state of technology of capacitive wireless power transfer," Sep. 01, 2021, *MDPI*. doi: 10.3390/en14185862.
- [37] IEEE Power & Energy Society, IEEE Power Electronics Society, and Institute of Electrical and Electronics Engineers, *ESTS 2019 : IEEE Electric Ship Technologies Symposium : Emerging Technologies for Future Electric Ships : August 14-16, 2019, Westin Crystal City Hotel, Arlington, VA*.
- [38] IEEE Power & Energy Society, IEEE Power Electronics Society, and Institute of Electrical and Electronics Engineers, *ESTS 2019 : IEEE Electric Ship Technologies Symposium : Emerging Technologies for Future Electric Ships : August 14-16, 2019, Westin Crystal City Hotel, Arlington, VA*.
- [39] H. Zhang, F. Lu, H. Hofmann, W. Liu, and C. C. Mi, "Six-Plate Capacitive Coupler to Reduce Electric Field Emission in Large Air-Gap Capacitive Power Transfer," *IEEE Trans Power Electron*, vol. 33, no. 1, pp. 665–675, Jan. 2018, doi: 10.1109/TPEL.2017.2662583.

- [40] IEEE Power Electronics Society, IEEE Microwave Theory and Techniques Society, Institute of Electrical and Electronics Engineers, and K. O. Wireless Power Week (2020 : Seoul, *2020 IEEE PELS Workshop on Emerging Technologies: Wireless Power Transfer (Wow)* : Nov. 15-19, 2020, Seoul, Korea.
- [41] E. Rong, P. Sun, K. Qiao, X. Zhang, G. Yang, and X. Wu, "Six-Plate and Hybrid-Dielectric Capacitive Coupler for Underwater Wireless Power Transfer," *IEEE Trans Power Electron*, vol. 39, no. 2, pp. 2867–2881, Feb. 2024, doi: 10.1109/TPEL.2023.3334888.
- [42] Y. Liu, X. L. Li, C. K. Tse, and C. Zhu, "A Comparative Study of Compensation Topologies for Capacitive Power Transfer based on Sensitivity Analysis."
- [43] Z. Wang, Y. Zhang, X. He, B. Luo, and R. Mai, "Research and Application of Capacitive Power Transfer System: A Review," Apr. 01, 2022, *MDPI*. doi: 10.3390/electronics11071158.
- [44] C. Y. Liou, C. J. Kuo, and S. G. Mao, "Wireless-Power-Transfer System Using Near-Field Capacitively Coupled Resonators," *IEEE Transactions on Circuits and Systems II: Express Briefs*, vol. 63, no. 9, pp. 898–902, Sep. 2016, doi: 10.1109/TCSII.2016.2535042.
- [45] A. Shakya and M. Kumar, "Implementation of Inductive Wireless Power Transmission system for Battery Charging applications," in *2022 2nd International Conference on Advances in Electrical, Computing, Communication and Sustainable Technologies, ICAECT 2022*, Institute of Electrical and Electronics Engineers Inc., 2022. doi: 10.1109/ICAECT54875.2022.9808083.
- [46] I. IEEE Transportation and Electrification Conference and Expo 2017 Chicago, Institute of Electrical and Electronics Engineers, Ill. IEEE Transportation and Electrification Conference and Expo 2017.06.22-24 Chicago, and Ill. ITEC 2017.06.22-24 Chicago, *2017 IEEE Transportation and Electrification Conference and Expo (ITEC) Chicago, Illinois, June 22-24, 2017*.
- [47] J. Dai and D. C. Ludois, "Capacitive Power Transfer Through a Conformal Bumper for Electric Vehicle Charging," *IEEE J Emerg Sel Top Power Electron*, vol. 4, no. 3, pp. 1015–1025, Sep. 2016, doi: 10.1109/JESTPE.2015.2505622.
- [48] X. Wu, W. Gong, J. Xiao, S. Chen, Y. Mo, and R. Deng, "A Multi-Channel Wireless Power Transfer Method for Electric Vehicles Based on Magnetic Field Coupling," in *2023 IEEE 3rd International Conference on Data Science and Computer Application, ICDSCA 2023*, Institute of Electrical and Electronics Engineers Inc., 2023, pp. 230–235. doi: 10.1109/ICDSCA59871.2023.10392921.
- [49] V. M. Ponnuswamy and S. B. Veeranna, "Transmitter-Side Controlled Series-Series Compensated Wireless Charging System without Wireless Communication for Electric Vehicles," in *IECON Proceedings (Industrial Electronics Conference)*, IEEE Computer Society, 2022. doi: 10.1109/IECON49645.2022.9968700.
- [50] D. Wang, J. Zhang, S. Cui, Z. Bie, F. Chen, and C. Zhu, "The state-of-the-arts of underwater wireless power transfer: A comprehensive review and new perspectives," Jan. 01, 2024, *Elsevier Ltd*. doi: 10.1016/j.rser.2023.113910.
- [51] M. Lu, M. Bagheri, A. P. James, and T. Phung, "Wireless Charging Techniques for UAVs: A Review, Reconceptualization, and Extension," May 26, 2018, *Institute of Electrical and Electronics Engineers Inc*. doi: 10.1109/ACCESS.2018.2841376.
- [52] M. Simic, C. Bil, and V. Vojisavljevic, "Investigation in wireless power transmission for UAV charging," in *Procedia Computer Science*, Elsevier B.V., 2015, pp. 1846–1855. doi: 10.1016/j.procs.2015.08.295.
- [53] R. Sedehi *et al.*, "A Wireless Power Method for Deeply Implanted Biomedical Devices via Capacitively Coupled Conductive Power Transfer," *IEEE Trans Power*

- Electron*, vol. 36, no. 2, pp. 1870–1882, Feb. 2021, doi: 10.1109/TPEL.2020.3009048.
- [54] R. Narayanamoorthi, “Modeling of Capacitive Resonant Wireless Power and Data Transfer to Deep Biomedical Implants,” *IEEE Trans Compon Packaging Manuf Technol*, vol. 9, no. 7, pp. 1253–1263, Jul. 2019, doi: 10.1109/TCPMT.2019.2922046.
- [55] Institute of Electrical and Electronics Engineers, *2018 IEEE/MTT-S International Microwave Symposium : 10-15 June 2018, Philadelphia, Pennsylvania, USA*.
- [56] IEEE Power Electronics Society, IEEE Microwave Theory and Techniques Society, Institute of Electrical and Electronics Engineers, and K. O. Wireless Power Week (2020 : Seoul, *2020 IEEE PELS Workshop on Emerging Technologies: Wireless Power Transfer (Wow) : Nov. 15-19, 2020, Seoul, Korea*).
- [57] IEEE Industry Applications Society and Institute of Electrical and Electronics Engineers, *2019 22nd International Conference on Electrical Machines and Systems (ICEMS)*.
- [58] S. Kodeeswaran, M. Nandhini Gayathri, A. Kannabhiran, and S. S. Williamson, “Design of a Static Capacitive Power Transfer System with Six-Plate Coupler for Electric Vehicle Wireless Charging,” *IEEE Transactions on Transportation Electrification*, 2023, doi: 10.1109/TTE.2023.3316710.
- [59] IEEE Power Electronics Society, IEEE Microwave Theory and Techniques Society, Institute of Electrical and Electronics Engineers, and K. O. Wireless Power Week (2020 : Seoul, *2020 IEEE PELS Workshop on Emerging Technologies: Wireless Power Transfer (Wow) : Nov. 15-19, 2020, Seoul, Korea*).
- [60] IEEE Power & Energy Society, IEEE Power Electronics Society, and Institute of Electrical and Electronics Engineers, *ESTS 2019 : IEEE Electric Ship Technologies Symposium : Emerging Technologies for Future Electric Ships : August 14-16, 2019, Westin Crystal City Hotel, Arlington, VA*.
- [61] T. Ohira, “Extended k-Q product formulas for capacitive- and inductive-coupling wireless power transfer schemes,” *IEICE Electronics Express*, vol. 11, no. 9, Apr. 2014, doi: 10.1587/elex.11.20140147.
- [62] C. Jiang, B. Wei, C. Xu, X. Wu, and H. He, “Efficiency Improvement Under Coupler Misalignment for Dual-Transmitter and Single-Receiver Capacitive Power Transfer System,” *IEEE Trans Power Electron*, vol. 38, no. 12, pp. 14872–14883, Dec. 2023, doi: 10.1109/TPEL.2023.3314746.
- [63] M. Fadel *et al.*, “Capacitive power transfer for wireless batteries charging,” *Automatica (EEA)*, vol. 66, no. 4, pp. 40–51, 2018, [Online]. Available: <https://www.researchgate.net/publication/330183455>
- [64] IEEE Microwave Theory and Techniques Society and Institute of Electrical and Electronics Engineers, *2020 IEEE International Symposium on Radio-Frequency Integration Technology (RFIT)*.
- [65] Institute of Electrical and Electronics Engineers, *2019 IEEE MTT-S International Microwave Symposium (IMS)*.
- [66] Institute of Electrical and Electronics Engineers, *Proceedings of the 2019 Asia-Pacific Microwave Conference (APMC) : 10-13 December 2019, Marina Bay Sands, Singapore*.
- [67] *2020 IEEE International Symposium on Radio-Frequency Integration Technology (RFIT)*. IEEE, 2020.
- [68] *2018 IEEE/MTT-S International Microwave Symposium - IMS*. IEEE, 2018.

APPENDICES

Appendix A

```
clc;
clear;

% Define constants
eo = 8.854e-12;      % Permittivity of free space (F/m)
erair = 1.0006;     % Relative permittivity of air
erfw = 78.5;        % Relative permittivity of freshwater
ersea = 81.5;       % Relative permittivity of seawater

% Define the fixed area and the range of distances
area = 100;         % Fixed area in square meters
distances = [1,5,10,15,20,30,50]; % Distances in meters

% Preallocate arrays for capacitance values
capacitances_air = zeros(1, length(distances));
capacitances_fw = zeros(1, length(distances));
capacitances_sea = zeros(1, length(distances));

% Calculate the product AT for air, freshwater, and seawater
AT_air = area * eo * erair;
AT_fw = area * eo * erfw;
AT_sea = area * eo * ersea;

% Loop over each distance to calculate capacitance
for j = 1:length(distances)
    d = distances(j);
    capacitances_air(j) = AT_air / d; % Calculate capacitance for given distance in air
    capacitances_fw(j) = AT_fw / d; % Calculate capacitance for given distance in freshwater
    capacitances_sea(j) = AT_sea / d; % Calculate capacitance for given distance in seawater
end

% Display the results for air
fprintf('Air Capacitance (F)\n');
fprintf('Distance (m)\t');
fprintf('%0.2f\t', distances);
fprintf('\n');
fprintf('Capacitance\t');
fprintf('%0.2e\t', capacitances_air);
fprintf('\n');

% Display the results for freshwater
fprintf('\nFreshwater Capacitance (F)\n');
fprintf('Distance (m)\t');
fprintf('%0.2f\t', distances);
fprintf('\n');
fprintf('Capacitance\t');
fprintf('%0.2e\t', capacitances_fw);
fprintf('\n');
```

Appendix B

```
% Display the results for seawater
fprintf('\nSeawater Capacitance (F)\n');
fprintf('Distance (m)\t');
fprintf('%0.2f\t', distances);
fprintf('\n');
fprintf('Capacitance\t');
fprintf('%0.2e\t', capacitances_sea);
fprintf('\n');

% Plotting the results for air
figure;
plot(distances, capacitances_air, '-o', 'DisplayName', sprintf('Area = %d m^2 (Air)', area));
xlabel('Distance (m)');
ylabel('Capacitance (F)');
title('Capacitance vs Distance (Air)');
legend show;
grid on;

% Plotting the results for freshwater
figure;
plot(distances, capacitances_fw, '-o', 'DisplayName', sprintf('Area = %d m^2 (Freshwater)', area));
xlabel('Distance (m)');
ylabel('Capacitance (F)');
title('Capacitance vs Distance (Freshwater)');
legend show;
grid on;

% Plotting the results for seawater
figure;
plot(distances, capacitances_sea, '-p', 'DisplayName', sprintf('Area = %d m^2 (Seawater)', area));
xlabel('Distance (m)');
ylabel('Capacitance (F)');
title('Capacitance vs Distance (Seawater)');
legend show;
grid on;

% Combine results into a single plot
figure;
hold on; % This allows plotting multiple lines on the same figure

plot(distances, capacitances_air, '-*', 'DisplayName', 'Air');
plot(distances, capacitances_fw, '-o', 'DisplayName', 'Freshwater', 'Color', 'k');
plot(distances, capacitances_sea, '-p', 'DisplayName', 'Seawater', 'Color', 'r');

hold off; % This turns off hold mode for subsequent plots (if any)

xlabel('Distance (m)');
ylabel('Capacitance (F)');
title('Capacitance vs Distance (Air, Freshwater, Seawater)');
legend show;
grid on;
```

Appendix C

```

clc;
clear;

% Constant parameters
Lm = 60e-9; % Inductance Lm in Henries
Cm = 180e-12; % Mutual capacitance Cm in Farads
Cs = 72e-12; % Self-capacitance Cs in Farads
LR = 122e-9; % Inductance LR in Henries
CR = 5.5e-12; % Capacitance CR in Farads

% Constants for medium
E0 = 8.8542e-12; % Permittivity of free space (F/m)
ERair = 1.0006; % Relative permittivity of air
ERfw = 79; % Relative permittivity of freshwater
ERsea = 81.5; % Relative permittivity of seawater
sigma = 0.011; % Conductivity (S/m)

% Define specific frequencies in Hz from 0 to 300 MHz with a step of 20 MHz
frequencies = 0:20e6:300e6;

% efficiency results
nmaxair_percentages = zeros(1, length(frequencies));
nmaxfw_percentages = zeros(1, length(frequencies));
nmaxsea_percentages = zeros(1, length(frequencies));

% Calculate A and B
A = (CR + 2 * Cs) * Cm * Lm * Cs * LR;
B = (((2 * Cs + Cm) * CR) + (4 * Cs * (Cs + Cm))) * LR + (Cm * Cs * Lm);

% Display header for calculated values
disp('Frequency (MHz) Qair Qfw Qsea kp kQair kQfw kQsea');
nmax (Air, %) nmax (Freshwater, %) nmax (Seawater, %));
disp(
('UNIVERSITI TEKNIKAL MALAYSIA MELAKA',
% Loop over specified frequencies to calculate efficiencies
for i = 1:length(frequencies)
    f = frequencies(i); % Current frequency in Hz
    omega = 2 * pi * f; % Angular frequency

    % Calculate Q factors for freshwater and air
    Qair = (omega * ERair * E0) / sigma;
    Qfw = (omega * ERfw * E0) / sigma;
    Qsea = (omega * ERsea * E0) / sigma;

    % Calculate D and E
    D = abs(Cm * (1 - (omega^2) * CR * LR));
    E = abs((A * (omega^4)) - (B * (omega^2)) + (2 * Cs + Cm));

```

Appendix D

```

% Calculate kp
kp = D / E;
kp_values(i) = kp; % Store kp value

% Calculate kQ for freshwater , air and seawater
kQair = kp * Qair;
kQfw = kp * Qfw;
kQsea = kp * Qsea;

% Calculate nmax for freshwater, air and seawater
nmaxair = 1 - (2 / (1 + sqrt(1 + (kQair)^2)));
nmaxfw = 1 - (2 / (1 + sqrt(1 + (kQfw)^2)));
nmaxsea = 1 - (2 / (1 + sqrt(1 + (kQsea)^2)));

% nmax in percentage
nmaxair_percentages(i) = nmaxair * 100;
nmaxfw_percentages(i) = nmaxfw * 100;
nmaxsea_percentages(i) = nmaxsea * 100;

% Display Q, kp, kQ, and nmax values for each frequency
fprintf('%10.0f MHz      %8.2f %8.2f %8.2f %8.2f %8.2f %8.2f %8.2f %20.2f \n', ...
        frequencies(i)/1e6, Qair, Qfw, Qsea, kp, kQair, kQfw, kQsea,
        nmaxair_percentages(i), nmaxfw_percentages(i), nmaxsea_percentages(i));
end

% Combined plot for Air, Freshwater, and Seawater
figure;
plot(frequencies/1e6, nmaxair_percentages, 'r-o', 'DisplayName', 'Air');
hold on;
plot(frequencies/1e6, nmaxfw_percentages, 'b-o', 'DisplayName', 'Freshwater');
plot(frequencies/1e6, nmaxsea_percentages, 'g-o', 'DisplayName', 'Seawater');
xlabel('Frequency (MHz)');
ylabel('Maximum Power Transfer Efficiency (%)');
title('Maximum Power Transfer Efficiency vs Frequency');
legend('show');

% plot for Air
figure;
plot(frequencies/1e6, nmaxair_percentages, 'r-o', 'DisplayName', 'Air');
xlabel('Frequency (MHz)');
ylabel('Maximum Power Transfer Efficiency (%)');
title('Maximum Power Transfer Efficiency vs Frequency (Air)');
legend('show');
for i = 1:length(frequencies)
    text(frequencies(i)/1e6, nmaxair_percentages(i), sprintf('%8.2f%%',
nmaxair_percentages(i)), 'VerticalAlignment', 'bottom', 'HorizontalAlignment',

```

Appendix E

```
'right');
end

% plot for Freshwater
figure;
plot(frequencies/1e6, nmaxfw_percentages, 'b-o', 'DisplayName', 'Freshwater');
xlabel('Frequency (MHz)');
ylabel('Maximum Power Transfer Efficiency (%)');
title('Maximum Power Transfer Efficiency vs Frequency (Freshwater)');
legend('show');
for i = 1:length(frequencies)
    text(frequencies(i)/1e6, nmaxfw_percentages(i), sprintf('%.2f%%',
nmaxfw_percentages(i)), 'VerticalAlignment', 'bottom', 'HorizontalAlignment',
'right');
end

% plot for Seawater
figure;
plot(frequencies/1e6, nmaxsea_percentages, 'g-o', 'DisplayName', 'Seawater');
xlabel('Frequency (MHz)');
ylabel('Maximum Power Transfer Efficiency (%)');
title('Maximum Power Transfer Efficiency vs Frequency (Seawater)');
legend('show');
for i = 1:length(frequencies)
    text(frequencies(i)/1e6, nmaxsea_percentages(i), sprintf('%.2f%%',
nmaxsea_percentages(i)), 'VerticalAlignment', 'bottom', 'HorizontalAlignment',
'right');
end

% Plot for kp vs Frequency
figure;
plot(frequencies/1e6, kp_values, 'm-o', 'DisplayName', 'kp');
xlabel('Frequency (MHz)');
ylabel('kp');
title('kp vs Frequency');
legend('show');
for i = 1:length(frequencies)
    text(frequencies(i)/1e6, kp_values(i), sprintf('%.2f', kp_values(i)),
'VerticalAlignment', 'bottom', 'HorizontalAlignment', 'right');
end

% Plot for kp vs Frequency (Air Medium)
figure;
plot(frequencies/1e6, kp_values, 'r-o', 'DisplayName', 'Air Medium');
xlabel('Frequency (MHz)');
ylabel('kp');
title('kp vs Frequency (Air Medium)');
legend('show');
for i = 1:length(frequencies)
    text(frequencies(i)/1e6, kp_values(i), sprintf('%.2f', kp_values(i)),
```

Appendix F

```
'VerticalAlignment', 'bottom', 'HorizontalAlignment', 'right');
end

% Plot for kp vs Frequency (Freshwater Medium)
figure;
plot(frequencies/1e6, kp_values, 'b-o', 'DisplayName', 'Freshwater Medium');
xlabel('Frequency (MHz)');
ylabel('kp');
title('kp vs Frequency (Freshwater Medium)');
legend('show');
for i = 1:length(frequencies)
    text(frequencies(i)/1e6, kp_values(i), sprintf('%.2f', kp_values(i)),
        'VerticalAlignment', 'bottom', 'HorizontalAlignment', 'right');
end

% Plot for kp vs Frequency (Seawater Medium)
figure;
plot(frequencies/1e6, kp_values, 'g-o', 'DisplayName', 'Seawater Medium');
xlabel('Frequency (MHz)');
ylabel('kp');
title('kp vs Frequency (Seawater Medium)');
legend('show');
for i = 1:length(frequencies)
    text(frequencies(i)/1e6, kp_values(i), sprintf('%.2f', kp_values(i)),
        'VerticalAlignment', 'bottom', 'HorizontalAlignment', 'right');
end
```

UNIVERSITI TEKNIKAL MALAYSIA MELAKA

Appendix G

```

% Given Parameters
Lp = 15.8e-9; % Parasitic Inductance (H)
Gp = 1.97e-3; % Parasitic Conductance (S)
Cp = 2.73e-12; % Parasitic Capacitance (F)
Cm = 198e-12; % Mutual Coupling Capacitance (F)
Gm = 0.689; % Mutual Conductance (S)
Cs = 3.62e-12; % Self-Coupling Capacitance (F)
Gs = 20.7e-3; % Self-Coupling Conductance (S)
CR = 5.5e-12; % Parasitic Capacitance (F)

% Frequency range from 0 MHz to 300 MHz
frequencies = linspace(0, 300e6, 1000); % Frequency range (Hz)
K_approx_values = zeros(size(frequencies)); % Initialize array for K_approx
F_values = zeros(size(frequencies)); % Initialize array for F

for i = 1:length(frequencies)
    f = frequencies(i); % Current frequency
    omega = 2 * pi * f; % Angular frequency (rad/s)

    % Calculate F (Equation (10))
    F_values(i) = Lp * ((2 * Gm + Gs) * ((4 * Gm + Gp + 2 * Gs) * Gp * Lp - 2 * Cp) * ω
    omega^2 + Gp + 2 * Gm);

    % Equation (11): Further Approximation of K
    K_approx_values(i) = Gm / sqrt((Gs + Gm)^2 - Gm^2);
end

% Select frequencies from 0 MHz to 300 MHz in 20 MHz intervals
frequencies_sampled = 0:20e6:300e6;
K_approx_sampled = zeros(size(frequencies_sampled));
F_sampled = zeros(size(frequencies_sampled));

for j = 1:length(frequencies_sampled)
    f = frequencies_sampled(j); % Current sampled frequency
    omega = 2 * pi * f; % Angular frequency (rad/s)

    % Calculate F (Equation (10)) for sampled points
    F_sampled(j) = Lp * ((2 * Gm + Gs) * ((4 * Gm + Gp + 2 * Gs) * Gp * Lp - 2 * Cp) * ω
    * omega^2 + Gp + 2 * Gm);

    % Equation (11): Further Approximation of K for sampled points
    K_approx_sampled(j) = Gm / sqrt((Gs + Gm)^2 - Gm^2);
end

% Display the table
disp(table_sampled_data);

% Plot F vs Frequency
figure;
plot(frequencies / 1e6, F_values, 'g-', 'LineWidth', 1.5);
hold on;
scatter(frequencies_sampled_MHz, F_sampled, 'r', 'filled');
xlabel('Frequency (MHz)');
ylabel('F');
title('F vs Frequency');
grid on;
hold off;

```

Appendix H

```

clc;
clear;

% Constant parameters
Lm = 60e-9;    % Inductance Lm in Henries
Cm = 180e-12; % Mutual capacitance Cm in Farads
Cs = 72e-12;  % Self-capacitance Cs in Farads
LR = 122e-9;  % Inductance LR in Henries
CR = 5.5e-12; % Capacitance CR in Farads

% Constants for medium
E0 = 8.8542e-12; % Permittivity of free space (F/m)
ERair = 1.0006;  % Relative permittivity of air
ERfw = 79;       % Relative permittivity of freshwater
ERsea = 81.5;    % Relative permittivity of seawater
sigma = 0.011;   % Conductivity (S/m)

% Define specific frequencies in Hz from 0 to 300 MHz with a step of 20 MHz
frequencies = 0:20e6:300e6;

% Efficiency results
nmaxair_percentages = zeros(1, length(frequencies));
nmaxfw_percentages = zeros(1, length(frequencies));
nmaxsea_percentages = zeros(1, length(frequencies));

% Calculate A and B
A = (CR + 2 * Cs) * Cm * Lm * Cs * LR;
B = (((2 * Cs + Cm) * CR) + (4 * Cs * (Cs + Cm))) * LR + (Cm * Cs * Lm);

% Calculations
% f_k1 and f_k3
fk1 = (1 / (2 * pi)) * sqrt((B - sqrt(B^2 - (4 * A * (2 * Cs + Cm)))) / (2 * A));
fk3 = (1 / (2 * pi)) * sqrt((B + sqrt(B^2 - (4 * A * (2 * Cs + Cm)))) / (2 * A));

% f_k0
fk0 = 1 / (2 * pi * sqrt(CR * LR));

% f_k2 and f_k4
fk2 = (1 / (2 * pi)) * sqrt((1 / (CR * LR)) - sqrt((1 / (CR^2 * LR^2)) - (B / (CR * LR * A)) + (2 * Cs + Cm) / A));
fk4 = (1 / (2 * pi)) * sqrt((1 / (CR * LR)) + sqrt((1 / (CR^2 * LR^2)) - (B / (CR * LR * A)) + (2 * Cs + Cm) / A));

% Convert frequencies to MHz
fk1 = fk1 / 1e6;
fk3 = fk3 / 1e6;
fk0 = fk0 / 1e6;
fk2 = fk2 / 1e6;
fk4 = fk4 / 1e6;

```